



1 **Copernicus Atmosphere Monitoring Service - Regional Air Quality Production System v1.0**

2 Augustin Colette¹, Gaëlle Collin², François Besson², Etienne Blot², Vincent Guidard^{2,14}, Frédéric Meleux¹, Adrien Royer²,
3 Valentin Petiot^{2,14}, Claire Miller², Oihana Fermond², Alizé Jeant², Mario Adani^{5,16}, Joaquim Arteta¹⁴, Anna Benedictow¹⁰,
4 Robert Bergström¹¹, Dene Bowdalo⁸, Jorgen Brandt⁴, Gino Briganti⁵, Ana. C. Carvalho¹¹, Jesper Heile Christensen⁴, Florian
5 Couvidat¹, Ilia D'Elia⁵, Massimo D'Isidoro⁵, Hugo Denier van der Gon¹², Gaël Descombes¹, Enza Di Tomaso^{3, 8}, John
6 Douros¹³, Jeronimo Escribano⁸, Henk Eskes¹³, Hilde Fagerli¹⁰, Yalda Fatahi⁹, Johannes Flemming³, Elmar Friese⁶, Lise Frohn⁴,
7 Michael Gauss¹⁰, Camilla. Geels⁴, Guido Guarneri⁵, Marc Guevara⁸, Antoine Guion¹, Jonathan Guth¹⁴, Risto Hänninen⁹, Kaj
8 Hansen⁴, Ulas Im⁴, Ruud Janssen¹², Marine Jeoffrion², Mathieu Joly¹⁴, Luke Jones³, Oriol Jorba⁸, Evgeni Kadantsev⁹, Michael
9 Kahnert¹¹, Jacek W. Kaminski⁷, Rostislav Kouznetsov⁹, Richard Kranenburg¹², Jeroen Kuenen¹², Anne Caroline Lange⁶,
10 Joachim Langner¹¹, Victor Lannuque¹, Francesca Macchia⁸, Astrid Manders¹², Mihaela Mircea⁵, Agnes Nyiri¹⁰, Miriam Olid⁸,
11 Carlos Pérez García-Pando^{8,15}, Julia Palamarchuk⁹, Antonio Piersanti⁵, Blandine Raux¹, Miha Razinger³, Lennard Robertson¹¹,
12 Arjo Segers¹², Martijn Schaap¹², Pilvi Siljamo⁹, David Simpson¹⁰, Mikhail Sofiev⁹, Anders Stangel⁹, Joanna Struzewska⁷,
13 Carles Tena⁸, Renske Timmermans¹², Thanos Tsikerdekis¹³, Svetlana Tsyro¹⁰, Svyatoslav Tyuryakov⁹, Anthony Ung¹,
14 Andreas Uppstu⁹, Alvaro Valdebenito¹⁰, Peter van Velthoven¹³, Lina Vitali⁵, Zhuyun Ye⁴, Vincent-Henri Peuch³, Laurence
15 Rouil^{1, ^a}

16 ¹INERIS: Institut National de l'Environnement Industriel et des Risques, Verneuil en Halatte, 60550, France

17 ²Météo-France, Saint-Mandé, 94165, France

18 ³ECMWF: European Centre for Medium-Range Weather Forecasts, Reading, RG2 9AX, United Kingdom

19 ⁴Aarhus University: Roskilde, 4000, Denmark

20 ⁵ENEA: Italian National Agency for New Technologies, Energy and Sustainable Economic Development, Bologna, 40129,
21 Italy

22 ⁶Forschungszentrum Jülich GmbH, ICE-3, Institute of Climate and Energy Systems - Troposphere, 52428 Jülich, Germany

23 ⁷IEP-NRI: Institute of Environmental Protection - National Research Institute, Warsaw, 00-001, Poland

24 ⁸BSC: Barcelona Supercomputing Center, Barcelona, 08034, Spain

25 ⁹FMI, Finnish Meteorological Institute, Helsinki, 00-001, Finland

26 ¹⁰MET Norway: Norwegian Meteorological Institute, Oslo, 0372, Norway

27 ¹¹SMHI: Swedish Meteorological and Hydrological Institute. Norrköping, SE-601 76, Sweden

28 ¹²TNO: Netherlands Organisation for applied scientific research, Utrecht, 3584, The Netherlands



- 29 ¹³ KNMI: Royal Netherlands Meteorological Institute, De Bilt, 3730, The Netherlands
- 30 ¹⁴: Centre National de Recherches Météorologiques - UMR 3589 CNRS/Météo-France, Toulouse, 31000, France
- 31 ¹⁵. Catalan Institution for Research and Advanced Studies (ICREA), 08010, Barcelona, Spain
- 32 ¹⁶Centro Euro-Mediterraneo sui Cambiamenti Climatici, 40127 Bologna, Italy
- 33 ^{^a}: now at: ECMWF: European Centre for Medium-Range Weather Forecasts, Reading, RG2 9AX, United Kingdom
- 34 *Correspondence to:* Augustin Colette (augustin.colette@ineris.fr)

35



36 **Abstract**

37 The Copernicus Atmosphere Monitoring Service (CAMS) delivers a range of **full**, free and open products in relation to
38 atmospheric composition at global and regional scales. The CAMS Regional Service produces daily forecasts, analyses, and
39 reanalyses of air quality in Europe. This Service relies on a distributed modelling production by eleven teams in ten European
40 countries: CHIMERE (France), DEHM (Denmark), EMEP (Norway), EURAD-IM (Germany), GEM-AQ (Poland), LOTOS-
41 EUROS (The Netherlands), MATCH (Sweden), MINNI (Italy), MOCAGE (France), MONARCH (Spain), SILAM (Finland).
42 The project management and coordination of the service is devoted to a Centralised Regional Production Unit. Each model
43 produces every day 24h analyses for the previous day and 97h forecasts for 19 chemical species over a spatial domain at
44 0.1x01. degree resolution (approximately 10km x 10km) with 420 points in latitude and 700 in longitude and 10 vertical levels.
45 Six pollen species are also delivered for the surface forecasts. The eleven individual models are then combined into an
46 ENSEMBLE median. In total, more than 82 billion data points are made available for public use on a daily basis.

47 The design of the system follows clear technical requirements in terms of consistency in the model setup and forcing fields
48 (meteorology, surface anthropogenic emission fluxes, and chemical boundary conditions). But it also benefits from a diversity
49 of in the description of atmospheric processes through the design of the eleven European Chemistry Transport Models (CTM)
50 involved.

51 The present article aims to provide a comprehensive technical documentation, both for the setup as well as for the diversity of
52 **CTM** involved in the Service. We also include an overview of the main output products, their public dissemination and the
53 related evaluation and quality control strategy.



54 1 Introduction

55 The Copernicus Atmosphere Monitoring Service (CAMS, atmosphere.copernicus.eu/) is the core global and regional
56 atmospheric environmental service operated by the European Centre for Medium-Range Weather Forecast (ECMWF) within
57 the European Union Copernicus Earth Observation Programme. It provides a range of **full**, free, open, and quality assured
58 products in relation to global and regional air quality, inventory-based emissions, observation-based surface fluxes of
59 greenhouse gases and from biomass burning, solar energy, ozone and UV radiation, and climate forcings (Peuch et al., 2022).

60 We focus here on the regional production service (<https://atmosphere.copernicus.eu/european-air-quality-forecast-plots/>)
61 which provides daily 4-day forecasts of the main air quality species and analyses of the day before, as well as posterior re-
62 analyses using the latest observation datasets available for assimilation. It constitutes today the reference air quality forecasting
63 system at European scale by building upon a distributed production of eleven chemistry transport models operated in ten
64 European countries, with a Centralised Regional Production Unit to ensure a consistent implementation. Such a comprehensive
65 air quality forecasting system operated at continental scale has no equivalent in the world.

66 Air quality monitoring and forecasting constitute an essential activity to improve the knowledge of atmospheric composition
67 and air pollution patterns and identify short and long-term mitigation strategies. In the European legislation, the Directive (Ec,
68 2008) on ambient air quality and cleaner air for Europe of the European Parliament and of the European Council, defines limit
69 and target values for regulatory ambient air concentrations and improvement of ambient air quality to avoid, prevent or reduce
70 harmful effects on human health and the environment. To this end, it sets out the methodological requirements for the
71 assessment of ambient air quality in Member States which are based on the implementation of adequate monitoring systems,
72 typically relying on reference and standardised instruments operated at air quality monitoring stations whose data are reported
73 to the Air Quality e-reporting database maintained by the European Environment Agency (which subsequently makes the data
74 publicly available). A revision of the Ambient Air Quality Directive was adopted by the European Council in October 2024,
75 the revision includes amongst other features, a stronger emphasis on the use of air quality models as well as an explicit reference
76 to the Copernicus Atmosphere Monitoring Service as a trusted source of information products and supplementary tools to
77 support reporting activities in relation to forecasting and management of air pollution episodes.

78 Modelling comes as a complementary information on ambient air quality. Fitness for forecasting purposes of air quality
79 modelling has been widely documented (Zhang et al., 2012a, b), but air quality models are also essential to produce exposure
80 maps through data assimilation or data fusion. In such processes, the prior modelled estimates of surface air concentrations of
81 the main air pollutants are combined with in situ or remote sensing observations to produce improved mapping of air pollution,
82 typically for use in health impact assessment or epidemiological studies (Shaddick et al., 2020). Air quality modelling and
83 reanalyses are also typically used to anticipate ex-ante and assess ex-post the effectiveness of policy mitigation strategies. The



84 projections and hindcasts performed in the framework of the Convention on Long Range Transboundary Air Pollution
85 (CLRTAP) of the United Nations Economic Commission for Europe Geneva Air Convention and its Gothenburg Protocol
86 constitute a good example of atmospheric modelling activities in support of policy decisions at European scale (Maas and
87 Grennfelt 2016).

88 Whereas several European countries or selected metropolitan areas operate their own air quality modelling system, there is
89 also a need to produce air quality forecasts and analyses over the whole European continent: to provide background data for
90 those local systems (chemical boundary conditions), for the areas not covered by any national system, or just as complementary
91 information. The Copernicus Atmosphere Monitoring Service has played that role since 2015. It builds upon the earlier
92 research and development phases initiated since 2005 through European collaborative research and innovation projects: GEMS
93 (Hollingsworth, 2008) and MACC, MACC-II, and MACC-III (Marécal et al., 2015; Peuch et al., 2014).

94 The unique setup of the system allows it to reach an unprecedented level of quality and robustness by relying on a set of
95 stringent common requirements combined with a large variety of Chemistry-Transport Models (CTMs). Since 2022, an
96 ensemble of eleven CTMs have been used: CHIMERE (INERIS, France), DEHM (Aarhus Univ., Denmark), EMEP (Met
97 Norway), EURAD-IM (Forschungszentrum Juelich, Germany), GEM-AQ (IEP-NRI, Poland), LOTOS-EUROS (TNO and
98 KNMI, The Netherlands), MATCH (SMHI, Sweden), MINNI (ENEA, Italy), MOCAGE (Météo-France, France),
99 MONARCH (BSC, Spain), SILAM (FMI, Finland). Using an ensemble of CTMs allows at the same time to minimize the risk
100 of failure in the daily operational production, and to increase the skill of the forecast (Galmarini et al., 2013). But consistency
101 in the implementation is key to ensure the continuous improvement of the system, hence the crucial role of the CAMS Regional
102 Central Production Unit led by Météo-France and INERIS.

103 Each model delivers every day 24h analyses and 97h forecast for 19 chemical species over a spatial domain at 0.1x0.1 degree
104 resolution (approximately 10km x 10km) with 420 points in latitude and 700 in longitude and 10 vertical levels. Additionally,
105 surface forecasts of six pollen species are delivered. With the 11 individual models and one ENSEMBLE median, it is a total
106 of almost 82 billion data point made available for public use every day.

107 The results of the CAMS Regional Service are made publicly available as quick looks on the website
108 atmosphere.copernicus.eu/european-air-quality-forecast-plots and the numerical outputs are disseminated on the Copernicus
109 Atmosphere Data Store: ads.atmosphere.copernicus.eu. The typical use of the forecasts is as background information used by
110 national and local air quality agencies, in addition to their knowledge about specific local air pollution sources. This can be
111 done either qualitatively by the consultation of available online viewers, or by using the numerical data to feed downstream
112 chemistry-transport, gaussian, or machine-learning models. The use of reanalyses is rather for policy applications (for



113 regulatory reporting obligations or to assess the impact policy interventions through trends analyses) or exposure assessment
114 in health impact studies.

115 The aim of the present article is to provide a transparent and detailed documentation to serve as a reference for the user of
116 CAMS Regional Air quality Products. It constitutes an update of the previous similar article devoted to the MACC regional
117 forecast system (Marécal et al., 2015), whereas the system was still in research mode at the time and not fully operational. A
118 focus on regional activities within the overall CAMS portfolio was also described in (Peuch et al., 2022). The CAMS Regional
119 production system has evolved continuously over the past. In the present article, we provide a detailed description of the system
120 as it stands in 2024. But since the near real time production of forecast and analysis remains available for public use with a 3-
121 year retention time, and reanalysis data remain available since the beginning of the production, we also provide some
122 information about the major evolutions in the recent past.

123 The main characteristics of the centralised production system are introduced in Section 2. This section covers the overall
124 production workflow, but also the common features and requirements which apply to the distributed production of individual
125 modelling teams such as the common external forcing data. Since the use of an ensemble of eleven different chemistry transport
126 models is an important specificity of the service, we devote a large part of the paper in Section 3 to summarize the formulation
127 of each model and how they adapt specifically to the requirement of the CAMS Regional Production System. The post-
128 processing as well as some elements regarding the evaluation and quality control or the main uses of the production are
129 presented in Section 4. In the conclusion (Section 5) we refer to the short and long-term development priorities to ensure the
130 performance and sustainability of the system over the long term.



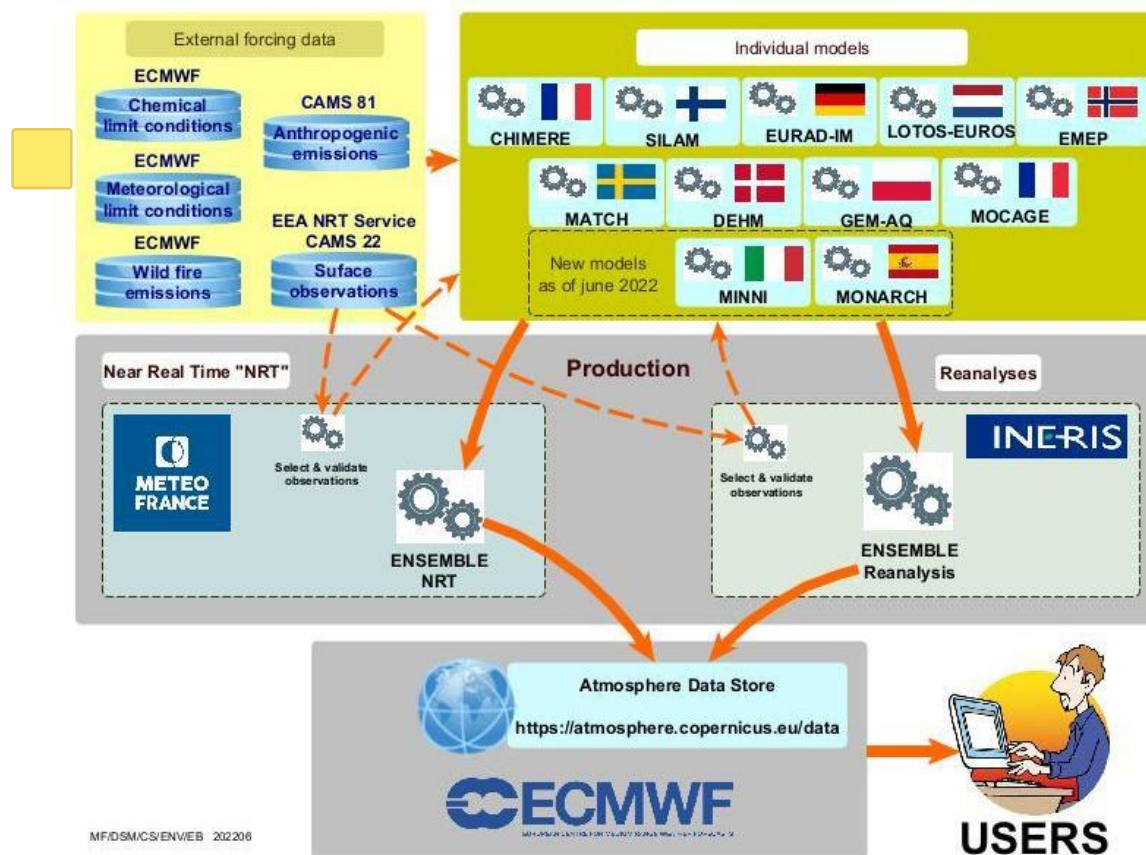
131 2 Centralised Regional Production Unit

132 2.1 Organisation of the production system

133 The CAMS regional production relies on a quite unique ensemble of 11 individual models whose daily operation is distributed
134 amongst 11 modelling centres in ten European countries. The coordination is handled by the Central Regional Production Unit
135 (CRPU) which is led by Météo-France, with the support of INERIS for model development matters and reanalysis production
136 (Figure 1).

137 The CRPU defines the design of the regional production system under the auspices of ECMWF. This includes setting the
138 guidance and requirements for the implementation of individual models as well as continuous evolution in order to maintain
139 the system within the state of the art. The CRPU is also in charge of contractual matters and relations with the providers of
140 input data as well as the delivery of model results to the Atmosphere Data Store for public use (Section 4.3).

141 In earlier MACC phases and the first CAMS regional project, only 7 models were contributing to the distributed operational
142 production: CHIMERE, EMEP, EURAD-IM, LOTOS-EUROS, MATCH, MOCAGE, and SILAM. As of October 2019,
143 DEHM and GEM-AQ joined the operational system. As of June 2022, MINNI and MONARCH joined the production.



144

145 *Figure 1: Schematic of the CAMS Regional Production workflow. Top-left the external forcings (anthropogenic emissions, meteorology,*
146 *boundary conditions) and in-situ observations for assimilation and evaluation. Top right: eleven regional chemistry-transport model*
147 *operated in ten European countries. Middle: Meteo-France (for the near real time) and INERIS (for the reanalysis) centralise the individual*
148 *productions. Bottom: the results are disseminating to the Atmosphere Data Store.*

149 2.2 Modelling products

150 The CAMS regional system includes both daily 4-days forecasts and several analysis products. All of them are provided from
151 both eleven individual CTMs results and an ENSEMBLE product which is constituted by the median of individual models at
152 each grid point.

153 Hourly near-real time forecasts (NRT/FC) are released every day with a 4 days horizon (from 0 to 96hrs forecasts). They rely
154 on chemistry-transport outputs, some of which are initialised on the basis of the previous analysis (see details in Section 3).
155 The ENSEMBLE NRT/FC fields are made available publicly each day at 08:00 UTC for forecast horizon 0 to 48hrs (day 1
156 and day 2), and at 10:00 UTC for forecast horizon 49 to 96hrs (day 3 and days 4).



157 As of January 2024, the list of species in the NRT/FC includes the following gases: ozone (O₃), nitrogen oxide (NO), nitrogen
158 dioxide (NO₂), carbon monoxide (CO), sulphur dioxide (SO₂), glyoxal (CHOCHO), formaldehyde (HCHO), ammonia (NH₃),
159 total Non-Methane Volatile Organic Compounds (NMVOC), total Peroxy-Acetyl Nitrates (PANs). Particulate matter (PM)
160 are included as : PM_{2.5} (smaller than 2.5µm), PM₁₀ (smaller than 10µm). The following tracers in the PM_{2.5} fraction are also
161 provided: secondary inorganic aerosols (SIA), total elemental carbon (EC), EC fraction related to residential emissions, total
162 organic matter. In the PM₁₀ fraction, the tracers include desert dust, sea salt and wildfires. In addition, six pollen species are
163 included: birch, olive, grass, alder, mugwort and ragweed.

164 Hourly near-real time analysis (NRT/AN) are released each day by 12:00 UTC for the previous day. Here, each individual
165 model is corrected to minimise error with observed air pollutant concentrations over Europe. For the latest reanalysis available
166 on the ADS as of January 2024 (covering the year 2021), the list of species is: for O₃, NO, NO₂, CO, NH₃, NMVOC, PM₁₀,
167 PM_{2.5}, PM₁₀ wildfires, PM₁₀ dust, EC total, EC residential, PAN, SIA, SO₂. For earlier years, not all of these species are
168 available, and in the future the list will continue expanding to catch up with the full species set in the daily forecast production.
169 Note that observations are not available for all of those species, individual components contributing to the total PM₁₀ or PM_{2.5}
170 mass are scaled according to the assimilation of total PM₁₀ or PM_{2.5} measurements, and pollen species are not assimilated.

171 The daily analyses products are supplemented by an interim reanalysis (IRA) and a validated reanalysis (VRA). Both rely on
172 the same modelling tools as the NRT production, including assimilation strategy. But the observations taken into account
173 differ. Acknowledging that for the NRT/AN production some observations can be missing or not validated, daily analyses are
174 reproduced with a 20 days delay in the IRA. This time gap is considered sufficient to fix most failures in NRT data flows and
175 maximise the number of available measurement data. The interim reanalysis is subsequently consolidated and delivered in the
176 first months of Y+1. Since all observations are only definitively validated by European member states by the end of the
177 following year (Y+1), the full year Y is reprocessed in Y+2 to produce the VRA of the corresponding year.

178 **2.3 Air quality observations**

179 The gathering, filtering and selection of observations is centralised by the CRPU and subsequently disseminated to individual
180 modelling teams which apply different assimilation algorithms even though the exact same stations are assimilated by each
181 model (see details in Section 3). All observation data are obtained from the Air Quality e-reporting database¹ maintained by
182 the European Environment Agency where near real time “up-to-date” (UTD) and validated observations are reported, in
183 particular for countries of the European Union which are expected to do so with respect to the European Directives.

¹ <https://www.eea.europa.eu/data-and-maps/data/aqereporting-9>, last accessed 30/10/2024



184 An important step lies in the filtering and selection of data, where an objective classification is applied based upon the temporal
185 variability patterns of the air pollutant concentrations to differentiate background and proximity stations (Joly and Peuch,
186 2012). Traffic and industrial sites are excluded from the assimilation strategy, but since November 2020 stations falling in
187 classes 1-7 of the Joly & Peuch classification are included, which means broadly that urban background sites are taken into
188 account, whereas earlier than November 2020, only suburban and rural sites were included. This way, even if the spatial
189 resolution of the CAMS Regional Production is 10x10km, we ensure the relevance of the modelling setup to capture urban
190 background air quality.

191 Approximately 2-third of the stations' data are distributed by the CRPU for assimilation (both for NRT/AN and IRA&VRA),
192 while the rest of the data are kept for evaluation (see Section 4.2).

193 At present there is no centralisation of the dissemination of any satellite observation of atmospheric composition even if many
194 individual modelling teams already assimilate satellite data, and this is expected to further develop in the coming years (See
195 details in the presentation of individual models in Section 3).

196 **2.4 Modelling domain**

197 The modelling domain covers Europe within 25°W to 45°E longitude and 30°N to 72°N latitude at a 0.1°x0.1° resolution.
198 Whereas in earlier phases of the project some individual models were operating at slightly lower resolution (about 0.2°), today
199 all models operate on a native resolution of about 0.1°. Covering the whole region is a strong requirement, and all models
200 deliver data over the entire domain, which means that some of them perform the forecast on a slightly larger domain in order
201 to include a buffer area or cope with differing geographic projection (see details in Section 3). The spatial extent has evolved
202 marginally in recent years, it was only reaching up to 70°N until June 2019.

203 The strategy for the vertical discretisation is left open for individual contributing models, but there is a common requirement
204 in the delivery of model results on common vertical levels. As of January 2024, the complete list of vertical levels is: surface,
205 50m, 100m, 250m, 500m, 750m, 1000m, 2000m, 3000m, and 5000m above ground. This has evolved substantially in recent
206 years, only surface concentrations were provided in the earlier phases of CAMS, and different lists of vertical levels have been
207 archived in the past for near real time forecast, analyses, and reanalysis products.

208 **2.5 Meteorology and chemical boundary conditions**

209 The meteorological fields used to force the individual operational CTMs are from the operational IFS (Integrated Forecasting
210 System) daily meteorological forecasts of the European Centre for Medium-Range Weather Forecasts (ECMWF). The spatial
211 resolution of the IFS forecast has increased in time, it is about 9km as of 2024. The exact list of meteorological parameters



212 used to drive the individual CTMs differs depending on the models (see details in Section 3). Most of them use the forecast
213 starting at 12:00 UTC on D–1 but there might also be some deviations to account for operational constraints.

214 The chemical boundary conditions are also obtained from ECMWF but using the configuration of the IFS including chemistry
215 (Flemming et al., 2015; Rémy et al., 2019) operating at approximately 40km spatial resolution. This configuration of the IFS
216 model runs forecasts twice daily from 00 and 12 UTC and the data are available every hour (for surface fields) and every 3
217 hours (for el- and pressure-level fields). The model results are made available for further use as boundary conditions of
218 regional models through different dissemination routes including the MARS archive server of ECMWF, a dedicated ftp access
219 for the regional CAMS operational models and the atmosphere data store (ADS) of Copernicus.

220 The list of species used as boundary conditions for the regional CAMS models is given in Table 2. Further details are available
221 through the CAMS User Support website² and (Morcrette et al., 2009). All aerosol species are provided as dry PM, except for
222 sea salt, whose mass and size is provided at a relative humidity of 80%. The mass of the corresponding dry sea salt is 1/4.3
223 smaller and the radius is half of the sea salt at relative humidity of 80%.

224 **2.6 Surface emissions**

225 **2.6.1 Anthropogenic emissions**

226 Using identical anthropogenic emissions in all the eleven individual models is essential for the consistency of the CAMS
227 Regional products. The so-called TNO-MACC-III (Kuenen et al., 2014) emission inventory was used for several years in the
228 past. Since June 2019, it has been replaced by the CAMS-REG emissions inventory, which is regularly updated (Kuenen et
229 al., 2022). The CAMS-REG inventory is based on official national totals of air pollutant emissions reported in compliance
230 with the European Directive on National Emission Reduction Commitments (2016/2284/EU) and the Gothenburg Protocol of
231 the LRTAP Convention. Additional processing is applied to ensure consistency in the dataset by making corrections and
232 performing some gap-filling where information is missing. A consistent spatial distribution for gridded emission datasets is
233 applied at $0.05^\circ \times 0.1^\circ$ resolution. Since June 2021, the CAMS Regional production has used an improved version of the
234 CAMS-REG inventory which substituted national estimates of wood burning emission in order to cope with a well-established
235 inconsistency in the reporting of condensable emissions (Denier Van Der Gon et al., 2015).

236 The use of officially reported emissions induces a subsequent delay in the successive updates of the emission datasets. The
237 Emissions for year Y, are reported in March Y+2. Then they undergo verification, gap filling and spatialisation before being

² <https://confluence.ecmwf.int/display/CKB/CAMS%3A+Global+atmospheric+composition+forecast+data+documentation>
(last accessed 30/10/2024)



238 considered for implementation in the CAMS Regional production. The emissions being used for the day-to-day forecasts are
239 thus generally based on national emissions reported about 3 years earlier. In order to cope with this limitation, the CAMS-
240 REG emission inventory developed a proxy inventory for the recent years, still based on the officially reported emissions. This
241 way, the emission implemented in late 2023 in the regional production could be based on an estimate for the year 2022.

242 Only the spatialised annual fluxes of NO_x , SO_x , non-methane volatile organic compounds, (NMVOCs), NH_3 , CO , PM_{10} and
243 $\text{PM}_{2.5}$ emissions are prescribed for all models. The subsequent disaggregation required in CTMs in terms of (i)
244 hourly/daily/weekly/monthly profiles, (ii) vertical injection height, and (iii) mapping towards model chemical species is left
245 open for individual modelling teams. Default information is nevertheless provided regarding the temporal disaggregation
246 (Guevara et al., 2021) as well as the ventilation of total VOC or total PM on individual VOC species or aerosol species,
247 respectively.

248 **2.6.2 Biogenic, natural and wildfire emissions**

249 Biogenic emissions are left to the choice of individual operational models, most of which include their own online calculation
250 of emissions from vegetation and other natural sources. They include soil emissions for (i) mineral dust resuspension, (ii) soil
251 NO_x or even (iii) sea salt within the European domain.

252 The only coordination regarding ecosystem emissions concerns wildfires where all models are expected to use the Global Fire
253 Assimilation System (GFAS) product (Kaiser et al., 2012) provided by CAMS. GFAS is based on fire radiative power retrievals
254 from data of the Moderate Resolution Imaging Spectroradiometer (MODIS) instruments aboard the Terra and Aqua satellites.
255 GFAS provides hourly emission data with a 8-hr delay compared to real time. Each individual modelling team retrieves GFAS
256 emission when initiating their forecast. As the individual forecasts are initiated between 12:00 D-1 and 03:00 D+0 depending
257 on the regional systems, the only full day where GFAS wildfire emissions are available is D-2, and some systems also include
258 part of D-1 emissions. Each system therefore reconstructs a 24hr cycle of emission based either on D-2 only or also including
259 part of D-1 emissions. This cycle is used by all models for their analysis of D-1. For the forecast, persistence of this daily cycle
260 of emission is only maintained for D+0 and D+1 considering that the vast majority of wildfires in Europe are not persisting
261 for longer time periods.

262 **2.6.3 Pollen emission and dispersion**

263 The following pollen species are included in the CAMS Regional production: birch, grass, olive, ragweed, alder, and mugwort.
264 Their implementation in the individual operational CAMS models is more uniform than for the air pollutants as they all rely
265 on the documentation of (Sofiev et al., 2013). The pollen species differ in terms of their geographic distribution (source masks),
266 total amount of available pollen grains, start and end date of the season (heatsum thresholds), and the shape of the season



267 (source strength as function of time). The alder pollen emission model is similar to that of birch and olive, while the mugwort
268 source is a variation of the grass source. However, mugwort is implemented as five different sub-species, each with its own
269 spatially gridded start and end dates of the flowering season. Ragweed pollen follows the method described in (Prank et al.,
270 2013).

271 Once emitted, pollen species are advected in the model in the same way as other chemically inert species and are subject to
272 gravitational settling over time.





273 3 Individual Model Description

274 3.1 CHIMERE

275 3.1.1 Model Overview

276 CHIMERE is a multi-scale CTM developed jointly by INERIS and CNRS (Menut et al., 2021). Its development was initiated
277 in the early 2000s (Bessagnet et al., 2004; Vautard et al., 2005) and it has since then pioneered operational national air quality
278 forecasting in France (Rouïl et al., 2009). It is also extensively used for long-term simulations for emission control scenarios
279 (Colette et al., 2013; Meleux et al., 2007; Colette et al., 2015). It runs over a range of spatial scale from the hemispheric to the
280 urban scale, with resolutions from 100km to 1km (Colette et al., 2014; Bessagnet et al., 2017). The exact model version used
281 since June 2021 in the CAMS Regional Production is CHIMERE v2020r1.

282 3.1.2 Model geometry

283 For the CAMS regional forecasts, CHIMERE uses a regular latitude-longitude grid with a $0.1^\circ \times 0.1^\circ$ resolution which covers
284 25°W to 45°E and 30°N to 72°N and 9 vertical levels, extending from the surface up to 500 hPa, a lowermost layer about 20m
285 deep and about 7 layers below 2 km. No vertical downscaling is applied and concentrations in the lowermost model layer are
286 considered representative of the surface.

287 3.1.3 Forcing Meteorology

288 The forcing meteorology is retrieved from the IFS model vertical layers covering the CHIMERE vertical extent on a $0.2^\circ \times 0.2^\circ$
289 horizontal grid resolution with a temporal resolution of 3 hours. The forecast released at 00:00UTC of the previous days is
290 used. The three-dimensional meteorological parameters included to force the CHIMERE forecast are horizontal wind
291 components, temperature, specific humidity, orography, rain water/snow mixing ratios, cloud liquid and ice water contents.
292 The 2D variables included are: surface temperature, surface pressure, large scale and convective precipitations, boundary layer
293 height, sensible and latent heat fluxes at surface, surface solar radiation downwards, soil parameters (water and temperature)
294 for 4 layers (0-7 cm, 7-28 cm, 28-100 cm, 100-255 cm), sea ice cover, snow depth.

295 3.1.4 Chemical initial and boundary conditions

296 Lateral and top boundary conditions are taken from chemical species available in the global IFS forecast model of the previous
297 day at 3hr temporal resolution. The full list of species used from the IFS model is given in Table 2. The forecasts are initialised
298 by the CHIMERE forecasts of the previous day.

299



300 **3.1.5 Emissions**

301 The common annual anthropogenic emissions CAMS-REG are implemented as explained in Section 2.5.1. Temporal
302 disaggregation is based on TNO time profiles provided with CAMS-REG. Chemical disaggregation for VOCs is based on
303 (Passant, 2002). PM components are speciated using the splits provided with the CAMS-REG database.

304 Biogenic VOC emissions are computed online with the MEGAN 2.10 algorithm (Guenther et al., 2012) implemented in
305 CHIMERE and using high spatiotemporal data LAI (30 arcsec every 8 days) generated from MODIS (Yuan et al., 2011).
306 Biogenic emission factors are estimated based on the 30 arcsec USGS (US Geophysical Survey) land-use database and the
307 emission factors provided for each functional type by (Guenther et al., 2012).

308 The hourly GFAS wildfire emission for D-2 (i.e. the last full day available when launching the forecast system) are used for
309 the analysis (D-1) and the first two days of the forecast (D+0 and D+1). Fire emissions are set to zero for the remainder of the
310 forecast horizon.

311 Dust production within the European domain is included (Alfaro and Gomes, 2001). It is based on a scheme for saltation and
312 a vertical flux estimate using cohesion kinetic energies scheme (Marticorena and Bergametti, 1995).

313 **3.1.6 Solver, advection and mixing**

314 The numerical time solver is based on a splitting operator which solves separately transport (including deposition and
315 emissions), chemistry and aerosol formation.

316 Advection is based on the Piecewise Parabolic Method 3d order scheme (Colella and Woodward, 1984). Vertical turbulent
317 mixing takes place only in the boundary layer. The formulation uses K-diffusion parameterisation (Troen and Mahrt, 1986),
318 without counter-gradient term.

319 **3.1.7 Deposition**

320 Dry deposition of gaseous and particle species is parameterised as a downward flux out of the lowest model layer where the
321 deposition velocity is described through a resistance analogy (Wesely, 1989). Wet deposition of particles and gases are
322 computed by using a polydisperse distribution of rain droplets based on (Willis and Tattelman, 1989) and by computing the
323 efficiency of the collision. Below-cloud scavenging of gases is assumed irreversible and is therefore only accounted for the
324 most soluble compounds (HNO_3 , H_2O_2 , HCl , SO_2 and NH_3). In-cloud scavenging is accounted for all gases by computing the
325 gaseous and aqueous phases partitioning based on Henry's law constants and the pH of the clouds. Scavenging by snow is also
326 accounted for and is based on (Chang, 1984) for gases and on (Wang et al., 2014) for particles.



327 **3.1.8 Chemistry and aerosols**

328 In order to optimise computing time, the reduced MELCHIOR2 mechanism with 44 species and about 120 reactions is derived
329 from the full mechanism MELCHIOR (Derognat et al., 2003). The sectional aerosol module accounts for 7 species and 10 bins
330 from 10nm to 40 μ m (primary particle material, nitrate, sulphate, ammonium, biogenic secondary organic aerosol SOA,
331 anthropogenic SOA and water). Photolytic rates are attenuated using liquid water and relative humidity. The aerosol module
332 is described in great details in (Couvidat et al., 2018) and accounts for condensation, nucleation, and condensation/evaporation.
333 Aerosol thermodynamic equilibrium is achieved using the ISORROPIA model version 2.1. The secondary organic aerosol
334 formation mechanism used in the operational forecasting version of CHIMERE is described in (Bessagnet et al., 2008).

335 **3.1.9 Assimilation system**

336 The CHIMERE assimilation for operational purposes relies on a kriging based approach to assimilate hourly concentration
337 values for correcting the raw model results. For the analysis period, linear regression between a selected set of observations
338 (excluding mountain and proximity sites) and the raw CHIMERE model is performed (in moving neighbourhood). The
339 experimental variogram of the regression residuals is then computed and a variogram model is fitted; the model adequacy is
340 checked by cross validation. Ultimately, observations are kriged with the CHIMERE model as external drift (in moving
341 neighbourhood). This method is applied for O₃ and NO₂. For PM₁₀ and PM_{2.5}, an ordinary co-kriging of the observations (main
342 variable) and CHIMERE (secondary variable) is applied to ensure consistency between both pollutants. Only in-situ surface
343 observations are used.

344 Further evolution of the CHIMERE assimilation system using an ensemble Kalman Filter approach is under development, in
345 particular to pave the way for assimilation of satellite data. It has however not yet demonstrated to provide better skill score
346 than the geostatistical method.

347



348 **3.2 DEHM**

349 **3.2.1 Model Overview**

350 The Danish Eulerian Hemispheric Model (DEHM) is a 3-dimensional, offline, large-scale, Eulerian, atmospheric chemistry
351 transport model developed to study long-range transport of air pollution in the Northern Hemisphere. DEHM was originally
352 developed in the early 1990's in order to study the atmospheric transport of sulphur-dioxide and sulphate into the Arctic
353 (Christensen, 1997; Heidam et al., 2004). The model has been modified, extended and updated continuously since then and
354 now includes a flexible setup with the possibility for nested domains with higher resolutions over targeted areas (Brandt et al.,
355 2012; Geels et al., 2021). Apart from standard air pollution components and pollen, the DEHM model also includes mercury
356 (Christensen et al., 2004), CO₂ (Lansø et al., 2019) and POPs (Hansen et al., 2008).

357 **3.2.2 Model geometry**

358 The horizontal domain is defined on a regular latitude-longitude grid of 0.1° resolution with grid centre points covering
359 longitude 24.95°W to 44.95°E and latitude 30.05°N to 71.95°N. The vertical discretization is defined on 29 terrain-following
360 sigma levels up to about 100hPa. The 12 lowest layers are within the lowest 1 km of the atmosphere and the thickness of the
361 lowest layer is about 20m. The model includes an option for downscaling to the surface, but this is not applied in the operational
362 setup.

363 **3.2.3 Forcing Meteorology**

364 The forcing meteorology is retrieved from the IFS model vertical layers covering the DEHM vertical extent on a 0.2°x0.2°
365 horizontal grid resolution with a temporal resolution of 3 hours. The forecast released at 12:00 UTC of the previous days is
366 used. The meteorological parameters included to force the DEHM forecast are: 3D fields of the horizontal wind components
367 (U,V), temperature, specific humidity, cloud liquid water contents, cloud ice water contents, rain water contents, snow water
368 contents and fraction of cloud cover. The 2D fields are land-sea mask, surface pressure, geopotential height, skin temperature,
369 Ustar, large scale and convective rain, snow depth, sensible heat flux, latent heat flux, net solar radiation, boundary layer
370 height, 2 m temperature, 2 m dew point temperature, 10 m wind (U,V), albedo, sea ice area fraction and surface roughness.

371 **3.2.4 Chemical initial and boundary conditions**

372 Lateral and top boundary conditions are taken from chemical species available in the global IFS forecast model of the previous
373 day at 3 hr temporal resolution. The full list of species used from the IFS model is given in Table 2. The DEHM forecasts are
374 initialised by the DEHM forecasts of the previous day.



375 **3.2.5 Emissions**

376 The common annual anthropogenic emissions CAMS-REG are implemented as explained in Section 2.5.1. Originally the
377 temporal disaggregation was based on the GENEMIS tables, using a GNFR to SNAP matrix. From 2021 the new CAMS-
378 TEMPO (Guevara et al., 2021) profiles for annual, monthly, weekly and daily distribution of emissions have been included in
379 the operational version of DEHM. PM components are speciated using the splits provided with the CAMS-REG emissions.
380 The speciation of VOCs from the emission input of total non-methane VOCs is based on the global speciated NMVOC
381 emission database EDGAR 4.3.2 (Huang et al., 2017).

382 Natural emissions of the Biogenic Volatile Organic Compounds (BVOCs) isoprene and monoterpenes are estimated in the
383 DEHM model based on the MEGAN model (Zare et al., 2012). The production of sea salt aerosols at the ocean surface is
384 based on two parameterisation schemes describing the bubble-mediated sea spray production of smaller and larger aerosols.
385 In each time step, the production is calculated for 10 size bins and thereafter summed up to give an aggregated production of
386 fine (with dry diameters $<1.3 \mu\text{m}$) and coarse (with dry diameters ranging $1.3\text{-}6\mu\text{m}$) aerosols (Soares et al., 2016). Soil and
387 lightning emissions are based on data from the Global Emissions Inventory Activity (Yienger and Levy, 1995).

388 The hourly GFAS wildfire emissions are retrieved as soon as they are available (i.e. with a 8-hr delay from real time) in order
389 to obtain a recent 24hr cycle spanning over D-2 and D-1. This cycle is used for the analysis (D-1) and the first two days of the
390 forecast (D+0 and D+1). Fire emissions are set to zero for the remainder of the forecast horizon. Hourly injection heights are
391 calculated based on the hourly data of ‘Mean altitude of maximum injection’ and ‘Altitude of plume top’.

392 **3.2.6 Solver, advection and mixing**

393 The horizontal advection is solved numerically using the higher order Accurate Space Derivatives scheme, documented to be
394 very accurate (Dabdub and Seinfeld, 1994), especially when implemented in combination with a Forester filter (Forester,
395 1977). The vertical advection as well as the dispersion sub-models is solved using a finite elements scheme (Pepper et al.,
396 1979) for the spatial discretization. For the temporal integration of the dispersion, the q-method (Lambert, 1991) is applied and
397 the temporal integration of the 3-dimensional advection is carried out using a Taylor series expansion to third order. Time
398 integration of the advection is controlled by the Courant-Friedrich-Lewy (CFL) stability criterion. A wind adjustment is
399 included in order to ensure mass conservation.

400 The vertical diffusion is configured by Kz profiles (Hertel et al., 1995), based on Monin-Obukhov similarity theory for the
401 surface layer. This Kz profile is extended to the whole boundary layer by using a simple extrapolation, which ensures that Kz
402 is decreasing in the upper part of the boundary layer. The planetary boundary layer (PBL) height is obtained directly from the
403 IFS meteorology.



404 3.2.7 Deposition

405 Gaseous and aerosol dry-deposition velocities are calculated based on the resistance method for 16 different land-use types
406 and are configured similar to the EMEP model (Emberson et al., 2000b; Simpson et al., 2003), except for the dry deposition
407 of species on water surfaces, where the deposition depends on the solubility of the chemical species and the wind speed (Hertel
408 et al., 1995).

409 Wet deposition includes in-cloud and below-cloud scavenging and is calculated as the product of scavenging coefficients and
410 the concentration of gases and particles in air (Simpson et al., 2003). The in-cloud scavenging coefficients are dependent on
411 Henry's law constants and the rate at which precipitation is formed.

412 3.2.8 Chemistry and aerosols

413 The basic chemical scheme in DEHM now includes 74 different species and 158 reactions. It is based on the original scheme
414 by (Strand and Hov, 1994). The original Strand and Hov scheme has been modified in order to improve the description of,
415 amongst other things, the transformations of nitrogen containing compounds. The chemical scheme has been extended with a
416 detailed description of the ammonia chemistry through the inclusion of ammonia (NH_3) and related species: ammonium-nitrate
417 (NH_4NO_3), ammonium bisulphate (NH_4HSO_4), ammonium sulphate ($(\text{NH}_4)_2\text{SO}_4$) and particulate nitrate (NO_3) formed from
418 nitric acid (HNO_3) using an aerosol equilibrium approach with reaction rates dependent on the equilibrium (Frohn, 2004).
419 Furthermore, reactions concerning the wet-phase production of particulate sulphate have been included. The photolysis rates
420 are calculated by using a 2-stream version of the Phodis model (Kylling et al., 1995). The original rates for inorganic and
421 organic chemistry have been updated with rates from the chemical scheme applied in the EMEP model (Simpson et al., 2003).
422 SOA formation is included via a VBS-based approach (Bergström et al., 2012b; Zare et al., 2014). In total, DEHM includes
423 nine classes of particulate matter ($\text{PM}_{2.5}$, PM_{10} , TSP, seasalt < 2.5 mm, sea-salt > 2.5 mm, smoke from wood stoves, fresh black
424 carbon, aged black carbon, and organic carbon).

425 3.2.9 Assimilation system

426 Since the system upgrade in November 2020, the assimilation in DEHM has been based on an updated version of the
427 comprehensive 3D-var data assimilation scheme previously described in (Silver et al., 2016). The NMC method (Kahnert,
428 2008; Parrish and Derber, 1992) is used to estimate the background error covariance matrix. Two 1-year runs of DEHM using
429 analysed and forecasted ECMWF weather data are performed and their differences are used to estimate the background errors
430 in spectral space for O_3 , NO_2 , SO_2 , CO , $\text{PM}_{2.5}$, and PM_{10} . For the analysis and reanalysis runs, surface in-situ observations of
431 the six species are assimilated at an hourly basis in DEHM.



432 3.3 EMEP

433 3.3.1 Model Overview

434 The EMEP MSC-W (European Monitoring and Evaluation Programme Meteorological Synthesizing Centre-West) model is a
435 chemical transport model developed at the Norwegian Meteorological Institute under the EMEP programme of the United
436 Nations Geneva Convention on Long-range Transboundary Air Pollution. The EMEP MSC-W model system allows several
437 options with regard to the chemical schemes used and the possibility of including aerosol dynamics. (Simpson et al., 2012)
438 described an early version of the EMEP MSC-W model in detail, while updates to the model since 2012 have been documented
439 and evaluated in the annual status reports of EMEP (see (Emep, 2023) and references therein). The forecast version of the
440 EMEP MSC-W model (EMEP-CWF) has been in operation since June 2006. The scheduled model updates in CAMS ensure
441 that the model version stays as close as possible to the official EMEP Open Source version³. Nevertheless, the EMEP-CWF
442 results and performances in CAMS might differ from those presented in the annual EMEP Status Reports, because of different
443 input data (emissions and meteorological driver) and model configurations (Forecast in EMEP-CWF versus Hindcast in EMEP
444 Status Reports).

445 3.3.2 Model geometry

446 The EMEP-CWF covers the European domain [30°N-76°N] x [30°W-45°E] on a geographic projection with a horizontal
447 resolution of 0.1° x 0.1° (longitude-latitude). Vertically the model uses 20 levels defined as sigma coordinates. The 10 lowest
448 model levels are within the PBL, and the top of the model domain is at 100 hPa. The lowermost layer has a thickness of
449 approximately 50 meters. Vertical downscaling is used to derive surface concentrations at 3 meters altitude, as described in
450 (Simpson et al., 2012).

451 3.3.3 Forcing Meteorology

452 The forcing meteorology is retrieved from the IFS model vertical layers covering the EMEP vertical extent on a 0.1°x0.1°
453 horizontal grid resolution with a temporal resolution of 3 hours. The forecast released at 12:00UTC of the previous days is
454 used. The meteorological parameters included to force the EMEP forecast are: 3D fields of the horizontal wind components
455 (U,V), potential temperature, specific humidity, and cloud fraction. The 2D fields are land-sea mask, surface pressure, friction
456 velocity (u^*), large scale and convective precipitation, soil water, snow depth, fraction of snow cover, fraction of ice cover,
457 sensible heat flux, latent heat flux, sea surface temperature, 2m temperature and 2m relative humidity. The IFS forecasts do
458 not include 3D precipitation, which is needed by the EMEP-CWF model. Therefore, a 3D precipitation estimate is derived
459 from large-scale precipitation and convective precipitation (surface variables).

³ <https://github.com/metno/emep-ctm> (last accessed 30/10/2024)



460 **3.3.4 Chemical initial and boundary conditions**

461 Boundary conditions are taken from chemical species available in the global IFS forecast model of the previous day at 3hr
462 temporal resolution (Table 2). In cases where IFS chemical boundary conditions are not available, default boundary conditions
463 are specified for O₃, CO, NO, NO₂, CH₄, HNO₃, PAN, SO₂, isoprene, C₂H₆, some VOCs, Sea salt, Saharan dust and SO₄, as
464 annual mean concentrations along with a set of parameters for each species describing seasonal, latitudinal and vertical
465 distributions. The EMEP forecasts are initialised by the EMEP 3D VAR analysis of the previous day.

466 **3.3.5 Emissions**

467 The common annual anthropogenic emissions CAMS-REG are implemented as explained in Section 2.5.1. Temporal
468 disaggregation is based on CAMS-REG-TEMPO v4.1. Chemical disaggregation for PM species follows the tables that come
469 with CAMS-REG while VOC emissions are speciated for each source-sector based on a lumped-species approach as described
470 in (Simpson et al., 2012; Bergström et al., 2022) .

471 The hourly GFAS wildfire emission for D-2 (i.e. the last full day available when launching the forecast system) are used for
472 the analysis (D-1) and the first two days of the forecast (D+0 and D+1). Fire emissions are set to zero for the remainder of the
473 forecast horizon.

474 The mineral dust source in the EMEP model is based on (Alfaro and Gomes, 2001; Fécan et al., 1998; Gomes et al., 2003;
475 Marticorena and Bergametti, 1995; Marticorena et al., 1997).

476 Natural emissions of Biogenic Volatile Organic Compounds (BVOCs) are based on Table 3 of (Simpson et al., 2012).

477 **3.3.6 Solver, advection and mixing**

478 The numerical solution of the advection terms of the continuity equation is based on the scheme of (Bott, 1989). The fourth
479 order scheme is utilized in the horizontal directions. In the vertical direction, a second order version applicable to variable grid
480 distances is employed.

481 The turbulent diffusion coefficients (K_z) are first calculated for the whole 3D model domain on the basis of local Richardson
482 numbers. The planetary boundary layer (PBL) height is then calculated using methods described in (Simpson et al., 2012). For
483 stable conditions, K_z values are retained. For unstable situations, new K_z values are calculated for layers below the mixing
484 height using the O'Brien interpolation.



485 3.3.7 Deposition

486 Parameterisation of dry deposition is based on a resistance formulation. The deposition module makes use of a stomatal
487 conductance algorithm which was originally developed for ozone fluxes, but which is now applied to all gaseous pollutants
488 when stomatal control is important (Emberson et al., 2000a; Simpson et al., 2003; Tuovinen et al., 2004). Non-stomatal
489 deposition for NH_3 is parameterised as a function of temperature, humidity, and the molar ratio SO_2/NH_3 .

490 Both gaseous and particulate nitrogen species are scavenged in the EMEP model according to their wet scavenging ratios and
491 collection efficiencies listed in Table S20 of (Simpson et al., 2012). In-cloud and sub-cloud scavenging ratios are considered
492 for gases and in-cloud scavenging ratios and sub-cloud scavenging efficiencies for particles.

493 3.3.8 Chemistry and aerosols

494 The EmChem19 chemical scheme couples the sulphur and nitrogen chemistry to the photochemistry and organic aerosol
495 formation using about 200 reactions between ca. 130 species (Bergström et al., 2022; Simpson et al., 2020b; Andersson-
496 Sköld and Simpson, 1999). The standard model version distinguishes 2 size fractions for aerosols, fine aerosol ($\text{PM}_{2.5}$) and
497 coarse aerosol ($\text{PM}_{2.5-10}$). The aerosol components presently accounted for are SO_4 , NO_3 , NH_4 , anthropogenic primary PM,
498 organic aerosols, and sea salt. Also aerosol water is calculated. Dry deposition parameterisation for aerosols follows standard
499 resistance-formulations, accounting for diffusion, impaction, interception, and sedimentation. Wet scavenging is treated with
500 simple scavenging ratios, taking into account in-cloud and sub-cloud processes. For secondary organic aerosol (SOA) a
501 volatility-basis set approach (Simpson et al., 2012) is used, which is a somewhat simplified version of the mechanisms
502 discussed in detail by (Bergström et al., 2012a). The EmChem19a scheme also has explicit toluene and benzene with different
503 SOA yields to the o-xylene surrogate that was used previously.

504 3.3.8 Assimilation system

505 The EMEP data assimilation system (EMEP-DAS) is based on the 3D-Var implementation for the MATCH model (Kahnert,
506 2008). The background error covariance matrix is estimated following the NMC method (Parrish and Derber, 1992). Recent
507 changes involved increased computational efficiency, tuning of model and observation representation uncertainties, and
508 improved impact of the assimilation in the vertical.

509 The EMEP-DAS delivers analyses of yesterday (driven by the operational IFS forecast of 00UTC of yesterday) assimilating
510 O_3 , NO_2 , CO , $\text{PM}_{2.5}$, and PM_{10} surface observations. For NO_2 , satellite observations from OMI used to be assimilated up to
511 2021 too.



513 **3.4 EURAD-IM**

514 **3.4.1 Model Overview**

515 The EURAD-IM (European Air pollution Dispersion - Inverse Model) system consists of 5 major parts: the meteorological
516 driver WRF (Weather Research and Forecasting⁴), the pre-processors EEP and PREP for preparation of anthropogenic
517 emission data and observations, the EURAD-IM Emission Model EEM, and the chemistry transport model EURAD (Hass et
518 al., 1995; Memmesheimer et al., 2004). EURAD-IM is a Eulerian meso-scale chemistry transport model involving advection,
519 diffusion, chemical transformation, wet and dry deposition and sedimentation of tropospheric trace gases and aerosols. It
520 includes 3d-var and 4d-var chemical data assimilation (Elbern et al., 2007) and is able to run in nesting mode.

521 **3.4.2 Model geometry**

522 To cover the CAMS domain from 25°E to 45°W and 30°N to 72°N, two lambert conformal projections subdomains with
523 respectively 45 km (199x166 grid boxes) and 9 km horizontal resolution (581x481 grid boxes) are used. The model domain
524 with the finer resolution covering the entire European part of the CAMS domain is nested within the halo domain with the
525 coarser resolution.

526 Variables are horizontally staggered using an Arakawa C grid. Vertically, the atmosphere is divided by 23 terrain-following
527 sigma coordinate layers between the surface and the 100 hPa pressure level. About 15 layers are within the first 2 km of the
528 atmosphere. The thickness of the lowest layer is about 35 m. No vertical downscaling is used to derive surface concentrations
529 from the first model level.

530 **3.4.3 Forcing Meteorology**

531 The Weather Research and Forecast (WRF) model is used for the calculation of meteorological fields needed to drive the
532 EURAD-IM CTM. Initial and boundary values for the WRF simulations are derived from 3-hourly IFS meteorological fields.
533 The main motivation to use WRF is to improve the spatial and temporal interpolation of IFS fields towards the EURAD-IM
534 geometry.

535 **3.4.4 Chemical initial and boundary conditions**

536

⁴ <https://www.mmm.ucar.edu/models/wrf>, last accessed 30/10/2024



537 The CAMS Global IFS 00:00 UTC forecast for the previous day is extracted from the MARS archive at ECMWF using 36
538 model levels with a temporal resolution of 3 hours. The full list of species used from the IFS model is given in Table 2. Sea
539 salt concentrations from IFS are divided by the constant 4.3 for the conversion from wet to dry mass.

540 **3.4.5 Emissions**

541 The common annual anthropogenic emissions CAMS-REG are implemented as explained in Section 2.5.1. The VOC and PM
542 split, the vertical distribution of area sources, and the emission strength per hour are calculated within the EURAD-IM CTM
543 with the distribution profiles provided with the CAMS-REG-AP_v6.1/2019 inventory (Kuenen et al., 2022). The VOC and
544 PM split depends on source category and country, the vertical distribution only depends on the source category. The CAMS-
545 TEMPO v4.1 (Guevara et al., 2021) profiles are used for the annual, monthly, weekly and daily distribution of emissions.

546 Biogenic emissions and NO_x emissions from soil are calculated within the EURAD-IM CTM with the Model of Emissions of
547 Gases and Aerosols from Nature (MEG [REDACTED] Guenther et al., 2012). Fire emissions are taken into account using hourly data
548 from the Global Fire Assimilation System Version 1.2 (GFASv1.2) product (Kaiser et al., 2012). Zero fire emissions are
549 assumed for D+2 and D+3 forecasts.

550 **3.4.6 Solver, advection and mixing**

551 The positive definite advection scheme of (Bott, 1989), implemented in a one-dimensional realisation, is used to solve the
552 advective transport. An operator splitting technique is employed (Mcrae et al., 1982) to handle the varying numerical
553 specificities of processes to be solved.

554 An Eddy diffusion approach is used to parameterize the vertical sub-grid-scale turbulent transport. The calculation of vertical
555 Eddy diffusion coefficients is based on the specific turbulent structure in the individual regimes of the planetary boundary
556 layer (PBL) according to the PBL height and the Monin-Obukhov length (Holtslag and Nieuwstadt, 1986). A semi-implicit
557 (Crank-Nicholson) scheme is used to solve the diffusion equation.

558 The sub-grid cloud scheme in EURAD-IM was derived from the cloud model in the EPA Models-3 Community Multiscale
559 Air Quality (CMAQ) modelling system (Roselle and Binkowski, 1999). Convective cloud effects on both gas phase species
560 and aerosols are considered.

561 **3.4.7 Deposition**

562 The gas phase dry deposition modelling follows the method proposed by (Zhang et al., 2003). Dry deposition of aerosol species
563 is treated size dependent, using the resistance model of (Petroff and Zhang, 2010) with consideration of the canopy. Dry
564 deposition is applied as lower boundary condition of the diffusion equation.



565 Wet deposition of gases and aerosols is derived from the cloud model in the CMAQ modelling system (Roselle and Binkowski,
566 1999). The wet deposition of pollen is treated according to (Baklanov and Sørensen, 2001).

567 Size dependent sedimentation velocities are calculated for aerosol and pollen species. The sedimentation process is
568 parameterized with the vertical advective transport equation and solved using the fourth order positive definite advection
569 scheme of (Bott, 1989).

570 **3.4.8 Chemistry and aerosols**

571 In the EURAD-IM CTM, the gas phase chemistry is represented by an extension of the Regional Atmospheric Chemistry
572 Mechanism (RACM) (Stockwell et al., 1997) based on the Mainz Isoprene Mechanism (MIM) (Geiger et al., 2003). A 2-step
573 Rosenbrock method is used to solve the set of stiff ordinary differentials equations (Sandu and Sander, 2006). Photolysis
574 frequencies are derived using the FTUV model (fast TUV) according to (Tie et al., 2003). The radiative transfer model therein
575 is based on the Tropospheric Ultraviolet-Visible Model (TUV) developed by (Madronich and Weller, 1990).

576 The modal aerosol dynamics model MADE (Ackermann et al., 1998) is used to provide information on the aerosol size
577 distribution and chemical composition. To solve for the concentrations of the secondary inorganic aerosol components, a
578 FEOM (fully equivalent operational model) version, using the HDMR (high dimensional model representation) technique
579 (Nieradzik, 2005; Rabitz and Aliş, 1999), of an accurate mole fraction based thermodynamic model (Friese and Ebel, 2010) is
580 used. The updated SORGAM module (Li et al., 2013) simulates secondary organic aerosol formation.

581 **3.4.9 Assimilation system**

582 The EURAD-IM assimilation system (Elbern et al., 2007) includes (i) the EURAD-IM CTM and its adjoint, (ii) the formulation
583 of both background error covariance matrices for the initial states and the emission, and their treatment to precondition the
584 minimisation problem, (iii) the observational basis and its related error covariance matrix, and (iv) the minimisation including
585 the transformation for preconditioning. The quasi-Newton limited memory L-BFGS algorithm described in (Liu and Nocedal,
586 1989; Nocedal, 1980) is applied for the minimisation.

587 Currently assimilated in the EURAD-IM analysis and interim re-analysis are surface in-situ observations of O₃, NO₂, SO₂, CO,
588 PM_{2.5}, PM₁₀.

589

590



591 3.5 GEM-AQ

592 3.5.1 Model Overview

593 GEM-AQ is a numerical weather prediction model where air quality processes (gas phase and aerosols) are implemented on-
594 line in the host meteorological model, the Global Environmental Multiscale (GEM) model, developed at Environment and
595 Climate Change Canada (Côté et al., 1998a). The model is used for operational air quality forecasting in Poland. Also, it is
596 used in a research project to investigate air quality in different environmental conditions (Struzewska and Kaminski, 2008,
597 2012; Struzewska et al., 2015; Struzewska et al., 2016). Application of the GEM-AQ to modelling of satellite retrieved NO₂
598 column was carried out by [redacted] ymankiewicz et al., 2014) and (Kawka et al., 2021).

599 3.5.2 Model geometry

600 The GEM-AQ model can be configured to simulate atmospheric processes over a broad range of scales, from the global scale
601 down to the meso-gamma scale. An arbitrarily rotated latitude-longitude mesh focuses resolution on any part of the globe. In
602 the CAMS regional production, the model is run in the limited area mode with a resolution of 0.1° x 0.1° on a spherical
603 coordinate system. The coordinates are the following: lower-left (17. [redacted] 22.1W), upper-right (58.6N/ 86.6E), and are
604 generated internally based on lower-left corner, grid extent and the numerical equator loc [redacted]. In the vertical, GEM-AQ uses
605 the generalised sigma vertical coordinate system. It has terrain-following sigma surfaces near the ground that transform to
606 pressure surfaces higher in the atmosphere. The model top is set at 10 hPa.

607 3.5.3 Forcing Meteorology

608 The operational IFS model provides meteorological fields for initial and boundary conditions used by the meteorological part
609 of the GEM-AQ model. The GEM-AQ model is started using the 12-hour forecast (valid at 00:00 UT of the following day) as
610 initial conditions. The IFS data are used as boundary conditions with a nesting interval of 3 hours. The IFS meteorological
611 fields are computed from spectral coefficients for the target GEM-AQ grid. Meteorological fields, within the GEM-AQ model
612 domain, are constrained and relaxed to the IFS global model every 3 hours. Thus, the meteorological fields are ‘dynamically
613 interpolated’ by the GEM meteorological model to the required transport and chemistry time steps.

614 3.5.4 Chemical initial and boundary conditions

615 Chemical species of the CAMS Global IFS forecast for the previous day are used with a temporal resolution of 3 hours (Table
616 2). For dust aerosols, the three available size bins from the IFS model are distributed uniformly over the 10 corresponding bins
617 in GEM-AQ. For organic matter aerosol, black carbon and sulphates, the same log-normal based profile was applied. For
618 organic aerosol and black carbon, hydrophobic and hydrophilic components were summed as “total organic aerosol” and “total
619 black carbon aerosol” before applying size-bin distribution profiles.



620 **3.5.5 Emissions**

621 The common annual anthropogenic emissions CAMS-REG are implemented as explained in Section 2.5.1. In those emissions,
622 the following fields are available: SO₂, NO_x, CO, NMVOC, NH₃, PM₁₀ and PM_{2.5}. Based on this information, emission fluxes
623 for 15 gaseous species (9 hydrocarbons and 6 inorganics) and 4 aerosol components (primary organic aerosol, black carbon,
624 sulphates, nitrates) are derived using factors provided by TNO. Total emission fluxes for each aerosol component are
625 distributed into 12 bins in the GEM-AQ aerosol module.

626 Anthropogenic emissions are distributed within the 7 lowest model layers (up to 1350 m) with injection height profiles for
627 each of the GNFR sectors re-mapped for the GEM-AQ levels. Temporal profiles modulating annual and diurnal variation of
628 emission fluxes for each GNFR are used.

629 For biogenic emissions, a monthly averaged MEGAN-MACC (Guenther et al., 2012) dataset valid for 2010 was used in order
630 to avoid short-term variability of reactive biogenic VOC generated on-line in the model.

631 **3.5.6 Solver, advection and mixing**

632 The set of non-hydrostatic Eulerian equations (with a switch to revert to the hydrostatic primitive equations) maintains the
633 model's dynamical validity right down to the meso-gamma scales. The time discretization of the model dynamics is fully
634 implicit, 2 time-level (Côté et al., 1998b; Côté et al., 1998a). The spatial discretization for the adjustment step employs a
635 staggered Arakawa C grid that is spatially offset by half a mesh length in the meridional direction. It is second-order accurate,
636 whereas the interpolations for the semi-Lagrangian advection are of fourth-order accuracy.

637 Deep convective processes are handled by Kain-Fritsch convection parameterisation (Kain and Fritsch, 1990). The vertical
638 diffusion of momentum, heat and tracers is a fully implicit scheme based on turbulent kinetic energy (TKE) theory.

639 **3.5.7 Deposition**

640 The effects of dry deposition are included as a flux boundary condition in the vertical diffusion equation. Dry deposition
641 velocities are calculated from a 'big leaf' multiple resistance model (Wesely, 1989; Aamaas et al., 2013) with aerodynamic,
642 quasi-laminar layer, and surface resistances acting in series. The process assumes 15 land-use types and takes snow cover into
643 account. Wet deposition takes into account cloud scavenging for soluble gas species and aerosols.

644 **3.5.8 Chemistry and aerosols**

645 The gas-phase chemistry mechanism currently used in the GEM-AQ model is based on a modification of version 2 of the Acid
646 Deposition and Oxidants Model (ADOM) (Venkatram et al., 1988), derived from the condensed mechanism of (Lurmann et



647 al., 1986). The ADOM-II mechanism comprises 47 species, 98 chemical reactions and 16 photolysis reactions. In order to
648 account for background tropospheric chemistry, 4 species (CH_3OOH , CH_3OH , CH_3O_2 , and $\text{CH}_3\text{CO}_3\text{H}$) and 22 reactions were
649 added. All species are solved using a mass-conserving implicit time stepping discretization, with the solution obtained using
650 Newton's method. Heterogeneous hydrolysis of N_2O_5 is calculated using the on-line distribution of aerosol. Although the model
651 meteorology is calculated up to 10 hPa, the focus of the chemistry is in the troposphere where all species are transported
652 throughout the domain. To avoid the overhead of stratospheric chemistry in this version (a combined stratospheric/tropospheric
653 chemical scheme is currently being developed), both the ozone and NO_y fields are replaced with a climatology above 100 hPa
654 after each transport time step. Ozone fields are taken from the HALOE (Halogen Occultation Experiment) climatology (Hervig
655 et al., 1993), while NO_y fields are taken from the CMAM (Canadian Middle Atmosphere Model). Photolysis rates (J values)
656 are calculated on-line every chemical time step using the method of (Landgraf and Crutzen, 1998). In this method, radiative
657 transfer calculations are done using a delta-two stream approximation for 8 spectral intervals in the UV and visible applying
658 pre-calculated effective absorption cross sections. This method also allows for scattering by cloud droplets and for clouds to
659 be presented over a fraction of a grid cell. The host meteorological model provides both cloud cover and water content. The J
660 value package used was developed for MESSy (Jöckel et al., 2006) and is implemented in GEM-AQ.

661 The current version of GEM-AQ has 5 size-resolved aerosol types, viz. sea salt, sulphate, black carbon, organic carbon and
662 dust as well as nitrates. The microphysical processes that describe the formation and transformation of aerosols are calculated
663 by a sectional aerosol module (Gong et al., 2003). The particle mass is distributed into 12 logarithmically spaced bins from
664 0.005 to 10.24-micron radius. This size distribution leads to an additional 60 advected tracers. The following aerosol processes
665 are accounted for in the aerosol module: nucleation, condensation, coagulation, sedimentation and dry deposition, in-cloud
666 oxidation of SO_2 , in-cloud scavenging, and below-cloud scavenging by rain and snow.

667 **3.5.9 Assimilation system**

668 Data assimilation in the GEM-AQ modelling system is done with Optimal Interpolation method (Robichaud and Ménard,
669 2014) and is applied to the forecast. Error statistics are computed with the Hollingsworth - Lönnberg (HL) method
670 (Hollingsworth and Lönnberg, 1986). It estimates the correlation length and the ratio of observation to model error variances
671 by a least-square fit of a correlation model against the sample of the spatial autocorrelation of observation-minus-model
672 residuals.

673 Currently, data assimilation is done at each forecast hour for O_3 , NO_2 , SO_2 , CO, PM_{10} and $\text{PM}_{2.5}$, using surface observations.

674



675 3.6 LOTOS-EUROS

676 3.6.1 Model Overview

677 The LOTOS-EUROS model is a 3D chemistry transport model aimed to simulate air pollution in the lower troposphere. The
678 model has been used in a large number of studies for the assessment of particulate air pollution and trace gases (e.g. O₃, NO₂)
679 (Hendriks et al., 2016; Schaap et al., 2013; Thürkow et al., 2021; Timmermans et al., 2022). A detailed description of the
680 model is given in (Manders et al., 2017). At present the version used in the production is v2.2.009.

681 3.6.2 Model geometry

682 The domain of LOTOS-EUROS is the CAMS regional domain from 25°W to 45°E and 30°N to 72°N. The projection is regular
683 longitude-latitude, at 0.1°x0.1° grid spacing. In the vertical and for the forecasts there are currently 12 model layers and 2 more
684 reservoir layers at the top, defined by coarsening in a mass conservative way the first 77 model levels of the IFS. For the
685 analyses there are 4 dynamic layers up to 5km agl and a surface layer with a fixed depth of 25 m. The lowest dynamic layer is
686 the mixing layer, followed by 3 reservoir layers. The heights of the reservoir layers are determined by the difference between
687 the mixing layer height and 5 km. For output purposes, the concentrations at measuring height (usually 2.5 m) are diagnosed
688 by assuming that the flux is constant with height and equal to the deposition velocity times the concentration at height z. This
689 applies for several of the gaseous species, namely O₃, NO, NO₂, HNO₃, N₂O₅, H₂O₂, CO, SO₂ and NH₃. For aerosols, the same
690 approach is utilized, only sedimentation velocity is used instead of deposition velocity.

691 3.6.3 Forcing Meteorology

692 The forcing meteorology is retrieved from the 00:00 and 12:00 UTC runs of the IFS model at hourly (surface fields) or 3-
693 hourly temporal resolution (model layer fields). The meteorological data is retrieved on a regular horizontal resolution of about
694 15 km and for all layers covered by the model's vertical extent. The meteorological variables included are 3-hourly 3D fields
695 for wind direction, wind speed, temperature, humidity and density, substituted by hourly 2D gridded fields of mixing layer
696 height, surface wind and temperature, precipitation rates, heat fluxes, cloud cover and surface variables snow depth, sea ice
697 cover and volumetric soil water.

698 3.6.4 Chemical initial and boundary conditions

699 The lateral and top boundary conditions for trace gases and aerosols are obtained from the CAMS-global daily forecasts (see
700 Table 2). LOTOS-EUROS uses a bulk approach for the aerosol size distribution differentiating between a fine and a coarse
701 fraction, but for dust and sea salt there are 5 distinct size classes: ff: 0.1-1 μm, f:1-2.5 μm, ccc: 2.5-4 μm, cc: 4-7 μm, c:7-10
702 μm. When the chemical boundary conditions from IFS are missing, the model uses climatological boundary concentrations
703 derived from IFS data. The forecasts are initialised with the LOTOS-EUROS forecast of the previous day.



704

705 **3.6.5 Emissions**

706 The common annual anthropogenic emissions CAMS-REG are implemented as explained in Section 2.5.1. Injection height
707 distribution from the EuroDelta study is implemented, which is per SNAP (or more recently, GNFR) category. Time profiles
708 used are defined per country and GNFR emission category type.

709 Biogenic NMVOC emissions are calculated online using actual meteorological data and a detailed landuse and tree species
710 database including emission factors from (Köble and Seufert, 2001). The isoprene emissions follow the mathematical
711 description of the temperature and light dependence of the isoprene emissions, proposed by (Guenther et al., 1993). Sea salt
712 emissions are parameterised following (Martensson et al., 2003; Monahan, 1986) from the wind speed at 10-meter height.

713 The fire emissions are taken from the near real-time GFAS fire emissions database. For the forecast, we assume persistence,
714 so that the latest downloaded emission for the specific hour is used. When the hourly emission is more than 3 days old, it is
715 set to zero.

716 Mineral dust emissions within the modelling domain are calculated online based on the sand blasting approach by (Marticorena
717 and Bergametti, 1995) with soil moisture inhibition as described by (Fécan et al., 1998). Finally, a parameterization using land
718 cover and temperature is used for handling soil NO_x emissions, based on (Yienger and Levy, 1995).

719 **3.6.6 Solver, advection and mixing**

720 The transport consists of advection in 3 dimensions, horizontal and vertical diffusion, and entrainment/detrainment. The
721 advection is driven by meteorological fields (u,v), which are input every 3 hours. The vertical wind speed w is calculated by
722 the model as a result of the divergence of the horizontal wind fields. A linear advection scheme is used to ensure tracer mass
723 conservation, which also allows more efficient parallelization and reduced model complexity. This scheme uses piece-wise
724 linear functions to define sub-grid concentrations, which is sometimes referred to as MUSCL ("Monotonic **U**-centered
725 Scheme for Conservation Laws") following (Van Leer, 1984).

726 Vertical diffusion is described using the standard K_z theory. Vertical exchange is calculated employing the new integral scheme
727 by (Yamartino et al., 2007). For the forecasting set-up with 12 layers, atmospheric stability values and functions, including K_z
728 values, are derived based on the surface heat fluxes from ECMWF meteorology and similarity profiles following the IFS
729 approach (Ecmwf, 2021) to adapt for land-use specific conditions. For the 5-layer version in the assimilation, a correction is
730 made for the vertical diffusion to correct for the height difference between surface and mixing layer.



731 **3.6.7 Deposition**

732 The dry deposition in LOTOS-EUROS is parameterised following the resistance approach. The laminar layer resistance and
733 the surface resistances for acidifying components are described following the EDACS system (Van Zanten et al., 2010), the
734 deposition velocities for particles are based on (Zhang et al., 2001). Wet deposition is divided between in-cloud and below-
735 cloud scavenging. The in-cloud scavenging module is based on the approach described in (Seinfeld and Pandis, 1998) and
736 (Banzhaf et al., 2012).

737 **3.6.8 Chemistry and aerosols**

738 LOTOS-EUROS uses the TNO CBM-IV scheme, which is a modified version of the original CBM-IV (Gery et al., 1989).
739 N₂O₅ hydrolysis is described explicitly based on the available (wet) aerosol surface area (using $\gamma = 0.05$) (Schaap et al., 2004).
740 Aqueous phase and heterogeneous formation of sulphate is described by a simple first order reaction constant (Barbu et al.,
741 2009; Schaap et al., 2004). Inorganic aerosol chemistry is represented using ISORROPIA II (Fountoukis and Nenes, 2007)
742 and secondary organic aerosols formation based on a VBS scheme (Bergström et al., 2012a; Zare et al., 2014) **will be included**
743 **in the operational forecast version at the end of 2023**

744 **3.6.9 Assimilation system**

745 The LOTOS-EUROS model is equipped with a data assimilation package with the ensemble Kalman filter technique (Curier
746 et al., 2012). The ensemble is created by specification of uncertainties for emissions (NO_x, VOC, NH₃ and aerosol), ozone
747 deposition velocity, and ozone top boundary conditions. Currently, data assimilation is performed for O₃, NO₂, PM₁₀ and PM_{2.5}
748 surface observations, OMI NO₂ is also assimilated.

749



750 **3.7 MATCH**

751 **3.7.1 Model Overview**

752 The Multi-scale Atmospheric Transport and Chemistry model (MATCH) (Robertson et al., 1999) is an off-line chemical
753 transport model (CTM) with a flexible design, accommodating different weather data forcing on different resolutions and
754 projections, and a range of alternative schemes for deposition and chemistry.

755 **3.7.2 Model geometry**

756 **The model geometry is taken from the input weather data.** The vertical resolution is reduced with respect to the ECMWF
757 operational model by combining pairs of IFS layers; hybrid vertical coordinates are used. The horizontal geometry of the
758 MATCH simulation is the same as the meteorological forcing (currently a lat-lon grid with 0.1° resolution). The lowest 76
759 layers of the ECMWF model are lumped in 26 levels, which then are used for the air quality simulations. The model top is at
760 about 8000 m height. The model domain covers the area between 28.8° W to 45.8° E and 29.2° N to 72.0° N. The grid is an
761 Arakawa C-grid with staggered wind components. The current operational system uses various tiles of physiography derived
762 from CLC/SEI inventory⁵ (Simpson et al., 2012).

763 **3.7.3 Forcing Meteorology**

764 The forcing meteorology is retrieved from the 12:00 UTC run of the IFS modelling system on a 0.1°×0.1° spatial grid and with
765 a temporal resolution of one hour. For the analyses, the 00:00 UTC analysis of the IFS is used at 0.2°×0.2° resolution. The
766 meteorological variables included are 3D fields of the horizontal wind components (U, V), temperature, specific humidity,
767 cloud cover, cloud water content, cloud ice water content, and surface fields of surface pressure, logarithm of surface pressure,
768 surface temperature, sea surface temperature, snow depth, albedo, roughness height, total cloud cover, precipitation, and
769 volumetric soil water at the surface.

770 **3.7.4 Chemical initial and boundary conditions**

771 The lateral boundary conditions for trace gases and aerosols are obtained from the IFS global forecasts at 3-hourly resolution
772 for the following species: O₃, CO, HCHO, NO, NO₂, SO₂, HNO₃, PAN, CH₄, C₅H₈, o-xylene, sulphate and C₂H₆ (see Table
773 2). When the chemical boundary conditions from IFS are missing, the model uses seasonal climatological boundary
774 concentrations instead.

⁵ www.sei.org/projects/sei-european-land-cover-map (last accessed 30/10/2024)



775 3.7.5 Emissions

776 The common annual anthropogenic emissions CAMS-REG are implemented as explained in Section 2.5.1. Temporal
777 disaggregation is based on the GENEMIS tables (Ebel et al., 1997), using a GNFR to SNAP matrix. The vertical distribution
778 of the emissions depends on the sector. Near-surface emission sources (SNAP 2,6,7,8,10) are distributed in the lowest 90 m;
779 for other sectors the emissions are allocated over varying model levels up to a maximum of about 1100 m height. According
780 to the sector, the anthropogenic VOC emissions are split into the MATCH chemical mechanism surrogate species: C₂H₆,
781 NC₄H₁₀, C₂H₄, C₃H₆, OXYLENE, BENZENE, TOLUENE, CH₃OH, C₂H₅OH, HCHO, CH₃CHO, CH₃COC₂H₅; the particulate
782 matter components elemental carbon, organic matter, anthropogenic dust (other than soil and road dust) are allocated to two
783 bins (PM_{2.5} and PM-coarse), as well as the road dust estimated according to (Schaap et al., 2009) and (Omstedt et al., 2005),
784 and the teluric dust calculated according to (Zender et al., 2003).

785 Biogenic emissions of isoprene, monoterpenes and sesquiterpenes are calculated following (Simpson et al., 2012; Simpson et
786 al., 1995; Bergström et al., 2012a), taking into account temperature at 2 m, radiation fluxes and the vegetation cover. **Exception**
787 **is made for the isoprene oxidation for which the chain of reactions is following the Carter-1 chemical mechanism, which has**
788 **proven to give the comparable results with fewer reactions (Carter, 1996; Langner et al., 1998)**

789 The dimethyl sulphide - DMS – emissions from the Ocean and Baltic Sea are also considered; whereas the particulate matters
790 from sea salt are calculated according to the parameterisation proposed by (Sofiev et al., 2011).

791 The GFAS biomass burning emissions are taken into the model mapping the following species into the MATCH chemical
792 mechanism: NO_x, SO₂, CO, CH₄, C₂H₄, C₂H₆, C₃H₆, C₄H₁₀, C₈H₁₀, benzene, toluene, CH₃OH, C₂H₅OH, formaldehyde,
793 acetaldehyde, OC, BC, PM_{2.5}, and PM₁₀. Half of these grid emissions are vertically distributed between the surface **and the top**
794 **of the plume (GFAS meter)** according to a parabolic curve, and the other half is uniformly distributed among the same
795 levels.

796 3.7.6 Solver, advection and mixing

797 Mass conservative transport schemes are used for advection and turbulent transport. The advection is formulated as a Bott-like
798 scheme (Robertson et al., 1999). A second order transport scheme is used in the horizontal as well as the vertical. The vertical
799 diffusion is described by an implicit mass conservative first order scheme, where the exchange coefficients for neutral and
800 stable conditions are parameterized following (Holtslag and Nieuwstadt, 1986). In the convective case the turbulent Courant
801 number is directly determined from the turnover time in the boundary layer.

802 Part of the dynamical core is the initialisation and adjustment of the horizontal wind components. This is a very important step
803 to ensure mass conservative transport. The initialisation is based on a procedure proposed by (Heimann and Keeling, 1989),



804 where the horizontal winds are adjusted by means of the difference between the input surface pressure tendency, and the
805 calculated pressure tendency assumed to be an error in the divergent part of the wind field.

806 Boundary layer parameterisation is based on surface heat and water vapour fluxes as described by (Van Ulden and Holtslag,
807 1985) for land surfaces, and (Burridge, 1977) for sea surfaces. The boundary layer height is calculated from formulations
808 proposed by (Zilitinkevich and Mironov, 1996) for the neutral and stable case, and from (Holtslag et al., 1995) for the
809 convective case. These parameterisations drive the formulations for dry deposition and vertical diffusion.

810 **3.7.7 Deposition**

811 Dry deposition of gases and aerosols is modelled using a resistance approach (based on the scheme in (Simpson et al., 2012)),
812 which includes stomatal and non-stomatal pathways for vegetated surfaces. MATCH uses 3D-precipitation (estimated in the
813 model, based on the surface precipitation and 3D cloud water information from the IFS forecast) and separates wet scavenging
814 into in-cloud and sub-cloud scavenging. For most gaseous components the scavenging is assumed to be proportional to the
815 precipitation intensity (with higher scavenging ratios in-cloud than sub-cloud). For the particulate components in-cloud
816 scavenging is also treated using simple scavenging ratios while the sub-cloud scavenging is treated using a scheme based on
817 (Berge, 1993) with size dependent collection efficiencies (as in (Simpson et al., 2012)).

818 **3.7.8 Chemistry and aerosols**

819 The photochemistry scheme is based on the EMEP MSC-W chemistry scheme (Simpson et al., 2012), with a modified scheme
820 for isoprene, based on the so-called Carter-1 mechanism (Carter, 1996; Langner et al., 1998). The SOA description is based
821 on (Hodzic et al., 2016).

822 **3.7.9 Assimilation system**

823 The model for data assimilation is an integrated part of the MATCH modelling system. The data assimilation scheme as such
824 is a variational spectral scheme (Kahnert, 2008), implying that the background covariance matrices are modelled in spectral
825 space. The limitation is that covariance structures are described as isotropic and homogeneous. The advantage is that the
826 background error matrix becomes block diagonal, and there are no scale separations as the covariance between spectral
827 components are explicitly handled. The block diagonal elements are the covariance between wave components at model layers
828 and chemical compounds.

829 Modelling the background error covariance matrices is the central part in data assimilation. This is conducted by means of the
830 so-called NMC approach (Parrish and Derber, 1992). The CTM (MATCH) is run for a 3-month period for photochemistry and
831 aerosols with analysed and forecasted ECMWF weather data. The differences are assumed to mimic the background errors,



832 and the statistics in spectral space are generated for different combinations of the model compounds: O₃, NO₂, NO, SO₂, CO,
833 PM_{2.5}, PM₁₀.

834 The scheme is fully intermittent in hour-by-hour steps and the above-listed components are assimilated from in-situ
835 measurements. The analysed components are propagated by chemistry and transport into unobserved components as
836 NMVOCs, PAN and NH₃.

837



838 **3.8 MINNI**

839 **3.8.1 Model Overview**

840 MINNI (Italian Integrated Assessment Modelling System for supporting the International Negotiation Process on Air Pollution
841 and assessing Air Quality Policies at national/local level; (D'elia et al., 2021; Mircea et al., 2014) has been developed to support
842 the Italian Ministry for Environment and Territory and Sea. The core of the modelling system is the 3-dimensional offline
843 Eulerian CTM FARM (Flexible Air quality Regional Model, (Silibello et al., 2008) that accounts for the transport, chemistry
844 and removal of atmospheric pollutants.

845 **3.8.2 Model geometry**

846 For the CAMS regional forecast, the model is configured with a regular latitude-longitude grid of $0.15^\circ * 0.10^\circ$ resolution.
847 The domain spans from -25° to 45.05° degree East and from 30° to 72° degree North. The model uses z-level terrain following
848 mesh with the first central grid point at 20 m AGL (above ground level) and the last one at 6290 m AGL. No vertical
849 downscaling is applied to extrapolate concentrations from 20 meters above the ground to the surface.

850 **3.8.3 Forcing Meteorology**

851 The forcing meteorology is retrieved from the 12:00 UTC run of the IFS modelling system on a $0.1^\circ \times 0.1^\circ$ spatial grid and with
852 a temporal resolution of one hour. The meteorological variables included are 3D fields such as temperature, relative humidity,
853 pressure and wind velocity and 2D fields such as boundary layer height, roughness length, albedo, sea surface temperature,
854 total cloud cover and precipitation.

855 **3.8.4 Chemical initial and boundary conditions**

856 The lateral and top boundary conditions for trace gases and aerosols are obtained from the CAMS-global daily forecasts with
857 a 3-hr temporal resolution (see Table 2). The initial condition is taken from the previous forecast of the MINNI model.

858 **3.8.5 Emissions**

859 The common annual anthropogenic emissions CAMS-REG are implemented as explained in Section 2.5.1. Point emissions
860 are summed up to diffuse emissions for each GNFR sector, since no information was available about the characterization of
861 the point sources in terms of injection height. Conservative mass horizontal interpolation has been applied to map the emissions
862 on the actual model domain. Vertical splitting has been applied for each GNFR sector adapting the vertical injection profiles
863 provided by TNO to the actual model levels. Temporal emission profiles for each GNFR sector, as they were provided by
864 TNO, have been applied considering local hour (i.e. the time zones shift has been taken into account).



865

866 $PM_{2.5}$ has been speciated following the TNO table as a function of country and sector and AERO3 (Binkowski and Shankar,
867 1995; Binkowski, 1999) species size fractions below $2.5\mu m$. The coarse component ($PM_{10}-PM_{2.5}$) was associated to non-
868 speciated coarse mode since MINNI dispersion model considers all the secondary aerosol fraction as $PM_{2.5}$. This method leaves
869 the detailed chemical speciation out but ensures mass conservation.

870 The NMVOC speciation originated from the TNO table as a function of country and sector obtaining the v01-v25 species. The
871 mapping among the v01-v25 species to SAPRC99 species has been done in agreement with the choices made and tested in the
872 frame of EURODELTA III intercomparison exercise (Colette et al., 2017).

873 Biogenic emissions are computed with the MEGAN model v.2.04 (Guenther et al., 2006), and NO_x emissions from soil
874 following (Williams et al., 1992) approach.

875 Erosion and resuspension of the dust are calculated by means of method proposed by (Vautard et al., 2005). Road dust
876 emissions are parameterized following (Zender et al., 2003).

877 Fire emissions are taken into account using hourly data from the GFAS database considering emissions from D-1 for AN (D-
878 1) and FC (D+0 and D+1, zero for the remaining days).

879 **3.8.6 Solver, advection and mixing**

880 FARM is a 3-dimensional Eulerian model with first order turbulence closure. Physical and chemical processes influencing the
881 concentration fields within the modelling domain are described by a system of partial differential equations (PDE). The
882 numerical integration of the above system of PDEs is performed by a method that splits the multi-dimensional problem into
883 time dependent one-dimensional problems, which are then solved sequentially over the time step.


884 Partial differential equations involved in horizontal and vertical advection-diffusion operators are solved in FARM using the
885 schemes employed in CALGRID model (Yamartino et al., 1992). In particular, horizontal advection-diffusion operators are
886 solved using a finite elements method based on Blackman cubic polynomials. The coefficients of a cell-centered cubic
887 polynomial are constrained to maintain high-accuracy and low-diffusion characteristics and to avoid undesirable negative
888 concentrations. In addition, a filter is used for filling undesired short wavelength minima. The numerical integration of the
889 vertical diffusion equation is performed in a hybrid way employing a hybrid semi-implicit Crank-Nicholson / fully implicit
890 scheme (Yamartino et al., 1992).



891 The calculation of horizontal diffusion coefficients is based on Stress tensor formulation of (Smagorinsky, 1963) also including
892 a dependence on the local stability class and wind speed. For the calculation of vertical diffusion coefficients, the (Lange,
893 1989) approach to boundary layer scaling regimes is used. Mixing due to deep convection is not explicitly taken into account.

894 Two different schemes to compute the PBL scaling parameters are used. In the daytime, the (Maul et al., 1980) version of
895 (Carson, 1973)encroachment method is used. During night-time, the minimum value between (Nieuwstadt, 1981) and
896 (Venkatram, 1980) is used.

897 **3.8.7 Deposition**

898 The dry deposition velocities are modelled following a resistance analogy approach, as an inverse sum of a series of 3
899 resistances: the aerodynamic resistance, the quasi-laminar layer resistance and the surface resistance. Aerodynamic resistance
900 is dependent on surface characteristics and atmospheric stability conditions (described through friction velocity and Monin-
901 Obukhov length). Quasi-laminar layer resistance is parameterised using (Hicks et al., 1987). Surface resistance is approximated
902 as a set of parallel resistance associated with leaf stomata, leaf cuticles, lower canopy and surface soil, litter and water (Wesely,
903 1989). Deposition to water surfaces is based on (Slinn et al., 1978) work. 

904 The deposition velocity of particulate species also depends on particle size distribution and density because of gravitational
905 settling. Sedimentation velocity acts in parallel to the other resistances. Hygroscopic growth is considered over water for
906 particles less than 2 μm . For particles ranging from 0.1 to 1 μm deposition velocity is computed as the inverse of the resistance
907 computed from canopy height, friction velocity and Monin-Obukhov length.

908 The parameterization of wet deposition follows the (Simpson et al., 2012) approach, including in-cloud and below-cloud
909 scavenging of gas and particles.

910 **3.8.8 Chemistry and aerosols**

911 The gas-phase chemical mechanism used for CAMS forecast is SAPRC-99 with the inclusion of Polycyclic aromatic
912 hydrocarbons (PAHs) and Mercury chemistry; moreover, a simplified aqueous phase mechanism is included for SO_2 oxidation
913 and chemical processes involving Mercury in both gas and aqueous phases.

914 A simple approach is used to estimate photolysis rates based on look-up tables to calculate the rate constants for photolysis
915 reactions (Nenes et al., 1998). Photolysis rates are computed and adjusted according to local solar zenith angle using an
916 empirical formula based on (Peterson, 1976) data.



917 The aerosols module is AERO3 (Binkowski and Shankar, 1995; Binkowski, 1999). In AERO3 the representation of the particle
918 size is three-modal (Aitken, accumulation and coarse), following lognormal distributions. The aerosol dynamics takes into
919 account nucleation, condensation and coagulation processes. The gas/particle mass transfer is implemented by means of
920 ISORROPIA v1.7 (Nenes et al., 1998) and SORGAM (Schell et al., 2001a) for secondary inorganic and organic aerosol,
921 respectively.

922 **3.8.9 Assimilation system**

923 The assimilation scheme used **in CAMS** is optimal interpolation: the correlation function is factorized in vertical and horizontal
924 components. The horizontal component has pollutant dependent fixed correlation length with a terrain-following exponential
925 decay. The vertical component is modelled with a Cressman function dependent on the boundary layer height. The system
926 assimilates NO₂, O₃, SO₂, CO, PM₁₀ and PM_{2.5}. In case of aerosol components, the correction applied to each of them is
927 proportional to their content in PM. At present, only data from surface stations are assimilated. More details are available in
928 (Adani and Uboldi, 2023).

929



930 **3.9 MOCAGE**

931 **3.9.1 Model Overview**

932 The MOCAGE 3D multi-scale Chemistry and Transport Model has been designed for both research and operational
933 applications in the field of environmental modelling. Since 2000, MOCAGE has been allowing to cover a wide range of topical
934 issues ranging from chemical weather forecasting, tracking and backtracking of accidental point source releases, trans-
935 boundary pollution assessment, assimilation of remote sensing measurements of atmospheric composition, to studies of the
936 impact of anthropogenic emissions of pollutants on climate change.

937 **3.9.2 Model geometry**

938 For the CAMS Regional Service, MOCAGE operates on a regular latitude-longitude grid at 0.1 resolution covering the 28° to
939 72° North and 26°W to 46°E domain, for both forecast and assimilation. The products delivered for the CAMS service are
940 issued from the regional domain only. In the vertical, 47 hybrid levels go from the surface up to 5 hPa, with approximately 8
941 levels in the Planetary Boundary Layer (i.e. below 2km), 16 in the free troposphere and 24 in the stratosphere. The thickness
942 of the lowest layer is about 40 m. There is no downscaling applied to surface concentration.

943 **3.9.3 Forcing Meteorology**

944 The forcing meteorology is retrieved from the IFS model vertical layers covering the MOCAGE vertical extent on a 0.1°x0.1°
945 horizontal grid resolution with a temporal resolution of one hour for the 3 first forecast days and 3 hours for the last forecast
946 day. The forecast released at 12UTC of the previous days is used. The meteorological parameters used are: horizontal and
947 vertical winds, temperature, humidity, cloud fraction and surface pressure.

948 **3.9.4 Chemical initial and boundary conditions**

949 Chemical initial values in the regional domain are provided by MOCAGE 24h forecast from the day before. The boundary
950 conditions are taken from global CAMS operational suite for the species (chemical and aerosols) that are distributed (see Table
951 2). For aerosols, the 2 or 3 bins from IFS are summed to get total concentration and then distributed onto the 6 MOCAGE bins
952 considering Mean IFS bin size as emission modes. A factor 4.3 is applied to convert Sea Salt from wet to dry fractions. Aerm03
953 (of diameter larger than 10µm) is only marginally distributed within MOCAGE PM₁₀ sea salt because of the matching between
954 bins and log-normal modes. For the species not included in Table 2, the concentrations from the MOCAGE global domain are
955 used, which helps to introduce smoothly, on the horizontal as well as on the vertical, these chemical boundary conditions into
956 the CAMS regional domain.



957 **3.9.5 Emissions**

958 The common annual anthropogenic emissions CAMS-REG are implemented as explained in Section 3.2. Temporal
959 disaggregation is based on the GENEMIS tables (Ebel et al., 1997), using a GNFR to SNAP matrix. Chemical disaggregation
960 for PM species and VOCs is based on sector and country-dependent split factors proposed by TNO.

961 Isoprene biogenic emissions are computed online using MEGAN model (Guenther et al., 2012), while other biogenic emissions
962 are computed from CAMS global biogenic emission inventory (version 3.1). NO_x soil emissions are taken from the CAMS-
963 GLOB-SOILv2.2 emission inventory.

964 Concerning biomass burning sources, GFAS emissions are emitted according to an ‘umbrella’ profile, with a maximum
965 injecting height climatologically determined. GFAS “near real time” observation-based fire emissions are made available with
966 a 8-hr delay. So that when the forecast system is initiated, most GFAS emission cover Day-2 of the forecast to be produced.
967 As a consequence, the 2-day persistence is interpreted in a way that fire emissions are only applied for D+0.

968 **3.9.6 Solver, advection and mixing**

969 Concerning physical and chemical parameterisations, an operator splitting approach is used. Parameterisations are called
970 alternatively in forward and reverse order, with the objective to reduce systematic errors.

971 Meteorological forcings are read every 3 hours from IFS input data, and are linearly interpolated to yield hourly values, which
972 is the time-step for advection; smaller time-steps are used for physical processes and chemistry, but the meteorological
973 variables are kept constant over each hour. MOCAGE is based upon a semi-lagrangian advection scheme (Williamson and
974 Rasch, 1989), using a cubic polynomial interpolation in all 3 directions.

975 For sub-gridscale transport processes, vertical diffusion is treated following (Louis, 1979) and transport by convection is from
976 (Bechtold et al., 2001). Scavenging within convective clouds is following (Mari et al., 2000), allowing to compute wet removal
977 processes directly within the convective transport parameterisation. Wet deposition in stratiform clouds and below clouds
978 follows (Giorgi and Chameides, 1986).

979 **3.9.7 Deposition**

980 A description of MOCAGE surface exchanges module is presented in (Michou et al., 2005). The dry deposition
981 parameterisation relies on a fairly classical surface resistance approach (Wesely, 1989), but with a refined treatment of the
982 stomatal resistance, similar to the one used in Meteo-France numerical weather prediction models (Noilhan and Planton, 1989).
983 Sedimentation of aerosol follows (Nho-Kim et al., 2004).



984 **3.9.8 Chemistry and aerosols**

985 The MOCAGE configuration for CAMS comprises 118 species and over 300 reactions and photolysis. It is a merge of reactions
986 of the RACM scheme (Stockwell et al., 1997) with the reactions relevant to the stratospheric chemistry of REPROBUS
987 (Lefevre et al., 1994). Aqueous chemistry for the formation of sulphate is represented, following (Ménégoz et al., 2009).
988 Detailed heterogeneous chemistry on Polar Stratospheric Clouds (types I, II) is accounted for, as described in (Lefevre et al.,
989 1994). Other heterogeneous chemistry processes are currently not included.

990 Photolysis is taken into account using a multi-entry look-up table computed off-line with the TUV software version 4.6
991 (Madronich, 1987). Photolysis depends on month (including monthly aerosol climatologies), solar zenith angle, ozone column
992 above each cell (as the model extends to the mid-stratosphere, it is actually the ozone profile computed by MOCAGE which
993 is used at every time step), altitude and surface albedo in the UV. They are computed for clear-sky conditions and the impact
994 of cloudiness on photolysis rates is applied afterwards.

995 The aerosol module of MOCAGE includes the primary species dusts, black carbon, sea salts, organic carbon, and the secondary
996 inorganic species sulphate, nitrate and ammonium. The formation and the multi-phasic equilibrium of inorganic secondary
997 aerosols are modelled by the ISORROPIA-II module. Details on MOCAGE aerosol simulation evaluation can be found in
998 (Martet et al., 2009) for dusts, in (Nho-Kim et al., 2005) for black carbon, and in (Sič et al., 2015) for the latest version of
999 MOCAGE primary aerosol module. The implementation and the evaluation of secondary inorganic aerosols in MOCAGE are
1000 described by (Guth et al., 2016). Further improvements of the representation of aerosols in MOCAGE are expected in the
1001 future with on-going work regarding organic secondary aerosols.

1002 **3.9.9 Assimilation system**

1003 MOCAGE operations for CAMS use the assimilation system based upon MOCAGE and PALM (Lahoz et al., 2007). As a first
1004 approximation, background error standard deviations are prescribed as proportional to background amounts. In order to spread
1005 assimilation increments spatially, background error correlations are modelled using a generalized diffusion operator (Weaver
1006 and Courtier, 2001). Several assimilation strategies are available in PALM but for CAMS MOCAGE uses a 3D-VAR
1007 technique, with an assimilation window that is 1h every hour.

1008 For surface analyses (NRT, IRA and VRA), MOCAGE assimilates O₃, NO₂, CO, PM₁₀ and PM_{2.5} in-situ surface observations.
1009 The species are assimilated independently every hour without any cross-species covariances, and then the increments per
1010 species are added to the analysis that serves as initial condition for computing the background of the next hour of the
1011 assimilation process, in this reanalysis mode.



1012 An hourly assimilation cycle is also used to update the atmospheric state of aerosols, with the assimilation of French lidars
1013 (mini-MPL) and some ceilometers from the European network E-profile in the regional domain of MOCAGE. The quantity
1014 modified during the assimilation process is the 3D field of total mass of all aerosol types and all sizes all together. The split
1015 per aerosol type and particle size is not modified during the assimilation. This hourly assimilation cycle is the backbone and
1016 every day at 00 UTC, the +96h forecast is initialised from this assimilation cycle.
1017



1018 **3.10 MONARCH**

1019 **3.10.1 Model Overview**

1020 The MONARCH model is a fully online multiscale chemical weather prediction system for regional and global-scale
1021 applications (Badia and Jorba, 2015; Badia et al., 2017; Jorba et al., 2012; Klose et al., 2021; Pérez et al., 2011). The system
1022 is based on the meteorological Nonhydrostatic Multiscale Model on the B-grid (NMMB; (Janjic and Gall, 2012)), developed
1023 and widely verified at the National Center for Environmental Prediction (NCEP). The model couples online the NMMB with
1024 the gas-phase and aerosol continuity equations to solve the atmospheric chemistry processes in detail. The model is designed
1025 to account for the feedbacks among gases, aerosol particles and meteorology. Currently, it can consider the direct radiative
1026 effect of aerosols while ignoring cloud–aerosol interactions.

1027 **3.10.2 Model geometry**

1028 The hybrid pressure-sigma coordinate is used in the vertical direction and the Arakawa B-grid is applied in the horizontal
1029 direction. The regional model is formulated on a rotated longitude–latitude grid, with the Equator of the rotated system running
1030 through the middle of the integration domain, resulting in more uniform grid distances. In the operational regional CAMS
1031 forecasts, the model is configured for a regional domain covering Europe and part of northern Africa with a regular horizontal
1032 grid spacing on the rotated projection of 0.15° (lower-left corner at 16.37°N 22.14°W, upper-right corner at 58.56°N 88.18°E)
1033 and the top of the domain is set at 50hPa using 24 vertical layers. Surface concentrations of gases and aerosols are derived
1034 directly from the first model level; no particular vertical downscaling is implemented. The depth of the first vertical layer of
1035 the model is around 45 m and about 7 layers are set below 2 km.

1036 **3.10.3 Forcing Meteorology**

1037 The forcing meteorology is retrieved from the IFS model on a 0.125°x0.125° horizontal grid resolution with a temporal
1038 resolution of 6 hours and dynamically interpolated to the final chemistry grid and time steps using the meteorological
1039 component of MONARCH. The IFS forecast released at 12:00UTC of the previous days is used. The meteorological variables
1040 obtained from IFS are: Skin temperature, Soil temperature, Soil moisture, Snow depth, Sea-ice mask, Sea-level pressure, U
1041 component of the wind, V component of the wind, Temperature, Geopotential height, Relative humidity or specific humidity,
1042 Cloud water content.

1043 **3.10.4 Chemical initial and boundary conditions**

1044 The variables used from chemical species available in the global IFS forecast model are detailed in Table 2. Note that CH₄ is
1045 not used from IFS because the MONARCH chemical mechanism considers a constant CH₄ concentration of 1.85 ppmv. A



1046 remapping has been applied to couple the modal distribution of the IFS aerosols with the aerosols distribution of the
1047 MONARCH model (see Table 2). The forecasts are initialised by the model results of the previous day.

1048 **3.10.5 Emissions**

1049 The common annual anthropogenic emissions CAMS-REG are implemented as explained in Section 2.5.1. The High-Selective
1050 Resolution Modelling Emission System version 3 (HERMESv3; (Guevara et al., 2019)) is used to pre-process the
1051 anthropogenic, ocean and biomass burning emissions for the MONARCH model. HERMESv3 is an open source, parallel and
1052 stand-alone multiscale atmospheric emission modelling framework that processes gaseous and aerosol emissions for use in
1053 atmospheric chemistry models.

1054 CAMS_REG-AP NMVOC and PM_{2.5} emissions are speciated using the sector and country-dependent split factors proposed
1055 by TNO. In terms of NO_x, a fraction of 90% NO and 10% NO₂ is considered for all sectors except for road transport, in which
1056 the following fractions are applied: (i) 95% NO, 4.2% NO₂ and 0.8 HONO for gasoline road transport and (ii) 70% NO, 28.3%
1057 NO₂ and 1.7% HONO for diesel road transport (Rappenglück et al., 2013). The vertical distribution of anthropogenic emissions
1058 is performed following the sector-dependent profiles proposed by TNO. The temporal distribution follows the gridded CAMS-
1059 REG-TEMPO v4.1 profiles (Guevara et al., 2021).

1060 The biogenic emissions for NMVOC and NO are computed on-line within the MONARCH model using the Model of
1061 Emissions of Gases and Aerosols from Nature version 2.04 (MEGANv2.04; (Guenther et al., 2006)), while monthly oceanic
1062 emissions of DMS are obtained from the CAMS-GLOB-OCEA v3.1 dataset (Granier et al., 2019; Lana et al., 2011).

1063 Mineral dust emissions can be calculated online using one of the schemes described in (Klose et al., 2021). For sea salt aerosol
1064 emissions, multiple source functions are available (Spada et al., 2013).

1065 Finally, biomass burning emissions (forest, grassland and agricultural waste fires) of organic carbon, black carbon, SO₂, and
1066 DMS are taken from the GFASv1.3 dataset. This product reports hourly emissions at a horizontal gridded resolution of 0.1° x
1067 0.1°. The vertical allocation of GFAS emissions is done using the maximum fire plume injection height and distributing
1068 uniformly all the emissions across the layers below this height. The persistence of the fires in forecast mode is set to 2 days,
1069 afterwards biomass burning emissions are set to zero.

1070 **3.10.6 Solver, advection and mixing**

1071 Different chemical processes were implemented following a modular operator splitting approach to solve the advection,
1072 diffusion, emission, dry and wet deposition, and chemistry processes. In order to maintain consistency with the meteorological
1073 solver, the chemical species are advected and mixed at the corresponding time step of the meteorological tracers following the



1074 principles described in (Janjic and Gall, 2012) and references therein. The advection scheme is Eulerian, positive definite and
1075 monotone, maintaining a consistent mass conservation of the chemical species within the domain of study. Lateral diffusion
1076 is formulated following the Smagorinsky non-linear approach, while vertical diffusion is based on the Mellor–Yamada–Janjic
1077 level 2.5 turbulence closure scheme.

1078 The convective mixing, however, is treated differently for aerosols and gases. The scheme implemented for aerosols is
1079 described in detail in (Pérez et al., 2011) and follows a relaxation approach similar to the Betts–Miller–Janjic convective
1080 parameterization of the NMMB. On the other hand, the convective mixing of gases is solved following the sub-grid cloud
1081 scheme of (Foley et al., 2010) as described in (Badia et al., 2017).

1082 **3.10.7 Deposition**

1083 The deposition processes implemented in the MONARCH model are dry deposition, in-cloud grid-scale, and in-cloud subgrid-
1084 scale scavenging for gases and aerosols, and below cloud scavenging for aerosols only.

1085 For gases, the dry deposition scheme follows the classical deposition velocity analogy, enabling the calculation of deposition
1086 fluxes from airborne concentrations. The canopy resistance is simulated following (Wesely, 1989). The cloud-chemistry
1087 processes are included in the system considering both the sub-grid and grid-scale scheme described in (Foley et al., 2010). The
1088 processes included are the scavenging, vertical mixing and wet-deposition. Only in-cloud scavenging is considered in the
1089 current implementation (Badia et al., 2017).

1090 Regarding aerosols, the parameterization of the aerosol dry deposition is based on (Zhang et al., 2001) which includes
1091 simplified empirical parameterizations for the deposition processes of Brownian diffusion, impaction, interception and
1092 gravitational settling. Wet scavenging of aerosols by precipitation is computed separately for convective and grid-scale
1093 (stratiform) precipitation. The model includes parameterizations for in-cloud scavenging, and for below cloud scavenging.
1094 Detailed description of the schemes can be found in (Pérez et al., 2011).

1095 **3.10.8 Chemistry and aerosols**

1096 A gas-phase module combined with a hybrid sectional-bulk mass-based aerosol module is implemented in the MONARCH
1097 model. The gas-phase chemical mechanism used is the Carbon Bond 2005 chemical mechanism (CB05; (Yarwood. G. et al.,
1098 2005)) extended with Chlorine chemistry (Sarwar et al., 2012). The rate constants were updated based on evaluations from
1099 (Atkinson et al., 2004; Sander et al., 2006). The photolysis scheme used is the Fast-J scheme (Wild et al., 2000). It is coupled
1100 with physics of each model layer (e.g., aerosols, clouds, absorbers as ozone) and it considers grid-scale clouds from the
1101 atmospheric driver.



1102 The aerosol module in MONARCH model solves the life cycle of sea salt, dust, organic matter (both primary and secondary),
1103 black carbon, sulphate, and nitrate aerosols. While a sectional approach is used for dust and sea salt, a bulk description of the
1104 other aerosol species is adopted. A simplified gas–aqueous–aerosol mechanism accounts for sulphur chemistry (Spada, 2015).
1105 The production of secondary nitrate–ammonium aerosol is solved using the thermodynamic equilibrium model EQSAM
1106 (Metzger et al., 2002). The coarse nitrate production is computed with an uptake reaction of HNO₃ on dust and sea salt coarse
1107 particles. The formation of SOA is considered using a simple non-volatile scheme accounting for the contribution of
1108 anthropogenic, biomass burning, and biogenic formation (Pai et al., 2020). Hygroscopic growth is considered for all aerosol
1109 components except mineral dust.

1110 **3.10.9 Assimilation system**

1111 The MONARCH assimilation system (MONARCH-DA) is based on a Local Ensemble Transform Kalman Filter (LETKF)
1112 scheme (Di Tomaso et al., 2022; Di Tomaso et al., 2017; Escribano et al., 2022; Hunt et al., 2007; Miyoshi and Yamane, 2007;
1113 Schutgens et al., 2010) coupled to the model through I/O routines. MONARCH ensemble is created by perturbing
1114 anthropogenic, biomass burning, soil and ocean emissions that are pre-processed by HERMESv3 or that are modelled by
1115 MONARCH via a physically-based scheme for dust aerosol. For analysis production in CAMS, MONARCH ensemble is run
1116 at a horizontal resolution of 0.2° latitude × 0.2° longitude in a rotated grid and initialised by the ensemble forecast of the
1117 previous day.

1118 Hourly surface observations from in-situ measurements are currently assimilated operationally for O₃, NO₂, SO₂, CO, PM₁₀,
1119 PM_{2.5}. For near-real time operational analysis production, previous-day observations are combined with a MONARCH 24-
1120 hour ensemble forecast initialised at 12 UTC of the previous day.

1121



1122 **3.11 SILAM**

1123 **3.11.1 Model Overview**

1124 The System for Integrated modeLLing of Atmospheric coMposition SILAM (silam.fmi.fi) is a global-to-sub-km chemistry
1125 transport model developed for a wide range of atmospheric composition and air quality assessment tasks (Sofiev et al., 2015b),
1126 emergency decision support applications (Sofiev et al., 2008), and data assimilation and source inversion problems (Vira and
1127 Sofiev, 2015; Sofiev et al., 2013). The model incorporates Eulerian and Lagrangian dispersion frameworks (the Eulerian
1128 transport routine is used for CAMS) and a set of chemical and physical transformation modules for the troposphere and the
1129 stratosphere (Carslaw et al., 1995; Damski et al., 2007; Yarwood. G. et al., 2005; Sofiev, 2000; Sofiev et al., 2010). Apart from
1130 the transport and physico-chemical cores described below, SILAM includes a set of supplementary tools including a
1131 meteorological pre-processor, input-output converters, reprojection and interpolation routines, etc. In the operational forecasts,
1132 these enabled direct forcing of the model by the ECMWF IFS meteorological fields.

1133 SILAM has been extensively evaluated in a variety of regional and global air quality projects (Brasseur et al., 2019; Huijnen
1134 et al., 2010; Kouznetsov et al., 2020; Petersen et al., 2019; Sofiev et al., 2015b; Xian et al., 2019) and health impact assessment
1135 studies (Korhonen et al., 2008; Kukkonen et al., 2020; Lehtomäki et al., 2018).

1136 **3.11.2 Model geometry**

1137 The centre points of the model grid cover 25.05°W to 44.95°E and 30.05°N to 71.95°N on a regular latitude longitude grid of
1138 0.1°resolution. Following (Sofiev, 2002), SILAM uses a multi-vertical approach with the meteorology-resolving grid
1139 corresponding to the tropospheric part of the IFS vertical: hybrid levels from 69 to 137. The chemical transformations and
1140 vertical fluxes are computed based on 10 thick staggered layers, with the thickness increasing from 25 m for the lowest layer
1141 to 1000-2000 m in the free troposphere. The layer tops are located at 25, 75, 175, 375, 775, 1500, 2700, 4700, 6700 and 8700m
1142 above the surface. Within the thick layers, the sub-grid information is used to evaluate the weighted averages of the high-
1143 resolution meteorological parameters and effective diffusion coefficients after (Sofiev, 2002).

1144 **3.11.3 Forcing Meteorology**

1145 Meteorological forcing is the ECMWF IFS operational forecasts taken from the 12:00UTC forecast of the previous day
1146 extracted at a resolution of 0.1° and temporal frequency of one hour for the first 72 hours and three hours for the last day of
1147 the forecast. The list of meteorological parameters extracted is: U and V components of 10m wind [m/s], 2m temperature [K],
1148 dew point temperature 2m [K] accumulated large scale rain [kg/m²], accumulated convective rain [kg/m²], surface roughness
1149 [m], total cloud cover [fract], convective available potential energy [J/kg], U and V -wind components at model levels [m/s],



1150 temperature at model levels [K], cloud water at model levels [kg/kg], cloud ice at model levels [kg/kg], specific humidity at
1151 model levels [kg/kg], cloud cover at model levels[fract], logarithm of surface pressure.

1152 **3.11.4 Chemical initial and boundary conditions**

1153 Boundary conditions are taken from the C-IFS (see Table 2). The full fields are imported every 3 hours; in-between, the linear
1154 interpolation is applied. The forecasts are initialised with the SILAM forecast of the previous day.

1155 **3.11.5 Emissions**

1156 The common annual anthropogenic emissions CAMS-REG are implemented as explained in Section 3.2. The PM_{2.5} emissions
1157 are split into EC, OC and mineral components, and OC is mapped to the volatility bins according to (Shrivastava et al., 2008).
1158 Emissions of biogenic VOCs, wind-blown dust, and sea salt are computed online in dedicated SILAM modules (Poupkou et
1159 al., 2010; Sofiev et al., 2011; Soares et al., 2016; Sofieva et al., 2022). GFAS hourly emissions from wild-land fires are
1160 replicated from D-2 to D+1 for forecast and shut down after; in the analysis mode it is used as is.

1161 Emissions of 6 pollen species are computed online following the heat-sum approach for trees (Sofiev et al., 2015b),
1162 climatological season for grasses and mugwort species, and multi-criteria hybrid model for ragweed (Prank et al., 2013).

1163 **3.11.6 Solver, advection and mixing**

1164 The SILAM Eulerian transport core (Sofiev et al., 2015a) is based on the coupled developments: refined advection scheme of
1165 (Galperin and Sofiev, 1994) and vertical diffusion and dry deposition algorithm of (Sofiev, 2002)and (Kouznetsov and Sofiev,
1166 2012). The methods are compatible, in a sense that both use the same set of variables to determine the sub-grid distribution of
1167 tracer mass. The approach, in particular, allows computing correct vertical exchange using high-resolution input data but low-
1168 resolution chemistry and diffusion grids. The later feature is used in the vertical setup with thick layers.

1169 Diffusion is parameterised following the first-order K-theory based closure. Horizontal diffusion is embedded into the
1170 advection routine, which itself has zero numerical viscosity, thus allowing full control over the diffusion fluxes. The vertical
1171 diffusivity parameterisation follows the approach suggested by (Groisman and Genikhovich, 1997) and (Sofiev et al., 2010).
1172 The procedure diagnoses all the similarity theory parameters using the profiles of the basic meteorological quantities: wind,
1173 temperature and humidity. Output includes the value of eddy diffusivity for scalars at some reference height (taken to be 1m).

1174 The model uses process-wise splitting and 1-D advection implementation flipping the order of processes every other time step.



1175 **3.11.7 Deposition**

1176 Dry deposition parameterisation for gases generally follows the resistive analogy of (Wesely, 1989). Deposition velocities for
1177 aerosols are evaluated using the original (Kouznetsov and Sofiev, 2012) algorithm. Wet deposition parameterisation is based
1178 on the scavenging coefficient after (Sofiev, 2000) for gas species and follows the generalised formulations of (Kouznetsov and
1179 Sofiev, 2012) for aerosols.

1180 **3.11.8 Chemistry and aerosols**

1181 The main gas-phase chemical mechanism is CB05 with additions for SO_x from (Sofiev, 2000) and organics from VBS
1182 (Volatility-Basis Set, (Shrivastava et al., 2008)). The heterogeneous scheme is an updated version of the DMAT model scheme
1183 (Sofiev, 2000). The formation pathways of secondary inorganic aerosols follow the VBS approach extended with the feedback
1184 to the main gas-phase chemical module. The aerosol size distribution is represented via sectional approach, with species-
1185 specific bin selections. Each bin is characterised with its lower and upper borders, as well as the mass-mean diameter, which
1186 is precomputed / predefined for each bin and species from its size spectrum. Primary anthropogenic aerosols are emitted into
1187 bins with mass-mean diameter of 0.5 µm (fine aerosol, dry size) and 6 µm (coarse aerosols, dry size). Secondary inorganic
1188 aerosols were put into 0.2 and 0.7 µm bins, plus a separate 3 µm bin for coarse nitrates formed on the sea salt surface. The
1189 dust size spectrum is described with 4 bins from 0.3 µm up to 20 µm. Finally, the seasalt spectrum is represented with 5 bins,
1190 from 0.05 µm up to 20 µm of mass-mean nominal diameter. Throughout computations, the particles are transported in
1191 accordance with their mass-mean diameter corrected with regard to actual humidity and the particle solubility. External mixing
1192 is assumed.

1193 **3.11.9 Assimilation system**

1194 The embedded data assimilation is based on the 3d- and 4d-dimensional variational approach, as well as with the EnKF (Vira
1195 and Sofiev, 2012, 2015). Tangent-linear (if needed) and adjoint formulations exist for the transport module, the transformation
1196 schemes and for the deposition modules. The assimilation procedure has been tested for both initialising the concentration
1197 fields and for refinement of the emission (Sofiev, 2019). The observation operators exist for in-situ observations and for the
1198 vertically integrated columns observed by the nadir-looking satellites. For the near-real time operational analyses in CAMS,
1199 the previous-day observations are used in a 3D-VAR data assimilation suite. That routine assimilates in-situ observations of
1200 NO₂, O₃ and PM_{2.5}, PM₁₀, SO₂ and CO.

1201



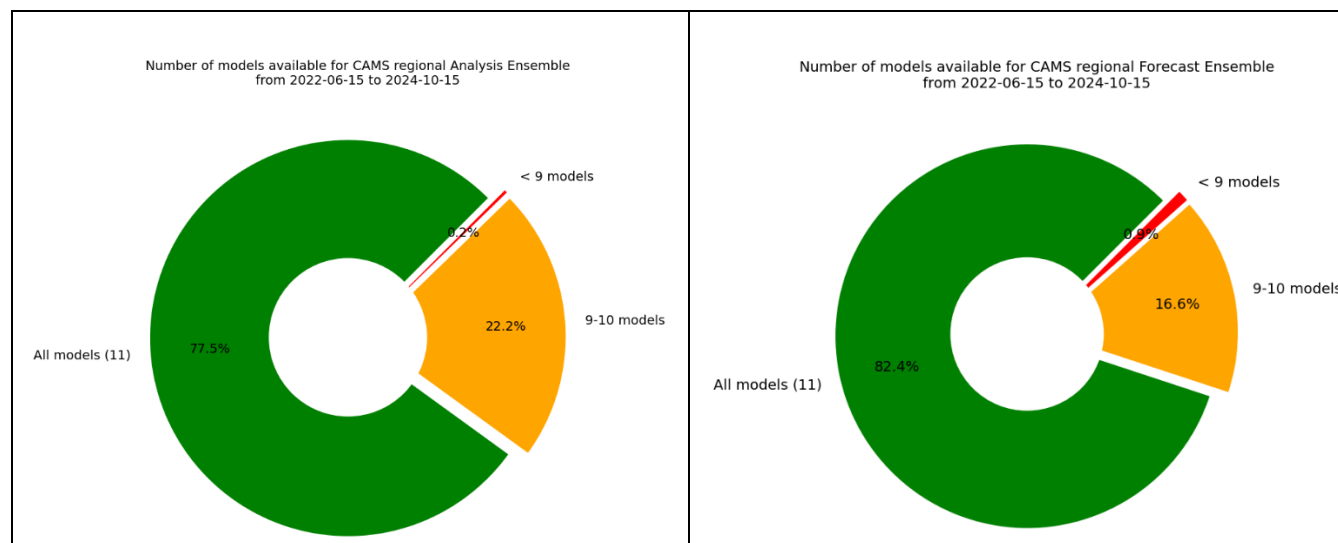
1202 4 Post-processing

1203 4.1 ENSEMBLE model

1204 All eleven individual operational model results deliver their results to the CRPU (Météo-France for NRT/FC and NRT/AN,
1205 and INERIS for IRA and VRA, using the product definition introduced in Section 2.2). An ENSEMBLE model is subsequently
1206 computed as a median of all available operational models. As explicated in Section 3, there are slight differences in the
1207 individual model geometry even if they are as close as possible to the common requirement **to deliver model output on the**
1208 **same grid**. The ENSEMBLE is computed across all models at each horizontal and vertical grid point of the common grid and
1209 for each species.

1210 Relying on 11 different models offer a very comprehensive view on the various possible representations of key atmospheric
1211 processes relevant to air quality (see the wide range of modelling design detailed in Section 3) and thus a characterisation of
1212 the intrinsic modelling uncertainty. The flipside of this diversity is a relatively higher risk of one model not being able to
1213 deliver in a timely basis. A median ENSEMBLE is computed everyday no matter how many models are successfully delivered
1214 for that given day. A Key Performance Indicator is documented to track the number of models which have delivered on time
1215 to be included in the ENSEMBLE for either the analyses or the forecasts (Figure 1).

1216 Using the median to compute such an ensemble is a very robust approach to cope with potential missing members, and it has
1217 been shown to outperform individual models for average performances (Galmarini et al., 2004). It is however a very
1218 conservative approach and developments are ongoing, in particular to improve the skills of the system to capture air quality
1219 exceedance detections by making use of machine learning algorithm coupled to the raw CAMS regional forecasts (Bertrand et
1220 al., 2022).





1221 *Figure 2: Distribution of the number of operational models having delivered on time to be included in the ENSEMBLE computation for the*
1222 *period 15/06/2022-15/10/2024: left NRT/AN (analysis) and right: NRT/FC (forecasts).*

1223 **4.2 Evaluation and Quality Control (EQC)**

1224 Evaluation and quality control is an essential part of CAMS in order to ensure the reliability and transparency of the products.
1225 For all the chemical species where a dense enough monitoring network allows a recurrent and statistically significant
1226 evaluation, synthetic performance reports are produced and made available on the CAMS website⁶. These evaluations focus
1227 primarily on the surface in-situ air quality regulatory monitoring networks for O₃, NO₂, PM₁₀, PM_{2.5}. For the assimilated
1228 products, the evaluation is performed on about one third of the stations, deliberately left out of the assimilation workflow
1229 (Section 2.3). The forecasts are evaluated using all available surface stations whose spatial representativity ranges from rural
1230 to urban background air quality. The skill scores are updated on a daily frequency and available publicly through an interactive
1231 interface on the CAMS EQC pages for the ENSEMBLE and individual models. Quarterly summaries are produced in publicly
1232 available reports. They also include an evaluation of the models in the troposphere against above-surface measurements
1233 (aircraft and space borne remote sensing and profiling). For the Interim and Validated reanalyses, the evaluation reports are
1234 produced on an annual basis.

1235 The present article is essentially a description of the system rather than a detailed analysis of its performance. Nevertheless,
1236 we present here a couple of evaluation diagnostics for illustration purposes. Therefore, the performances of individual models
1237 contributing to the ENSEMBLE are anonymised as it would be too complex to enter here in the details of the performances of
1238 each model, which relate to intrinsic parametrisations.

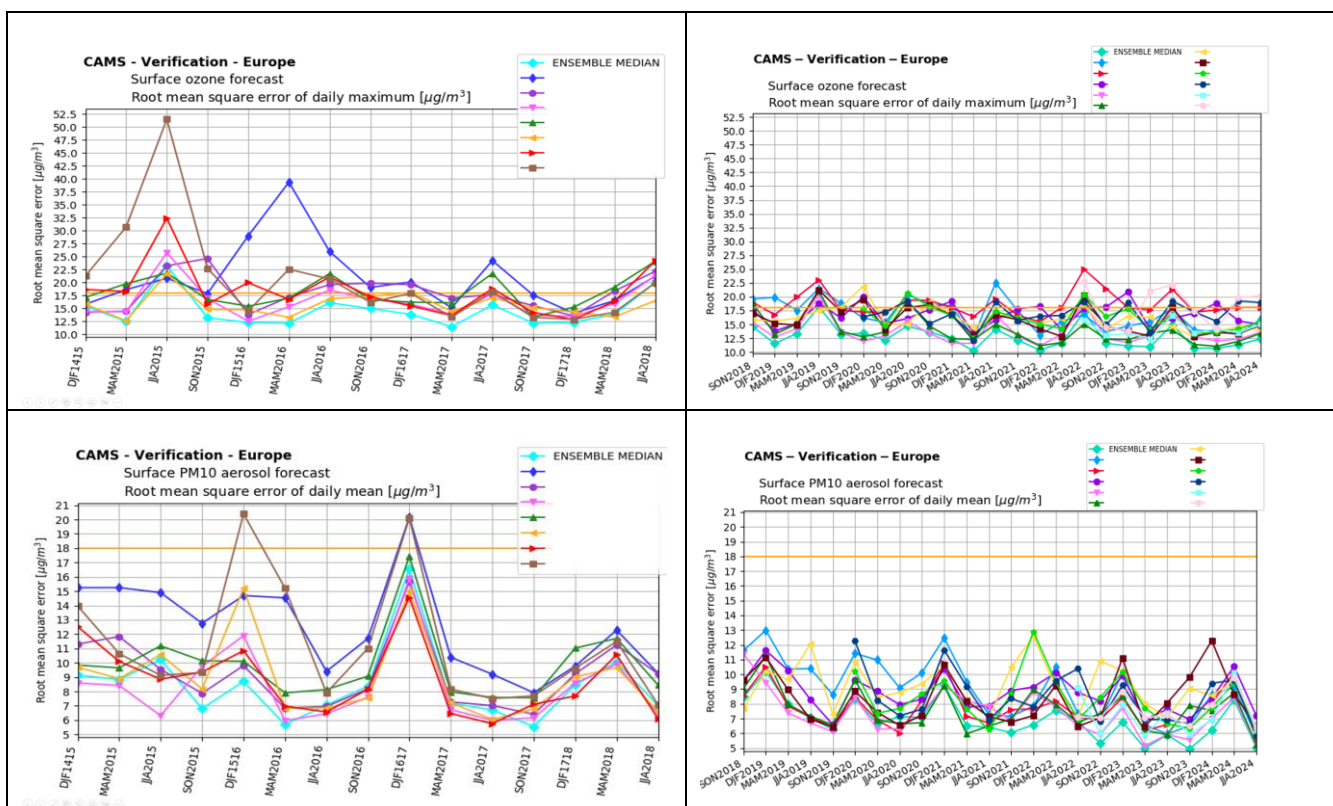
1239 In Figure 3 we show the root mean square error for surface ozone and PM₁₀ taken as the median over each quarter since the
1240 beginning of the CAMS production at the end of 2014 and over hundreds of European air quality monitoring stations. The
1241 figure is divided in two parts as urban background stations were only included in the evaluation as of fall 2018 (note also that
1242 the vertical scales differ). It appears clearly that while the spread of the models was still substantial in the first part of the
1243 period, the system has reached a level of maturity since 2017 with more homogeneous performances between the various
1244 models and very few outliers. The ENSEMBLE model appears to give better scores overall. It can be surpassed in terms of
1245 RMSE in some occasions but not always by the same model, therefore still illustrating the added value of the multi-model
1246 ensemble approach. The range of performances is today about 12-18µg/m³ for the RMSE of daily maxima ozone, so that the
1247 Key Performance Indicator of 18µg/m³ is not always met depending on the models and the season. For PM₁₀, the RMSE is
1248 between 5 to 8µg/m³ so that the same KPI of 18µg/m³ is usually met. Without entering in a more detailed analysis, it is visible

⁶ <https://atmosphere.copernicus.eu/regional-services>, last accessed 30/10/2024



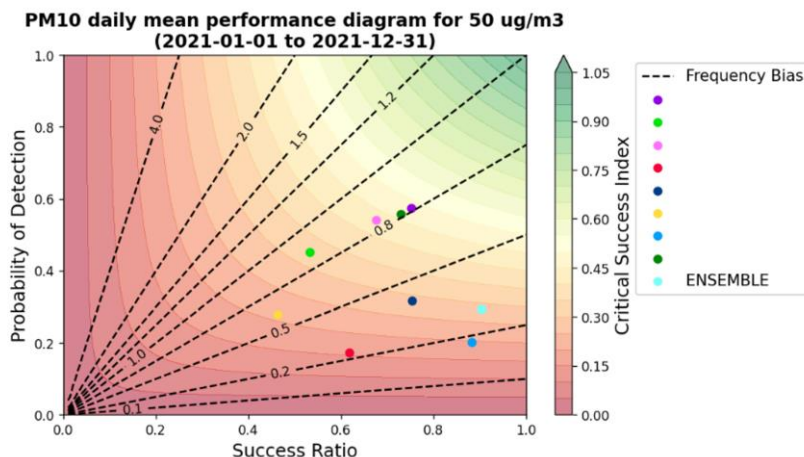
1249 that the scores are still gradually improving over the 2018-2023 period. Over the recent years, the median ENSEMBLE seems
 1250 to produce more systematically better performances and becomes more difficult to beat.

1251



1252 *Figure 3: Evolution of the skill scores of the CAMS Regional Air Quality Forecasts (individual models and ENSEMBLE median) between*
 1253 *2014 and 2024 (divided in two parts: before and after 2018 as urban background stations were not included in the evaluation over the first*
 1254 *period, and fewer models were available) Each point is the quarterly median of the RMSE ($\mu\text{g}/\text{m}^3$) computed at regulatory air quality*
 1255 *monitoring stations for top: daily maximum ozone and bottom: daily mean PM₁₀. The straight yellow line corresponds to the Key*
 1256 *Performance Indicator for RMSE of $18\mu\text{g}/\text{m}^3$.*

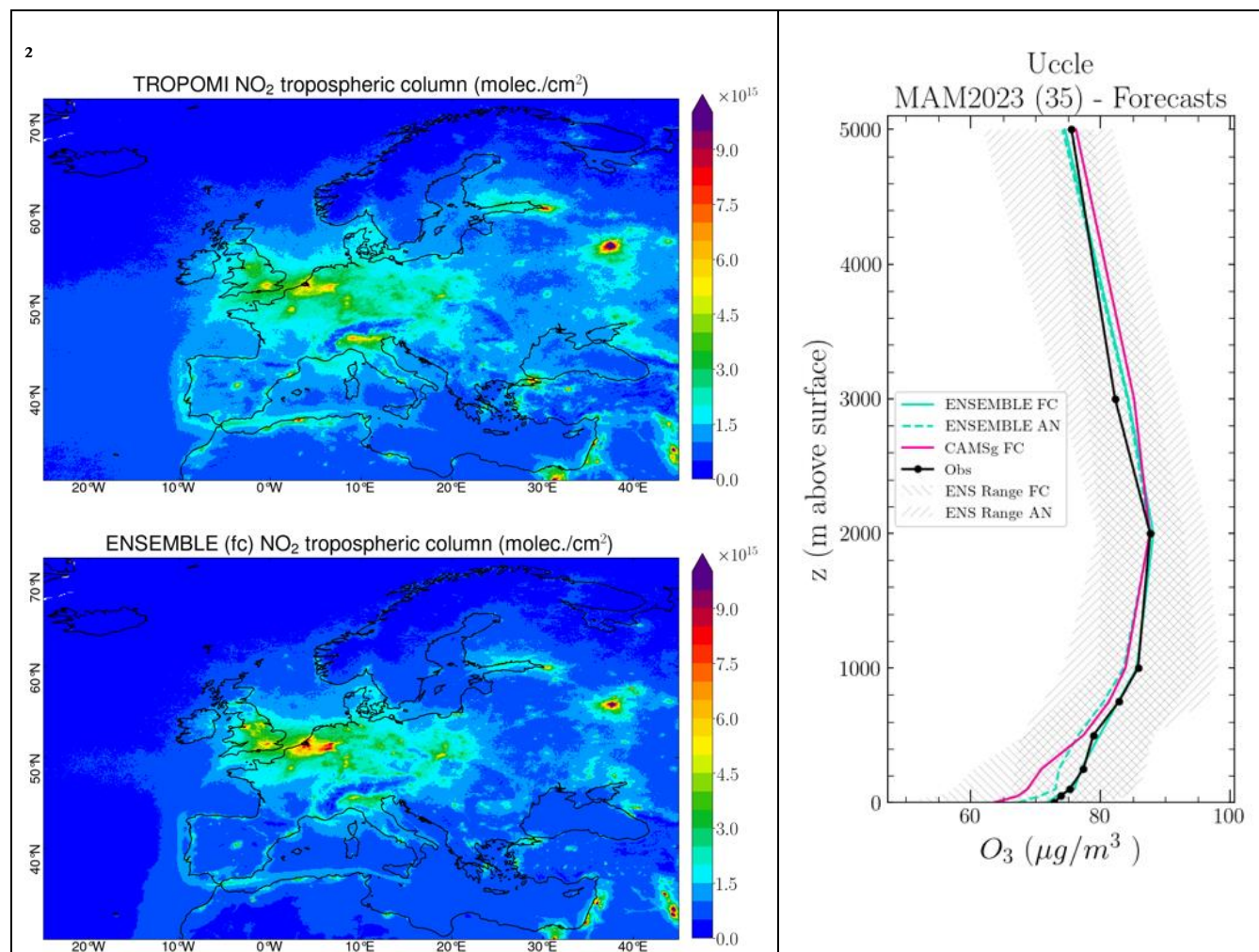
1257 In the European Air Quality regulation, detrimental air quality situations are identified in terms of various exceedance levels
 1258 depending on the air pollutants. For PM₁₀, the daily mean concentrations should not exceed $50\mu\text{g}/\text{m}^3$ more than 35 days (EC,
 1259 2008). The performance of the CAMS Regional reanalyses in capturing that threshold can be assessed through the performance
 1260 diagram presented in Figure 4. On the x-axis the success ratio is the number of hits divided by the number of hits and false
 1261 alarms. On the y-axis, the probability of detection is the number of hits divided by the number of hits and misses. For this
 1262 example, for the year 2021, the ENSEMBLE median has the best success ratio, but some individual models outperform in
 1263 terms of probability of detection.



1264

1265 *Figure 4: Performance of the CAMS Regional ENSEMBLE and individual models reanalyses in capturing air quality threshold detection*
1266 *for daily mean PM₁₀ above 50µg/m³ in 2021.*

1267 An illustration of the evaluation above the surface is provided in Figure 5. The total column of NO₂ in the CAMS regional
1268 ENSEMBLE forecast is compared to the TROPOMI instrument on board the Sentinel-5P satellite. The higher spatial resolution
1269 (approximately 5km) available since the launch of the instrument allows reaching out to urban level NO₂ concentrations
1270 therefore providing an excellent opportunity for the evaluation of spatial patterns of air pollution. Beyond surface and total
1271 columns, it is also essential to assess the performances of the vertical structure as illustrated for the comparison with ozone
1272 soundings in Belgium (Uccle). Here both the regional forecast and analyses are compared to assess the impact of surface
1273 assimilation of air quality measurement on the vertical profiles. The CAMS global model forecast is also included along with
1274 the CAMS regional ensemble range for the forecast and the analysis. A more detailed analysis of the comparison with satellite
1275 data can be found in (Douros et al., 2022).



1276 *Figure 5: Left: Evaluation over MAM-2023 of the CAMS Regional ensemble forecasts against TROPOMI satellite NO₂ tropospheric columns*
1277 *(10¹⁵ molecules/cm²). The CAMS NO₂ profiles have been multiplied with the TROPOMI kernels to remove the dependency on the retrieval a-*
1278 *priori profile shape. Right: Regional and global CAMS forecast and regional analyses of ozone compared to vertical profiles measured with*
1279 *ozone sondes over Uccle, Brussels, Belgium for MAM-2023 (μg/m³). source: CAMS2_83 Evaluation and Quality Control Service,*
1280 *<https://atmosphere.copernicus.eu/regional-services>*

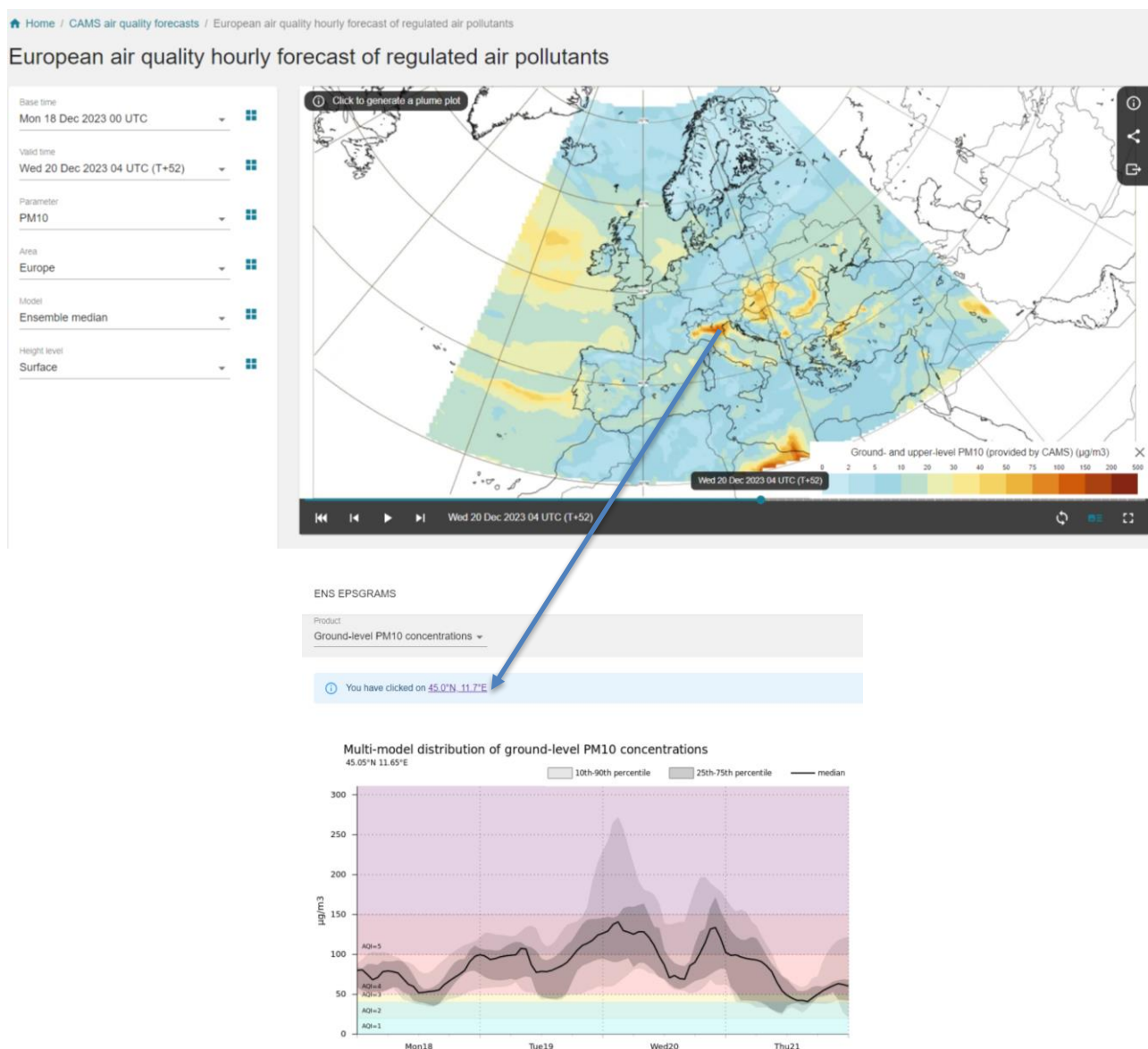
1281 4.3 Dissemination and further use of the CAMS Regional Products

1282 The results of the CAMS regional production system are made available publicly on the website
1283 <https://atmosphere.copernicus.eu/european-air-quality-forecast-plots> where maps and time series of the various air pollutant
1284 and pollen species can be displayed. The results of the median ENSEMBLE as well as each individual model are available for
1285 both forecast and analysis products. Daily means, daily maxima, and hourly fields are available. The list of vertical levels
1286 available for interactive plotting on the website is: surface, 100m, 1000m, 3000m and 5000m (note that more vertical levels



1287 are available on the ADS). The model spread can also be assessed by selecting any grid point in the map to display the time
1288 series of the 4 day forecast including modelled dispersion (Figure 6).

1289



1290 Figure 6: Screenshot of the CAMS Regional Production website displaying air quality forecasts over Europe (atmosphere.copernicus.eu6)



1291 The Copernicus Atmosphere Data Store (ADS) constitutes an important dissemination pathway for the CAMS Regional
1292 production system. All the numerical data can be freely retrieved through the website ads.atmosphere.copernicus.eu where
1293 automated requests can be built to download entire fields or custom extractions in either grib or netcdf formats.

1294 The typical use of CAMS Regional forecast product is for national and local air quality management agencies to understand
1295 the day-to-day air quality situation and anticipate major air pollution events. This can be done either by a qualitative analysis
1296 of quicklooks available on the CAMS website or external companies that have developed alternative visualisation tools.

1297 The numerical data obtained on the ADS can also be used as background information for national or local scale air quality
1298 modelling applications. Such uses range from the nesting of a Chemistry Transport Model as three-dimensional and hourly
1299 concentrations of several chemical species are available in the CAMS Regional Forecast. They can also be used to feed
1300 gaussian city-scale surface air quality models. There are also reported use of the CAMS Regional Forecast to inform machine-
1301 learning air quality statistical prediction tools (Bertrand et al., 2022; Petetin et al., 2022).

1302 The use of CAMS Regional reanalyses is rather to inform longer term air quality applications. They can be used as background
1303 information for land-use regression models used in air quality policy products or exposure assessment for health impact studies
1304 (Horálek et al., 2022). They are also the primary source of information for the Interim Assessment Report produced annually
1305 by the CAMS Policy Service and serves as background information for European Member States in the Regulatory Air Quality
1306 reporting obligations (Hamer et al., 2023).

1307 **5 Conclusion & Perspectives**

1308 The regional production of the Copernicus Atmosphere Monitoring Service is today a well-established reference for air quality
1309 forecast and analysis in European and beyond. It is constituted of a unique ensemble of eleven European Chemistry-Transport
1310 models operated in ten countries under the management of a Centralised Regional Production Unit. The system follows strict
1311 requirements in order to produce consistent air quality products through the ensemble of individual CTM. Those requirements
1312 include in particular forcing fields such as meteorology, chemical hemispheric boundary conditions, and surface fluxes of
1313 anthropogenic and wildfire emissions. But the added value of the use of an ensemble of models also lies in the diversity of the
1314 modelling strategy. As of today, the ensemble offers a very wide array of choices in terms of model design and structure, as
1315 well as regarding the formulation of underlying physical and chemical processes or forcing and coupling at the interfaces (land,
1316 sea, biosphere, ...).

1317 In the present paper, we provide a comprehensive scientific documentation of the technical characteristics for the common
1318 forcing requirements as well as the diversity in modelling design brought about by the individual contributing modelling



1319 groups. We also explained how the billions of data produced on a daily basis are aggregated centrally, evaluated and
1320 disseminated for a wide range of air quality applications. The CAMS Service has been operational since the end of 2014 and
1321 has reached today a high level of performance and stability. Since 2017 the spread of model performances has converged and
1322 it continues to improve gradually over the years.

1323 As an operational service, the Regional Production of CAMS follows closely the research developments in the field of air
1324 quality modelling. A substantial part of the model development is undertaken independently by the modelling teams through
1325 various research projects and PhD work at national level. The international benchmarking activities (such as the AQMEII or
1326 Eurodelta initiatives, (Galmarini et al., 2017; Colette et al., 2017)) are also an important source of information to identify
1327 model development priorities. More recently, the European Union has launched a series of research projects devoted to the
1328 Evolution of Copernicus in the Horizon Europe Programme⁷.

1329 In order to ensure a continuous improvement, the system follows a regular development cycle. The individual models are
1330 improved in time so that they remain in the state of the art of chemistry transport modelling. When the progress becomes
1331 mature enough, system upgrades are scheduled on a bi-annual basis to allow individual modelling groups to bring their
1332 development into the operational model version. These bi-annual upgrades are also the opportunity to carry coordinated
1333 changes, such as the regular update of anthropogenic emission fluxes. Through these upgrades, the portfolio of products is also
1334 continuously expanding. For instance, in addition to the 19 chemical species already being delivered, the current plan at the
1335 time of submission of the present article (i.e. for the year 2024) is to include new PM species such as ammonium nitrate and a
1336 tracer of shipping emissions.

1337 A large part of the research effort in relation to the Regional Production is related to Chemistry-Transport deterministic
1338 modelling. But there are also interesting prospects in the coupling between machine learning and physical and chemical
1339 modelling. The Regional Service is about to launch operational forecasts at station level on the basis of Model Output Statistics
1340 or any other Machine Learning Postprocessing which promises to open unprecedented performance in particular for air quality
1341 threshold detection (Bertrand et al., 2022). Novel methodologies to compute the ENSEMBLE model from the eleven individual
1342 production and move away from the conservative median approach are also under consideration.

1343 Besides the modelling developments, the uptake of innovative observations is also instrumental in the long-term perspective
1344 of CAMS. The production of deposition fluxes is a good illustration of the need to make the best of available observations.
1345 While CTMs are producing by nature deposition fluxes, they are not systematically quality checked and therefore the output
1346 products are limited at present to ambient air concentrations. A mid-term development is therefore ongoing to benchmark wet

⁷ <https://atmosphere.copernicus.eu/copernicus-research-whats-horizon>



1347 and dry deposition fluxes to ensure their robustness. To achieve this, CAMS relies on the network of deposition data collected
1348 in the EMEP network of rural supersites in Europe. But there are also promising prospects in the uptake of near-real-time
1349 advanced observations of atmospheric composition at the supersites of the ACTRIS European Research Infrastructure, in
1350 particular with regards to particulate matter chemical composition and source apportionment. Lastly, in the outlook of the
1351 future perspectives there are also high expectations regarding the uptake of geostationary satellite retrievals with the
1352 perspective of the launch of the Sentinel 4 satellite which will bring unprecedented high-frequency atmospheric composition
1353 information over Europe.

1354 **6 Data Availability**

1355 Copernicus is funded under the Copernicus Regulation and operated by ECMWF under the ECMWF Agreement. Access to
1356 all Copernicus (previously known as GMES or Global Monitoring for Environment and Security) Information and Data is
1357 regulated under Regulation (EU) No 1159/2013 of the European Parliament and of the Council of 12 July 2013 on the European
1358 Earth monitoring programme, under the ECMWF Agreement and under the European Commission's Terms and Conditions.
1359 Access to all Copernicus information is regulated under Regulation (EU) No 1159/2013 and under the ECMWF Agreement.

1360 The Copernicus Licence is free of charge, worldwide, non-exclusive, royalty free and perpetual. Access to Copernicus Products
1361 is given for any purpose in so far as it is lawful, whereas use may include, but is not limited to: reproduction; distribution;
1362 communication to the public; adaptation, modification and combination with other data and information; or any combination
1363 of the foregoing.

1364 The full terms of the Copernicus Licence are available at: [https://ads.atmosphere.copernicus.eu/api/v2/terms/static/licence-to-](https://ads.atmosphere.copernicus.eu/api/v2/terms/static/licence-to-use-copernicus-products.pdf)
1365 [use-copernicus-products.pdf](https://ads.atmosphere.copernicus.eu/api/v2/terms/static/licence-to-use-copernicus-products.pdf)

1366 **7 Code Availability**

1367 Following the Copernicus Programme Data Policy, the Regional Production data and information are available on a full, open,
1368 and free-of-charge basis, subject to limitations concerning registration, dissemination formats, and access restrictions. The
1369 Copernicus Atmosphere Data Store is located at: <https://ads.atmosphere.copernicus.eu/>.

1370 The CHIMERE v2020 model is available on its dedicated website at <https://www.lmd.polytechnique.fr/chimere/> and for
1371 download at <https://doi.org/10.14768/8afd9058-909c-4827-94b8-69f05f7bb46d>.

1372 The DEHM model is available for collaborative requests to J. H. Christensen; jc@envs.au.dk.



- 1373 The EMEP model is available at <https://github.com/metno/emep-ctm> under the GPLv3 licence. The model version for CAMS
1374 is updated once or twice a year in the frame of the regular updates in the CAMS regional service. The current version is close
1375 to the one archived on <https://doi.org/10.5281/zenodo.4230110>
- 1376 The EURAD-IM source code is not publicly available for download, but code and data are available on request by e-mail.
- 1377 The air quality part of the GEM-AQ model code is available upon request from the Institute of Environmental Protection. The
1378 meteorological part of the GEM-AQ model is available from Environment and Climate Change Canada
1379 (<https://github.com/ECCC-ASTD-MRD>).
- 1380 The LOTOS-EUROS model is available upon user request from the website [https://airqualitymodeling.tno.nl/lotos-
1381 euros/open-source-version/](https://airqualitymodeling.tno.nl/lotos-euros/open-source-version/).
- 1382 Access for implementation is only granted to the extent it is needed for the Parties concerned to carry out their tasks in the
1383 CAMS2_40 project and provided that SMHI can grant Access Rights to the MATCH CTM (Chemistry Transport Model),
1384 including version control, build environment, scripting system for production, and the legal restrictions or limits. This includes
1385 limitations imposed on licenses of software and data. Access Rights are subject to written request. The Access Rights are
1386 granted for the purpose of the CAMS Project only and may be restricted if this results in the infringement of third-party rights.
1387 All commercial and third-party software are excluded and no Access Rights are granted.
- 1388 The FARM code embedded in the MINNI System is available at <https://hpc-forge.cineca.it/projects/open/20>
- 1389 The MOCAGE source code is not publicly available for download, but code and data are available on request by e-mail.
- 1390 The MONARCH model is available at <https://earth.bsc.es/gitlab/es/monarch> under the GPLv3 licence.
- 1391 The SILAM code is available at <https://github.com/fmidev/silam-model> under the GPLv3 licence. The model is updated
1392 several times a year, including two CAMS-related updates. The GitHub release follows the most-recent operational release.
1393



1394
1395
1396

8 Author Contribution

1397

AC designed and drafted the overall manuscript and coordinated all contributions.

1398

1399

GC, FB, EB, VG, FM, AR, VP, CM, OF, AJ, VHP and LR contributed to drafting the centralised production specifics and general review of the draft.

1400

1401

1402

MA, JA, AB, RB, DB, JB, GB, AC, JHC, FC, IDE, MDI, GD, EDT, JD, JE, HF, YF, JF, EF, LF, MG, CG, GG, MG, AG, JG, RH, MK, JWK, RKo, RKr, ACL, JL, VL, FM, AM, MM, AN, MO, CPGP, JP, AP, BR, LR, AS, MS, PS, DS, MS, AS, JS, CT, RT, TT, ST, ST, AU_n, AU_p, AV, PvV, LV, ZY contributed to draft the specificities of individual model description.

1403

HE contributed to draft the text on model evaluation

1404

JK, HdV_G: contributed to draft the text on emissions.

1405

MR, OF, VP, AR, EB, provided plots and figures

1406

9 Competing Interest

1407

The authors declare that they have no conflict of interest.

1408

10 Acknowledgements

1409

1410

1411

The activities described in this paper have been funded by the Copernicus Atmosphere Monitoring Service. ECMWF implements the Copernicus Atmosphere Monitoring Service and the Copernicus Climate Change Service with funding from the European Union on behalf of the European Commission.

1412

1413

INERIS acknowledged the support of the French Ministry in Charge of Ecology for continuous support in developing the CHIMERE model and related air quality forecasting activities.

1414

1415

FMI acknowledges the support of Academy of Finland projects PS4A (grant 318194) and ALL-Impress (grant 329215) for the pollen module developments.

1416

1417

1418

1419

1420

The computing resources and the related technical support for MINNI forecast are provided by CRESCO/ENEAGRID High Performance Computing infrastructure and its staff. CRESCO/ENEAGRID High Performance Computing infrastructure is funded by ENEA, the Italian National Agency for New Technologies, Energy and Sustainable Economic Development and by Italian and European research programmes (see <http://www.cresco.enea.it/english>).



1421
1422

Table 1: Overview of the main characteristics and configurations of the eleven chemistry-transport models as used in the CAMS Regional Production

		CHIMERE	DEHM	EMEP	EURAD-IM	GEM-AQ	LOTOS-EUROS	MATCH	MINNI	MOCAGE	MONARCH	SILAM
Discretisation	Horizontal resolution	0.1° x 0.1° regular lat-lon	0.1° x 0.1° regular lat-lon	0.1° x 0.1° regular lat-lon	9x9 km Lambert conformal	0.1° x 0.1° lat-lon spherical grid	0.1° x 0.1° regular lat-lon	0.1° x 0.1° regular lat-lon	0.15° x 0.1° regular lat-lon	0.1° x 0.1° regular lat-lon	0.15° x 0.15° rotated regular lat-lon	0.1° x 0.1° regular lat-lon
	number of vertical levels	9	29	20	23	28	12	26	14	47	24	10
	top altitude	500hPa	100hPa	100hPa	100hPa	10hPa	200hPa	8000m	7040m	5hPa	50hPa	8700m
	depth of lowermost layer	20m	20m	50m	35m	20m	20m	45m	40m	40m	40m	25m
	number of lower layers	7 below 2km	12 below 1km	10 in PBL	15 below 2km	14 below 5km	7 below 1km	10 below 850hPa	8 below 1km	8 below 2km	7 below 2km	5 below 1km
Initial & boundary conditions & meteorology	Meteorological driver	D-1 00:00 UTC IFS, 3hrly	D-1 12:00 UTC IFS, 3hrly	D-1 12:00 UTC IFS, 3hrly	D-1 12:00 UTC IFS for FC, IFS analysis for AN, 3hrly for FC, 6hrly for AN, downscaled with WRF	D-1 12:00 UTC IFS, 3hrly	D-1 00:00/12:00 UTC IFS, 3hrly	D-1 12:00 UTC IFS, 3hrly	D-1 12:00 UTC IFS, 1hrly	D-1 12:00 UTC IFS for FC, 1hrly (from +00h to +72h), 3hrly (from +72h to +96h); D00:00 UTC IFS for AN, 1hrly	D-1 12:00 UTC IFS, 6hrly, downscaled with NMMB	D-1 12:00 UTC IFS, 1hrly (from +00h to +72h), 3hrly (from +72h to +96h)



		CHIMERE	DEHM	EMEP	EURAD-IM	GEM-AQ	LOTOS-EUROS	MATCH	MINNI	MOCAGE	MONARCH	SILAM
	Boundary values	CAMS-Global IFS	CAMS-Global IFS	CAMS-Global IFS	CAMS-Global IFS	CAMS-Global IFS	CAMS-Global IFS	CAMS-Global IFS	CAMS-Global IFS	CAMS-Global IFS + MOCAGE global for additional species	CAMS-Global IFS	CAMS-Global IFS & SILAM
	Initial values	Previous forecast	Previous forecast	Previous analysis	Previous forecast	Previous forecast	Previous forecast	Previous forecast	Previous forecast	Previous forecast	Previous forecast	Previous forecast
Emissions anthropogenic	Inventory	CAMS-REG v6.1 REF2 2022	CAMS-REG v6.1 REF2 2022	CAMS-REG v6.1 REF2 2022	CAMS-REG v6.1 REF2 2022	CAMS-REG v6.1 REF2 2022	CAMS-REG v6.1 REF2 2022	CAMS-REG v6.1 REF2 2022	CAMS-REG v6.1 REF2 2022	CAMS-REG v6.1 REF2 2022	CAMS-REG v6.1 REF2 2022	CAMS-REG v6.1 REF2 2022
	Temporal disaggregation	TNO	CAMS-REG-TEMPO_v4.1	CAMS-REG-TEMPO_v4.1	CAMS-REG-TEMPO_v4.1	CAMS-REG-TEMPO_v4.1	CAMS-REG-TEMPO_v4.1	GENEMIS	CAMS-REG-TEMPO_v3.2	GENEMIS	CAMS-REG-TEMPO_v4.1	TNO
Emissions: natural & biogenic	in-domain soil and road dust emissions	(Marticorena and Bergametti, 1995)	none	(Marticorena and Bergametti, 1995; Marticorena et al., 1997; Dabdub and Seinfeld, 1994; Gomes et al., 2003; Fécan et al., 1998) Road dust emissions currently switched off.	Based on DREAM model	(Marticorena and Bergametti, 1995)	(Marticorena and Bergametti, 1995) and soil moisture inhibition as in (Fécan et al., 1998)	Road dust from (Schaap et al., 2009) and (Omstedt et al., 2005) and mineral dust based on the DEAD model of (Zender et al., 2003) (mainly attributed to the Mediterranean area).	Erosion and resuspension from (Vautard et al., 2005), soil suitable for mobilization parameterized following (Zender et al., 2003)	(Ginoux et al., 2001) and ECOCLIMAP database	Mineral dust scheme based on (Klose et al., 2021) and (Pérez et al., 2011)	SILAM dust source, SILAM sea salt source, Silam BIO-VOC source



		CHIMERE	DEHM	EMEP	EURAD-IM	GEM-AQ	LOTOS-EUROS	MATCH	MINNI	MOCAGE	MONARCH	SILAM
	in-domain sea-salt emissions	(Martensson et al., 2003) (Monahan, 1986)	(Martensson et al., 2003) (Monahan, 1986)	(Martensson et al., 2003) (Monahan, 1986; Tsyro et al., 2011)	(Sofiev et al., 2011)	(Gong et al., 2003)	(Martensson et al., 2003) {Monahan, 1986 #822	(Sofiev et al., 2011)	(Zhang et al., 2005)	(Sič et al., 2015)	(Jaeglé et al., 2011)	(Sofiev et al., 2011)
	Birch, Grass, Olive, Ragweed,	yes	yes	yes	yes	yes	yes	yes	yes	yes	yes	yes
	Biogenic emissions	MEGAN V2.10 (Guenther et al., 2012)	MEGAN v2.04 (Guenther et al., 2006)	(Simpson et al., 2012)	MEGAN V2.10 (Guenther et al., 2012)	MEGAN-MACC climatology	(Guenther et al., 1993) with detailed tree types for Europe	(Simpson et al., 2012)	MEGAN v2.04 (Guenther et al., 2006)	CAMS-GLOB-BIOv3.1 (Sinderalova et al., 2022) isoprene from MEGAN v2.04 (Guenther et al., 2006)	MEGAN v2.04 (Guenther et al., 2006)	Dynamic biogenic, (Poupkou et al., 2010)
	Soil NOx	MEGAN V2.10 (Guenther et al., 2012)	GEIA (Yienger and Levy, 1995)	CAMS-GLOB-SOIL	MEGAN V2.10 (Guenther et al., 2012)	none	(Yienger and Levy, 1995)	none	(Williams et al., 1992)	CAMS-GLOB-SOILv2.2 (Simpson et al., 2021)	MEGAN v2.04 (Guenther et al., 2006)	none
	Wildfires emissions	Hourly emissions from D-2 cycled for AN (D-1) and FC (D+0 and D+1, zero for the remaining days)	last available 24h cycle over D-2 and D-1 cycled for AN (D-1) and FC (D+0 and D+1, zero for the remaining days)	Hourly emissions from D-2 cycled for AN (D-1) and FC (D+0 and D+1, zero for the remaining days)	last available 24h cycle over D-2 and D-1 cycled for AN (D-1) and FC (D+0 and D+1, zero for the remaining days)	last available 24h cycle over D-2 and D-1 cycled for AN (D-1) and FC (D+0 and D+1, zero for the remaining days)	Hourly emissions from D-2 cycled for AN (D-1) and FC (D+0 and D+1, zero for the remaining days)	Hourly emissions from D-1 for AN (D-1) and last available 24h from D-2 and D-1 cycled for FC (D+0 to D+4)	Hourly emissions from D-1 for AN (D-1) and FC (D+0 and D+1, zero for the remaining days)	Hourly emissions from D-2 cycled for AN (D-1) and FC (D+0 and D+1, zero for the remaining days)	Hourly emissions from D-2 cycled for AN (D-1) and FC (D+0 and D+1, zero for the remaining days)	Hourly emissions from D-2 cycled for AN (D-1) and FC (D+0 and D+1, zero for the remaining days)



		CHIMERE	DEHM	EMEP	EURAD-IM	GEM-AQ	LOTOS-EUROS	MATCH	MINNI	MOCAGE	MONARCH	SILAM
Chemistry/Physics	Gas phase chemistry	MELCHIOR2 (Derognat et al., 2003), 44 gaseous species and 120 reactions	Modified (Strand and Hov, 1994), 74 species and 158 reactions	EmChem 19a, 127 species and 198 reactions (Simpson et al., 2020a)	RACM-MM (Geiger et al., 2003)	Modified ADOM IIB mechanism, 51 species and 120 reactions	Modified CBM-IV (Schaap et al., 2004)	EmChem 09 (Simpson et al., 2012) and (Langner et al., 1998)	SAPRC 99 (Carter, 2000)	RACM (tropospheric) and REPROBUS (stratospheric)	CB05 (Yarwood, G. et al., 2005)	CBM-IV
	Heterogeneous chemistry	Conversion of NO ₂ into HNO ₃ and N ₂ O ₅ and Conversion of HO ₂ into H ₂ O ₂	Oxidation of NO ₂ by O ₃ on aerosols	Aerosol-uptake of HNO ₃ , HO ₂ and O ₃	Hydrolysis of N ₂ O ₅	Hydrolysis of N ₂ O ₅	Hydrolysis of N ₂ O ₅	Hydrolysis of N ₂ O ₅ , aerosol uptake of HNO ₃ and CH ₃ O ₂ H	none	only relevant for polar stratospheric clouds	Hydrolysis of N ₂ O ₅ and aerosol uptake of HNO ₃ on dust and sea salt	Sofiev (2000)
	Aerosol size distribution	10 bins from 10 nm to 40 μm	2 size fractions: PM _{2.5} and coarse fraction of PM ₁₀	2 size fractions: PM _{2.5} and coarse fraction of PM ₁₀	3 log-normal modes: 2 fine + 1 coarse	12 bins from 10nm to 20.5μm	5 size bins for dust and sea-salt, 2 size bins for other aerosols	2 size fractions: PM _{2.5} and coarse fraction of PM ₁₀	3 log-normal model: Aitken, accumulation and coarse	6 bins	8 bins for dust and sea salt. Fine mode for BC, OM, SO ₄ and NH ₄ . Coarse and fine mode for NO ₃	2 bins, except for dust (4 bins from 10nm to 30μm) and sea salt (5 bins from 10nm to 30μm)
Inorganic aerosols	(Couvidat et al., 2018): Thermodynamic equilibrium for particles under 1 μm and a dynamic approach for particles above 1 μm. Thermodynamic for the H ⁺ -NH ₄ ⁺ -SO ₄ ²⁻ -NO ₃ ⁻ -Na ⁺ -Cl ⁻ -H ₂ O system is based on ISORROPIA 2.1.	(Frohn, 2004)	MARS (Binkowski and Shankar, 1995), thermodynamic equilibrium for the H ⁺ -NH ₄ ⁺ -SO ₄ ²⁻ -NO ₃ ⁻ -H ₂ O system (Friese and Ebel, 2010)		(Gong et al., 2003)	ISORROPIA-2 (Fountoukis and Nenes, 2007)	(Mozurkewich, 1993)	ISORROPIA v1.7 (Nenes et al., 1998)	ISORROPIA-2 (Guth et al., 2016)	EQSAM (Metzger et al., 2002)	(Sofiev, 2000)	



	CHIMERE	DEHM	EMEP	EURAD-IM	GEM-AQ	LOTOS-EUROS	MATCH	MINNI	MOCAGE	MONARCH	SILAM
Secondary organic aerosols	(Bessagnet et al., 2009)	VBS approach (NPAS scheme of (Bergström et al., 2012a))	VBS approach (NPAS scheme, (Bergström et al., 2012a; Simpson et al., 2012))	updated SORGAM module (Li et al., 2013)	(Jiang, 2003)	not included	VBS schemes for ASOA and BSOA (Bergström et al., 2012a) (Hodzic et al., 2016)	SORGAM (Schell et al., 2001b)	(Castro et al., 1999)	non-volatile scheme for anthropogenic, biogenic and pyrogenic precursors (Pai et al., 2020)	VBS
Aqueous phase chemistry	SO ₂ oxidation by O ₃ and H ₂ O ₂	SO ₂ oxidation by O ₃ and H ₂ O ₂ (Jonson et al., 2000)	SO ₂ oxidation by ozone and H ₂ O ₂ and metal ion-catalyzed O ₂	10 gas/aqueous phase equilibria, 5 irreversible S(IV) → S(VI) transformations	SO ₂ oxidation	SO ₂ oxidation	SO ₂ oxidation	SO ₂ oxidation (Seinfeld and Pandis, 1998)	SO ₂ oxidation	SO ₂ oxidation by ozone and H ₂ O ₂	SO ₂ oxidation, nitrate formation (Sofiev, 2000), heterogeneous nitrate formation on sea salt particles
Dry deposition: gases	resistance approach (Wesely, 1989)	resistance approach (Simpson et al., 2003; Emberson et al., 2000a)	resistance approach, including non-stomatal deposition of NH ₃	resistance approach (Zhang et al., 2003)	resistance approach	resistance approach (Erisman et al., 1994)	resistance approach (Simpson et al., 2012)	resistance approach (Wesely, 1989)	resistance approach (Michou et al., 2005)	resistance approach (Wesely, 1989)	resistance approach (Wesely, 1989)
Dry deposition: aerosols	gravitational settling	gravitational settling (Simpson et al., 2003; Emberson et al., 2000a)	(Simpson et al., 2012)	resistance approach (Petroff and Zhang, 2010)	gravitational settling	(Zhang et al., 2001)	resistance approach (Simpson et al., 2012)	gravitational settling (Binkowski and Shankar, 1995)	(Sič et al., 2015)	(Zhang et al., 2001; Pérez et al., 2011)	(Kouznetsov and Sofiev, 2012)



		CHIMERE	DEHM	EMEP	EURAD-IM	GEM-AQ	LOTOS-EUROS	MATCH	MINNI	MOCAGE	MONARCH	SILAM
	Wet deposition	In-cloud scavenging for all gas/aerosols is taken into account. Below cloud by rain and snow falls is taken into account for soluble gas (HNO ₃ , H ₂ O ₂) and particles	(Simpson et al., 2003)	In-cloud and sub-cloud scavenging ratios for gases; in-cloud scavenging ratios and sub-cloud scavenging efficiencies for aerosols.	CMAQ (Salameh et al., 2007)	Below cloud scavenging for soluble gas species and aerosols	(Banzhaf et al., 2012)	gases: species dependent in-cloud and sub-cloud scavenging ratios; particles: in-cloud scavenging ratio, sub-cloud scavenging (Berge, 1993) and (Simpson et al., 2012)	(Simpson et al., 2003)	Convective: (Marrone et al., 2000) Stratiform: (Giorgi and Chameides, 1986), (Slinn et al., 1978; Slinn, 1983)	(Foley et al., 2010; Pérez et al., 2011)	SILAM
Assimilation	Assimilation method	Kriging-based analysis	3D-Var	Intermittent 3d-var	Intermittent 3d-var	Optimal Interpolation	ENKF	Intermittent 3d-var	Optimal Interpolation	3D VAR	LETKF (Di Tomaso et al., 2017)	Intermittent 3d-var
	Assimilated surface pollutants	NO ₂ , O ₃ , PM _{2.5} , PM ₁₀ , CO, SO ₂	NO ₂ , O ₃ , CO, SO ₂ , PM _{2.5} , PM ₁₀	NO ₂ , O ₃ , SO ₂ , CO, PM _{2.5} , PM ₁₀	NO ₂ , O ₃ , CO, SO ₂ , PM _{2.5} , PM ₁₀	NO ₂ , O ₃ , PM _{2.5} , PM ₁₀ , CO, SO ₂	NO ₂ , O ₃ , PM _{2.5} , PM ₁₀	NO ₂ , O ₃ , CO, SO ₂ , PM _{2.5} , PM ₁₀	NO ₂ , O ₃ , CO, SO ₂ , PM _{2.5} , PM ₁₀	NO ₂ , O ₃ , PM _{2.5} , PM ₁₀	NO ₂ , O ₃ , CO, SO ₂ , PM _{2.5} , PM ₁₀	NO ₂ , O ₃ , CO, SO ₂ , PM _{2.5} , PM ₁₀
	assimilated satellite	none	none	NO ₂ (OMI) until 2021, currently disabled	currently none	none	NO ₂ (OMI) until 2021	none	none	ground-based lidars from French network, ceilometers from e-profile, SO ₂ Tropomi	none	none
	Frequency of assimilation	Hourly	Hourly	Hourly	Hourly	Hourly	Hourly	Hourly	Hourly	Hourly	Hourly	Hourly



1424
1425

Table 2: Overview of the matching between chemical species used as boundary conditions from the global IFS model and the eleven regional models of the CAMS Regional production

IFS	CHIMERE	DEHM	EMEP	EURAD	GEM-AQ	LOTOS EUROS	MATCH	MINNI	MOCAGE	MONARCH	SILAM
aermr01 (wet) (sea salt 0.03-0.5 μm radius)	sea salt bins 3 to 5	SS_25=aermr01/4.3+0.5*aermr02/4.3	SS_25=aermr01/4.3+0.5*aermr02/4.3	not used	not used	SS bins 1=aermr01/4.3 (where SS_25 = SS bin 1 and 2)	SS_25=aermr01/4.3+0.4*aermr02/4.3	SS bin [1-2.5μm] = aermr01/4.3+0.40*aermr02/4.3	SS bins 1-6 = aermr01/4.3	SS bin 1=0.34*aermr01/4.3 + SS bin 2=0.30*aermr01/4.3 + 0.02*aermr02/4.3	SS bin 0.5μm = aermr01/4.3
aermr02 (wet) (sea salt 0.5-5 μm radius)	sea salt bins 6 to 8	SS_co=0.5*aermr02/4.3	SS_co=0.5*aermr02/4.3	not used	not used	SS bins 2=0.1*aermr02/4.3 SS bins 3=0.2*aermr02/4.3 SS bins 4=0.4*aermr02/4.3 SS bins 5=0.3*aermr02/4.3	SS_co=0.6*aermr02/4.3	SS bin [2.5-10μm] = 0.60*aermr02/4.3	SS bins 1-6 = aermr02/4.3	SS bin 3=0.13*aermr02/4.3 SS bin 4=0.18*aermr02/4.3 SS bin 5=0.35*aermr02/4.3 SS bin 6=0.32*aermr02/4.3 + 0.06*aermr03/4.3	SS bin 3μm = aermr02/4.3
aermr03 (wet) (sea salt 5-20 μm radius)	sea salt bin 9	not used	not used	not used	not used	not used	not used	not used	SS bins 1-6 = aermr03/4.3	SS bin 7=0.40*aermr03/4.3 SS bin 8=0.54*aermr03/4.3	SS bin 9μm = 0.5*aermr02/4.3 SS bin 20μm = 0.5*aermr02/4.3
aermr04 (dust 0.03-0.55 μm radius)	dust bins 4 to 6	DUST_25=aermr04+aermr05	DUST_25=aermr04+aermr05	DUST_acc=0.05 total IFS dust, DUST_coa=0.95 total IFS dust	dust bins 3-7	dust bin 1 = 0.2*aermr04+0.2*aermr05 dust bin 2 = 0.8*aermr04+0.8*aermr05	dust_25=aermr04+aermr05+0.11*aermr06	dust bin [1-2.5μm] = aermr04+aermr05+aermr06*0.11	Dust bins 1-6	DUST bin 1 = 0.03 * aermr04 DUST bin 2 = 0.14 * aermr04	Dust 0.3μm = 0.4*aermr04 Dust 1.5μm = 0.6*aermr04



aermr05 (dust 0.55-0.9 μm radius)	dust bin 7	not used	DUST_25= aermr04+ aermr05	DUST_acc=0.05 total IFS dust, DUST_coa=0.95 total IFS dust	dust bins 8		dust_25= aermr04+ aermr05+ 0.11*aer mr06	used above in dust bin [1- 2.5um]	Dust bins 1-6	DUST bin 3 = 0.82 * aermr04 + 0.11 * aermr05	Dust 6μm = aermr05
aermr06 (dust 0.9- 20 μm radius)	dust bins 7 to 10	DUST_co = 0,4*aerm r06	DUST_co =0,4*aer mr06	DUST_acc=0.05 total IFS dust, DUST_coa=0.95 total IFS dust	dust bins 9-12	dust bin 3 = 0.08*aer mr06 dust bin 4 = 0.16*aer mr06 dust bin 5 = 0.16*aer mr06	dust_co= 0.44*aer mr06	dust bin [2.5- 10μm] = aermr06* 0,44	Dust bins 1-6	DUST bin 4 = 0.89 * aermr05 + 0.01 * aermr06 DUST bin 5 = 0.11 * aermr06 DUST bin 6 = 0.23 * aermr06 DUST bin 7 = 0.50 * aermr06 DUST bin 8 = 0.14 * aermr06	Dust 6μm = 0.4*aerm r06 Dust 20μm = 0.6*aerm r06
aermr07 hydrophil ic OM	PPM bins 3 to 6	not used	not used	80% accumula tion mode, 20% Aitken mode	OC bins 1-12	POM_25	EC_25=0 .7*aermr 07; EC_co=0 .15*aerm r07	AORPA bin 0- 1μm = 0,00050* aermr07+ 0,00050* aermr08 AORPA bin 1- 2.5μm = 0,44955* aermr07+ 0,44955* aermr08 AORA bin 0- 1μm = 0,00050* aermr07 + 0,00050* aermr08 AORA bin 1- 2.5μm = 0,49950* aermr07	OC bins 1-6	hydrophil ic POM	Non- volatile bin of organic aerosol



								+ 0,49950* aermr08			
aermr08 hydrophobic OM	PPM bins 3 to 6	not used	not used	80% accumulation mode, 20% Aitken mode	OC bins 1-12	POM_25	EC_25=0.7*aermr08; EC_co=0.15*aermr08	AORB bin 0-1µm = 0,00010*aermr07 + 0,00010*aermr08 AORB bin 1-2.5µm = 0,09990*aermr07 + 0,09990*aermr08	OC bins 1-6	hydrophobic POM	Non-volatile bin of organic aerosol
aermr09 hydrophilic BC	PPM bins 3 to 6	BCfresh	not used	70% accumulation mode, 30% Aitken mode	BC bins 1-12	EC_25	OC_25=0.7*aermr09 OC_co=0.15*aermr09	AEC bin 0-1µm = 0,0011*aermr09+0,001*aermr10	BC bins 1-6	hydrophilic BC	EC
aermr10 hydrophobic BC	PPM bins 3 to 6	BCaged	not used	70% accumulation mode, 30% Aitken mode	BC bins 1-12	EC_25	OC_25=0.7*aermr10 OC_co=0.15*aermr10	AEC bin 1-2.5µm = 0,999*aermr09+0,999*aermr10	BC bins 1-6	hydrophobic BC	EC
aermr11 Sulphate Aerosol	SO4 bins 3 to 6	SO4	SO4	90% accumulation mode, 10% Aitken mode	SO4 bins 1-12	SO4_25	SO4	SO4 bin 0-1µm = 0,001*aermr11 SO4 bin 1-2,5µm = 0,999*aermr11	MOCAG E-global	SO4	SO4 split equally on 2 modes
aermr16 Nitrate fine mode	not used	not used	NO3_F (0-2.5 µm)	90% accumulation mode, 10%	not used	NO3_25	NO3_f	NO3 bin 0-1µm = 0,001*aermr16 NO3 bin	MOCAG E-global	not used	not used



				Aitken mode								1-2,5µm = 0,999*ae rmr16 + 0,55*ae rmr17
aermr17 Nitrate coarse mode	not used	not used	NO3_C (2.5-10 µm)	not used	not used	NO3_co	NITRATE(coarse)	Corse unspecified =0.45*ae rmr17	MOCAG E-global	not used	not used	
aermr18 Ammonium	not used	not used	NH4_F (0-2.5 µm)	90% accumulation mode, 10% Aitken mode	not used	NH4_25	NH4_f	NH4 bin 0-1µm = 0,001*ae rmr18 NH4 bin 1-2,5µm = 0,999*ae rmr18	MOCAG E-global	not used	not used	
aerm19 Biogenic SOA	OM	OM	not used	not used	BSOA	not used	SOA	BSOA	BSOA	not used	BSOA	
aerm20 Anthropogenic SOA	OM	OM	not used	not used	ASOA	not used	SOA	ASOA	ASOA	not used	ASOA	
CHOCHO (Glyoxal)	CHOCHO	not used	CHOCHO	CHOCHO	CHOCHO	not used	CHOCHO	CHOCHO	CHOCHO	not used	CHOCHO	
C2H6 (ethane)	C2H6	C2H6	C2H6	C2H6	C2H6	not used	C2H6	ALK1	MOCAG E-global	C2H6	2xPAR5	
C5H8 (isoprene)	C5H8	C5H8	C5H8	C5H8	C5H8	C5H8	C5H8	C5H8	MOCAG E-global	C5H8	C5H8	
CH4_c (methane)	CH4	not used	CH4	not used	CH4	CH4	CH4	CH4	MOCAG E-global	not used	not used	



CO (carbon monoxide)	CO	CO	CO	CO	CO	CO	CO	CO	CO	CO	CO
GO3 (ozone)	O3	O3	O3	O3	O3	O3	O3	O3	O3	O3	O3
H2O2 (hydrogen peroxide)	not used	not used	not used	H2O2	H2O2	not used	seasonal climatological conc used	not used	MOCAG E-global	H2O2	not used
HCHO (formaldehyde)	HCHO	HCHO	HCHO	HCHO	HCHO	HCHO	HCHO	HCHO	MOCAG E-global	HCHO	HCHO
HNO3 (nitric acid)	HNO3	HNO3	HNO3	HNO3	HNO3	HNO3	HNO3	HNO3	MOCAG E-global	HNO3	HNO3
NO (nitrogen monoxide)	not used	NO	NO	NO	NO	NO	NO	NO	MOCAG E-global	NO	NO
NO2 (nitrogen dioxide)	NO2	NO2	NO2	NO2	NO2	NO2	NO2	NO2	MOCAG E-global	NO2	NO2
PAN (Peroxyacetyl nitrate)	PAN	PAN	PAN	PAN	PAN	PAN	PAN	PAN	MOCAG E-global	PAN	PAN
SO2 (Sulphur dioxide)	SO2	SO2	SO2	SO2	SO2	SO2	SO2	SO2	SO2	SO2	SO2

1426

1427



1428

1429 **References**

1430

1431 Aamaas, B., Peters, G. P., and Fuglestedt, J. S.: Simple emission metrics for climate impacts, *Earth Syst. Dynam.*, 4, 145-
1432 170, 2013.

1433 Ackermann, I. J., Hass, H., Memmesheimer, M., Ebel, A., Binkowski, F. S., and Shankar, U.: Modal aerosol dynamics
1434 model for Europe: development and first applications, *Atmospheric Environment*, 32, 2981-2999,
1435 [http://dx.doi.org/10.1016/S1352-2310\(98\)00006-5](http://dx.doi.org/10.1016/S1352-2310(98)00006-5), 1998.

1436 Adani, M. and Uboldi, F.: Data assimilation experiments over Europe with the Chemical Transport Model FARM,
1437 *Atmospheric Environment*, 306, 119806, 2023.

1438 Alfaro, S. C. and Gomes, L.: Modeling mineral aerosol production by wind erosion: Emission intensities and aerosol size
1439 distributions in source areas, *Journal of Geophysical Research: Atmospheres*, 106, 18075-18084, 2001.

1440 Andersson-Sköld, Y. and Simpson, D.: Comparison of the chemical schemes of the EMEP MSC-W and IVL photochemical
1441 trajectory models, *Atmospheric Environment*, 33, 1111-1129, 1999.

1442 Atkinson, R., Baulch, D. L., Cox, R. A., Crowley, J. N., Hampson, R. F., Hynes, R. G., Jenkin, M. E., Rossi, M. J., and Troe,
1443 J.: Evaluated kinetic and photochemical data for atmospheric chemistry: Volume I - gas phase reactions of Ox, HOx, NOx
1444 and SOx species, *Atmos. Chem. Phys.*, 4, 1461-1738, 10.5194/acp-4-1461-2004, 2004.

1445 Badia, A. and Jorba, O.: Gas-phase evaluation of the online NMMB/BSC-CTM model over Europe for 2010 in the
1446 framework of the AQMEII-Phase2 project, *Atmospheric Environment*, 115, 657-669, 2015.

1447 Badia, A., Jorba, O., Voulgarakis, A., Dabdub, D., Pérez García-Pando, C., Hilboll, A., Gonçalves, M., and Janjic, Z.:
1448 Description and evaluation of the Multiscale Online Nonhydrostatic Atmosphere Chemistry model (NMMB-MONARCH)
1449 version 1.0: gas-phase chemistry at global scale, *Geoscientific Model Development*, 10, 609-638, 2017.

1450 Baklanov, A. and Sørensen, J.: Parameterisation of radionuclide deposition in atmospheric long-range transport modelling,
1451 *Physics and Chemistry of the Earth, Part B: Hydrology, Oceans and Atmosphere*, 26, 787-799, 2001.

1452 Banzhaf, S., Schaap, M., Kerschbaumer, A., Reimer, E., Stern, R., van der Swaluw, E., and Bultjes, P. J. H.:
1453 Implementation and evaluation of pH-dependent cloud chemistry and wet deposition in the chemical transport model REM-
1454 Calgrid, *Atmos. Environ.*, 49, 2012.

1455 Barbu, A., Segers, A., Schaap, M., Heemink, A., and Bultjes, P.: A multi-component data assimilation experiment directed
1456 to sulphur dioxide and sulphate over Europe, *Atmospheric Environment*, 43, 1622-1631, 2009.

1457 Bechtold, P., Bazile, E., Guichard, F., Mascart, P., and Richard, E.: A mass-flux convection scheme for regional and global
1458 models, *Quarterly Journal of the Royal Meteorological Society*, 127, 869-886, 2001.



- 1459 Berge, E.: Coupling of wet scavenging of sulphur to clouds in a numerical weather prediction model, *Tellus B: Chemical and*
1460 *Physical Meteorology*, 45, 1-22, 1993.
- 1461 Bergström, R., Hayman, G. D., Jenkin, M. E., and Simpson, D.: Update and comparison of atmospheric chemistry
1462 mechanisms for the EMEP MSC-W model system — EmChem19a, EmChem19X, CRIv2R5Em, CB6r2Em, and
1463 MCMv3.3Em, The Norwegian Meteorological Institute, Oslo, Norway, 2022.
- 1464 Bergström, R., Denier Van Der Gon, H., Prévôt, A. S., Yttri, K. E., and Simpson, D.: Modelling of organic aerosols over
1465 Europe (2002–2007) using a volatility basis set (VBS) framework: application of different assumptions regarding the
1466 formation of secondary organic aerosol, *Atmospheric Chemistry and Physics*, 12, 8499-8527, 2012a.
- 1467 Bergström, R., Denier van der Gon, H. A. C., Prévôt, A. S. H., Yttri, K. E., and Simpson, D.: Modelling of organic aerosols
1468 over Europe (2002–2007) using a volatility basis set (VBS) framework: application of different assumptions regarding the
1469 formation of secondary organic aerosol, *Atmos. Chem. Phys.*, 12, 8499-8527, doi:10.5194/acp-12-8499-2012, 2012b.
- 1470 Bertrand, J. M., Meleux, F., Ung, A., Descombes, G., and Colette, A.: Technical note: Improving the European air quality
1471 forecast of Copernicus Atmosphere Monitoring Service using machine learning techniques, *Atmos. Chem. Phys. Discuss.*,
1472 2022, 1-28, 10.5194/acp-2022-767, 2022.
- 1473 Bessagnet, B., Brignon, J.-M., Le Gall, A.-C., Meleux, F., Schucht, S., and Rouïl, L.: Politiques combinées de gestion de la
1474 qualité de l'air et du changement climatique (partie 1): enjeux, synergies et antagonismes, INERIS, Verneuil en Halatte,
1475 2009.
- 1476 Bessagnet, B., Hodzic, A., Vautard, R., Beekmann, M., Cheinet, S., Honore, C., Liousse, C., and Rouil, L.: Aerosol
1477 modeling with CHIMERE - preliminary evaluation at the continental scale, *Atmospheric Environment*, 38, 2803-2817,
1478 10.1016/j.atmosenv.2004.02.034, 2004.
- 1479 Bessagnet, B., Menut, L., Colette, A., Couvidat, F., Dan, M., Mailler, S., Létinois, L., Pont, V., and Rouil, L.: An Evaluation
1480 of the CHIMERE Chemistry Transport Model to Simulate Dust Outbreaks across the Northern Hemisphere in March 2014,
1481 *Atmosphere*, 8, 251, 2017.
- 1482 Bessagnet, B., Menut, L., Curci, G., Hodzic, A., Guillaume, B., Liousse, C., Moukhtar, S., Pun, B., Seigneur, C., and Schulz,
1483 M.: Regional modeling of carbonaceous aerosols over Europe—focus on secondary organic aerosols, *Journal of*
1484 *Atmospheric Chemistry*, 61, 175-202, 2008.
- 1485 Binkowski, F. and Shankar, U.: The Regional Particulate Matter Model .1. Model description and preliminary results, *J.*
1486 *Geophys. Res.*, 100, 26191–26209, 1995.
- 1487 Binkowski, F. S.: The aerosol portion of Models-3 CMAQ. In *Science Algorithms of the EPA Models-3 Community*
1488 *Multiscale Air Quality (CMAQ) Modeling System. Part II: Chapters 9-18*, National Exposure Research Laboratory, U.S.
1489 Environmental Protection Agency, Research Triangle Park, NC, 1999.
- 1490 Bott, A.: A Positive Definite Advection Scheme Obtained by Nonlinear Renormalization of the Advective Fluxes, *Mon.*
1491 *Wea. Rev.*, 117, 1006-1015, 1989.
- 1492 Brandt, J., Silver, J. D., Frohn, L. M., Geels, C., Gross, A., Hansen, A. B., Hansen, K. M., Hedegaard, G. B., Skjoth, C. A.,
1493 Villadsen, H., Zare, A., and Christensen, J. H.: An integrated model study for Europe and North America using the Danish



- 1494 Eulerian Hemispheric Model with focus on intercontinental transport of air pollution, *Atmospheric Environment*, 53, 156-
1495 176, 2012.
- 1496 Brasseur, G. P., Xie, Y., Petersen, A. K., Bouarar, I., Flemming, J., Gauss, M., Jiang, F., Kouznetsov, R., Kranenburg, R.,
1497 and Mijling, B.: Ensemble forecasts of air quality in eastern China—Part 1: Model description and implementation of the
1498 MarcoPolo—Panda prediction system, version 1, *Geoscientific Model Development*, 12, 33-67, 2019.
- 1499 Burridge, D.: THE METEOROLOGICAL OFFICE OPERATIONAL 10-LEVEL NUMERICAL WEATHER
1500 PREDICTION MODEL (DECEMBER 1975), 1977.
- 1501 Carslaw, K. S., Luo, B., and Peter, T.: An analytic expression for the composition of aqueous HNO₃-H₂SO₄ stratospheric
1502 aerosols including gas phase removal of HNO₃, *Geophysical Research Letters*, 22, 1877-1880, 1995.
- 1503 Carson, D.: The development of a dry inversion-capped convectively unstable boundary layer, *Quarterly Journal of the*
1504 *Royal Meteorological Society*, 99, 450-467, 1973.
- 1505 Carter, W. P. L.: Condensed atmospheric photooxidation mechanisms for isoprene, *Atmospheric Environment*, 30, 4275-
1506 4290, [http://dx.doi.org/10.1016/1352-2310\(96\)00088-X](http://dx.doi.org/10.1016/1352-2310(96)00088-X), 1996.
- 1507 Carter, W. P. L.: Documentation of the SAPRC-99 Chemical Mechanism for VOC Reactivity Assessment, 2000.
- 1508 Castro, L., Pio, C., Harrison, R. M., and Smith, D.: Carbonaceous aerosol in urban and rural European atmospheres:
1509 estimation of secondary organic carbon concentrations, *Atmospheric Environment*, 33, 2771-2781, 1999.
- 1510 Chang, T.: Rain and snow scavenging of HNO₃ vapor in the atmosphere, *Atmospheric Environment* (1967), 18, 191-197,
1511 1984.
- 1512 Christensen, J., Brandt, J., Frohn, L., and Skov, H.: Modelling of mercury in the Arctic with the Danish Eulerian
1513 Hemispheric Model, *Atmospheric Chemistry and Physics*, 4, 2251-2257, 2004.
- 1514 Christensen, J. H.: The Danish Eulerian hemispheric model—A three-dimensional air pollution model used for the Arctic,
1515 *Atmospheric Environment*, 31, 4169-4191, 1997.
- 1516 Colella, P. and Woodward, P. R.: The piecewise parabolic method (PPM) for gas-dynamical simulations, *Journal of*
1517 *computational physics*, 54, 174-201, 1984.
- 1518 Colette, A., Bessagnet, B., Meleux, F., Terrenoire, E., and Rouïl, L.: Frontiers in air quality modelling, *Geosci. Model Dev.*,
1519 7, 203-210, 2014.
- 1520 Colette, A., Bessagnet, B., Vautard, R., Szopa, S., Rao, S., Schucht, S., Klimont, Z., Menut, L., Clain, G., Meleux, F., Curci,
1521 G., and Rouïl, L.: European atmosphere in 2050, a regional air quality and climate perspective under CMIP5 scenarios,
1522 *Atmos. Chem. Phys.*, 13, 7451-7471, 2013.
- 1523 Colette, A., Andersson, C., Baklanov, A., Bessagnet, B., Brandt, J., Christensen, J. H., Doherty, R., Engardt, M., Geels, C.,
1524 Giannakopoulos, C., Hedegaard, G. H., Katragkou, E., Langner, J., Lei, H., Manders, A., Melas, D., Meleux, F., Rouïl, L.,
1525 Sofiev, M., Soares, J., Stevenson, D. S., Tombrou-Tzella, M., Varotsos, K. V., and Young, P.: Is the ozone climate penalty
1526 robust in Europe?, *Environmental Research Letters*, 10, 084015, 2015.



- 1527 Colette, A., Andersson, C., Manders, A., Mar, K., Mircea, M., Pay, M. T., Raffort, V., Tsyro, S., Cuvelier, C., Adani, M.,
1528 Bessagnet, B., Bergström, R., Briganti, G., Butler, T., Cappelletti, A., Couvidat, F., D'Isidoro, M., Doumbia, T., Fagerli, H.,
1529 Granier, C., Heyes, C., Klimont, Z., Ojha, N., Otero, N., Schaap, M., Sindelarova, K., Stegehuis, A. I., Roustan, Y., Vautard,
1530 R., van Meijgaard, E., Vivanco, M. G., and Wind, P.: EURODELTA-Trends, a multi-model experiment of air quality
1531 hindcast in Europe over 1990–2010, *Geosci. Model Dev.*, 10, 3255–3276, 10.5194/gmd-10-3255-2017, 2017.
- 1532 Côté, J., Gravel, S., Méthot, A., Patoine, A., Roch, M., and Staniforth, A.: The operational CMC–MRB global environmental
1533 multiscale (GEM) model. Part I: Design considerations and formulation, *Monthly Weather Review*, 126, 1373–1395, 1998a.
- 1534 Côté, J., Desmarais, J.-G., Gravel, S., Méthot, A., Patoine, A., Roch, M., and Staniforth, A.: The operational CMC–MRB
1535 global environmental multiscale (GEM) model. Part II: Results, *Monthly Weather Review*, 126, 1397–1418, 1998b.
- 1536 Couvidat, F., Bessagnet, B., Garcia-Vivanco, M., Real, E., Menut, L., and Colette, A.: Development of an inorganic and
1537 organic aerosol model (CHIMERE 2017 β v1.0): seasonal and spatial evaluation over Europe, *Geosci. Model Dev.*, 11, 165–
1538 194, 10.5194/gmd-11-165-2018, 2018.
- 1539 Curier, R., Timmermans, R., Calabretta-Jongen, S., Eskes, H., Segers, A., Swart, D., and Schaap, M.: Improving ozone
1540 forecasts over Europe by synergistic use of the LOTOS-EUROS chemical transport model and in-situ measurements,
1541 *Atmospheric environment*, 60, 217–226, 2012.
- 1542 D'Elia, I., Briganti, G., Vitali, L., Piersanti, A., Righini, G., D'Isidoro, M., Cappelletti, A., Mircea, M., Adani, M., and
1543 Zanini, G.: Measured and modelled air quality trends in Italy over the period 2003–2010, *Atmospheric Chemistry and
1544 Physics*, 21, 10825–10849, 2021.
- 1545 Dabdub, D. and Seinfeld, J. H.: Numerical advective schemes used in air quality models—sequential and parallel
1546 implementation, *Atmospheric Environment*, 28, 3369–3385, 1994.
- 1547 Damski, J., Thölix, L., Backman, L., Taalas, P., and Kulmala, M.: FinRose--middle atmospheric chemistry transport model,
1548 *Boreal environment research*, 12, 2007.
- 1549 Denier van der Gon, H. A. C., Bergström, R., Fountoukis, C., Johansson, C., Pandis, S. N., Simpson, D., and Visschedijk, A.
1550 J. H.: Particulate emissions from residential wood combustion in Europe – revised estimates and an evaluation, *Atmos.
1551 Chem. Phys.*, 15, 6503–6519, 10.5194/acp-15-6503-2015, 2015.
- 1552 Derognat, C., Beekmann, M., Baeumle, M., Martin, D., and Schmidt, H.: Effect of biogenic volatile organic compound
1553 emissions on tropospheric chemistry during the Atmospheric Pollution Over the Paris Area (ESQUIF) campaign in the Ile-
1554 de-France region, *Journal of Geophysical Research: Atmospheres*, 108, 2003.
- 1555 Di Tomaso, E., Schutgens, N. A. J., Jorba, O., and Pérez García-Pando, C.: Assimilation of MODIS Dark Target and Deep
1556 Blue observations in the dust aerosol component of NMMB-MONARCH version 1.0, *Geoscientific Model Development*, 10,
1557 1107–1129, 2017.
- 1558 Di Tomaso, E., Escribano, J., Basart, S., Ginoux, P., Macchia, F., Barnaba, F., Benincasa, F., Bretonnière, P. A., Buñuel, A.,
1559 Castrillo, M., Cuevas, E., Formenti, P., Gonçalves, M., Jorba, O., Klose, M., Mona, L., Montané Pinto, G., Mytilinaios, M.,
1560 Obiso, V., Olid, M., Schutgens, N., Votsis, A., Werner, E., and Pérez García-Pando, C.: The MONARCH high-resolution
1561 reanalysis of desert dust aerosol over Northern Africa, the Middle East and Europe (2007–2016), *Earth Syst. Sci. Data*, 14,
1562 2785–2816, 10.5194/essd-14-2785-2022, 2022.



- 1563 Douros, J., Eskes, H., van Geffen, J., Boersma, K. F., Compernelle, S., Pinardi, G., Blechschmidt, A. M., Peuch, V. H.,
1564 Colette, A., and Veeffkind, P.: Comparing Sentinel-5P TROPOMI NO₂ column observations with the CAMS-regional air
1565 quality ensemble, EGU sphere, 2022, 1-40, 10.5194/egusphere-2022-365, 2022.
- 1566 Ebel, A., Friedrich, R., and Rodhe, H.: GENEMIS: Assessment, improvement, and temporal and spatial disaggregation of
1567 European emission data, in: Tropospheric modelling and emission estimation, Springer, 181-214, 1997.
- 1568 EC: Directive 2008/50/EC of the European Parliament and of the Council of 21 May 2008 on ambient air quality and cleaner
1569 air for Europe, European Commission, Brussels, 2008.
- 1570 ECMWF: IFS Documentation CY47R3 - Part IV Physical processes, Reading, doi: 10.21957/eyrpir4vj, 2021.
- 1571 Elbern, H., Strunk, A., Schmidt, H., and Talagrand, O.: Emission rate and chemical state estimation by 4-dimensional
1572 variational inversion, Atmospheric Chemistry and Physics, 7, 3749-3769, 2007.
- 1573 Emberson, L., Ashmore, M., Cambridge, H., Simpson, D., and Tuovinen, J.-P.: Modelling stomatal ozone flux across
1574 Europe, Environmental Pollution, 109, 403-413, 2000a.
- 1575 Emberson, L. D., Ashmore, M. R., Simpson, D., Tuovinen, J.-P., and Cambridge, H. M.: Towards a model of ozone
1576 deposition and stomatal uptake over Europe, Norwegian Meteorological Institute, Oslo, Norway, 57, 2000b.
- 1577 EMEP: Transboundary particulate matter, photo-oxydants, acidifying and eutrophying components, EMEP, Oslo, Norway,
1578 2023.
- 1579 Erismann, J. W., Van Pul, A., and Wyers, P.: Parametrization of surface resistance for the quantification of atmospheric
1580 deposition of acidifying pollutants and ozone, Atmospheric Environment, 28, 2595-2607, [http://dx.doi.org/10.1016/1352-2310\(94\)90433-2](http://dx.doi.org/10.1016/1352-2310(94)90433-2), 1994.
1581
- 1582 Escribano, J., Di Tomaso, E., Jorba, O., Klose, M., Gonçalves Ageitos, M., Macchia, F., Amiridis, V., Baars, H., Marinou,
1583 E., Proestakis, E., Urbanneck, C., Althausen, D., Bühl, J., Mamouri, R. E., and Pérez García-Pando, C.: Assimilating
1584 spaceborne lidar dust extinction can improve dust forecasts, Atmos. Chem. Phys., 22, 535-560, 10.5194/acp-22-535-2022,
1585 2022.
- 1586 Fécan, F., Marticorena, B., and Bergametti, G.: Parametrization of the increase of the aeolian erosion threshold wind friction
1587 velocity due to soil moisture for arid and semi-arid areas, Annales Geophysicae, 149-157,
- 1588 Flemming, J., Huijnen, V., Arteta, J., Bechtold, P., Beljaars, A., Blechschmidt, A. M., Diamantakis, M., Engelen, R. J.,
1589 Gaudel, A., Inness, A., Jones, L., Josse, B., Katragkou, E., Marecal, V., Peuch, V. H., Richter, A., Schultz, M. G., Stein, O.,
1590 and Tsikerdekis, A.: Tropospheric chemistry in the Integrated Forecasting System of ECMWF, Geosci. Model Dev., 8, 975-
1591 1003, 10.5194/gmd-8-975-2015, 2015.
- 1592 Foley, K., Roselle, S., Appel, K., Bhave, P., Pleim, J., Otte, T., Mathur, R., Sarwar, G., Young, J., and Gilliam, R.:
1593 Incremental testing of the Community Multiscale Air Quality (CMAQ) modeling system version 4.7, Geoscientific Model
1594 Development, 3, 205-226, 2010.
- 1595 Forester, C.: Higher order monotonic convective difference schemes, Journal of Computational Physics, 23, 1-22, 1977.



- 1596 Fountoukis, C. and Nenes, A.: ISORROPIA II: a computationally efficient thermodynamic equilibrium model for K⁺–
1597 Ca²⁺–Mg²⁺–NH₄⁺–Na⁺–SO₄²⁻–NO₃⁻–Cl⁻–H₂O aerosols, *Atmos. Chem. Phys.*, 7, 4639-4659, doi:10.5194/acp-7-4639-
1598 2007, 2007.
- 1599 Friese, E. and Ebel, A.: Temperature dependent thermodynamic model of the system H⁺– NH₄⁺– Na⁺– SO₄²⁻– NO₃⁻–
1600 Cl⁻– H₂O, *The Journal of Physical Chemistry A*, 114, 11595-11631, 2010.
- 1601 Frohn, L.: A study of long-term high-resolution air pollution modelling, Ministry of the Environment, National
1602 Environmental Research Institute, Roskilde, Denmark, 2004.
- 1603 Galmarini, S., Kioutsioukis, I., and Solazzo, E.: E pluribus unum*: ensemble air quality predictions, *Atmos. Chem. Phys.*,
1604 13, 7153-7182, 10.5194/acp-13-7153-2013, 2013.
- 1605 Galmarini, S., Bianconi, R., Addis, R., Andronopoulos, S., Astrup, P., Bartzis, J., Bellasio, R., Buckley, R., Champion, H.,
1606 and Chino, M.: Ensemble dispersion forecasting—Part II: Application and evaluation, *Atmospheric Environment*, 38, 4619-
1607 4632, 2004.
- 1608 Galmarini, S., Koffi, B., Solazzo, E., Keating, T., Hogrefe, C., Schulz, M., Benedictow, A., Griesfeller, J. J., Janssens-
1609 Maenhout, G., Carmichael, G., Fu, J., and Dentener, F.: Technical note: Coordination and harmonization of the multi-scale,
1610 multi-model activities HTAP2, AQMEII3, and MICS-Asia3: simulations, emission inventories, boundary conditions, and
1611 model output formats, *Atmos. Chem. Phys.*, 17, 1543-1555, 10.5194/acp-17-1543-2017, 2017.
- 1612 Galperin, M. and Sofiev, M.: Errors in the validation of models for long-range transport and critical loads stipulated by
1613 stochastic properties of pollution fields., *EMEP Chemical Coordinating Centre, Lillestrom, Passau*, 162–179, 1994.
- 1614 Geels, C., Winther, M., Andersson, C., Jalkanen, J.-P., Brandt, J., Frohn, L. M., Im, U., Leung, W., and Christensen, J. H.:
1615 Projections of shipping emissions and the related impact on air pollution and human health in the Nordic region,
1616 *Atmospheric Chemistry and Physics*, 21, 12495-12519, 2021.
- 1617 Geiger, H., Barnes, I., Bejan, I., Benter, T., and Spittler, M.: The tropospheric degradation of isoprene: an updated module
1618 for the regional atmospheric chemistry mechanism, *Atmospheric Environment*, 37, 1503-1519, 2003.
- 1619 Gery, M. W., Whitten, G. Z., Killus, J. P., and Dodge, M. C.: A photochemical kinetics mechanism for urban and regional
1620 scale computer modeling, *Journal of Geophysical Research: Atmospheres*, 94, 12925-12956, 1989.
- 1621 Ginoux, P., Chin, M., Tegen, I., Prospero, J. M., Holben, B., Dubovik, O., and Lin, S. J.: Sources and distributions of dust
1622 aerosols simulated with the GOCART model, *Journal of Geophysical Research: Atmospheres*, 106, 20255-20273, 2001.
- 1623 Giorgi, F. and Chameides, W. L.: Rainout lifetimes of highly soluble aerosols and gases as inferred from simulations with a
1624 general circulation model, *Journal of Geophysical Research: Atmospheres*, 91, 14367-14376, 1986.
- 1625 Gomes, L., Rajot, J., Alfaro, S., and Gaudichet, A.: Validation of a dust production model from measurements performed in
1626 semi-arid agricultural areas of Spain and Niger, *Catena*, 52, 257-271, 2003.
- 1627 Gong, S., Barrie, L., Blanchet, J. P., Von Salzen, K., Lohmann, U., Lesins, G., Spacek, L., Zhang, L., Girard, E., and Lin, H.:
1628 Canadian Aerosol Module: A size-segregated simulation of atmospheric aerosol processes for climate and air quality models
1629 1. Module development, *Journal of Geophysical Research: Atmospheres*, 108, AAC 3-1-AAC 3-16, 2003.



- 1630 Granier, C., Darras, S., van der Gon, H. D., Doubalova, J., Elguindi, N., Galle, B., Gauss, M., Guevara, M., Jalkanen, J. P.,
1631 and Kuenen, J.: The Copernicus Atmosphere Monitoring Service global and regional emissions (April 2019 version),
1632 Copernicus Atmosphere Monitoring Service, 10.24380/d0bn-kx16, 2019.
- 1633 Groisman, P. Y. and Genikhovich, E. L.: Assessing surface–atmosphere interactions using former Soviet Union standard
1634 meteorological network data. Part I: Method, *Journal of climate*, 10, 2154–2183, 1997.
- 1635 Guenther, A., Zimmerman, P., Harley, P., Monson, R., and Fall, R.: Isoprene and monoterpene rate variability: model
1636 evaluations and sensitivity analyses, *J. Geophys. Res.*, 98, 12609–12617, 1993.
- 1637 Guenther, A., Karl, T., Harley, P., Wiedinmyer, C., Palmer, P. I., and Geron, C.: Estimates of global terrestrial isoprene
1638 emissions using MEGAN (Model of Emissions of Gases and Aerosols from Nature), *Atmos. Chem. Phys.*, 6, 3181–3210,
1639 2006.
- 1640 Guenther, A., Jiang, X., Heald, C. L., Sakulyanontvittaya, T., Duhl, T. a., Emmons, L., and Wang, X.: The Model of
1641 Emissions of Gases and Aerosols from Nature version 2.1 (MEGAN2. 1): an extended and updated framework for modeling
1642 biogenic emissions, *Geoscientific Model Development*, 5, 1471–1492, 2012.
- 1643 Guevara, M., Tena, C., Porquet, M., Jorba, O., and Pérez García-Pando, C.: HERMESv3, a stand-alone multi-scale
1644 atmospheric emission modelling framework–Part 1: global and regional module, *Geoscientific Model Development*, 12,
1645 1885–1907, 2019.
- 1646 Guevara, M., Jorba, O., Tena, C., Denier van der Gon, H., Kuenen, J., Elguindi, N., Darras, S., Granier, C., and Pérez
1647 García-Pando, C.: Copernicus Atmosphere Monitoring Service TEMPoral profiles (CAMs-TEMPO): global and European
1648 emission temporal profile maps for atmospheric chemistry modelling, *Earth Syst. Sci. Data*, 13, 367–404, 10.5194/essd-13-
1649 367-2021, 2021.
- 1650 Guth, J., Josse, B., Marécal, V., Joly, M., and Hamer, P.: First implementation of secondary inorganic aerosols in the
1651 MOCAGE version 2.15.0 chemistry transport model, *Geosci. Model Dev.*, 9, 137–160, 10.5194/gmd-9-137-2016, 2016.
- 1652 Hamer, P., Fjaeraa, A.-M., Soares, J., Meleux, F., Colette, A., Ung, A., Raux, B., and Tarrason, L.: Copernicus Atmosphere
1653 Monitoring Service Interim Annual Assessment Report on European Air Quality in 2022, ECMWF, Bonn,
1654 [https://policy.atmosphere.copernicus.eu/reports/CAMS271_2021SCx_D1.1.1_202306_2022_Interim_Assessment_Report_v](https://policy.atmosphere.copernicus.eu/reports/CAMS271_2021SCx_D1.1.1_202306_2022_Interim_Assessment_Report_v1.pdf)
1655 [1.pdf](https://policy.atmosphere.copernicus.eu/reports/CAMS271_2021SCx_D1.1.1_202306_2022_Interim_Assessment_Report_v1.pdf), 2023.
- 1656 Hansen, K. M., Christensen, J. H., Brandt, J., Frohn, L. M., Geels, C., Skjøth, C. A., and Li, Y. F.: Modeling short-term
1657 variability of α -hexachlorocyclohexane in Northern Hemispheric air, *Journal of Geophysical Research: Atmospheres*, 113,
1658 2008.
- 1659 Hass, H., Jakobs, H., and Memmesheimer, M.: Analysis of a regional model (EURAD) near surface gas concentration
1660 predictions using observations from networks, *Meteorology and Atmospheric Physics*, 57, 173–200, 1995.
- 1661 Heidam, N. Z., Christensen, J., Wählin, P., and Skov, H.: Arctic atmospheric contaminants in NE Greenland: levels,
1662 variations, origins, transport, transformations and trends 1990–2001, *Science of the Total Environment*, 331, 5–28, 2004.
- 1663 Heimann, M. and Keeling, C. D.: A three-dimensional model of atmospheric CO₂ transport based on observed winds: 2.
1664 Model description and simulated tracer experiments, Max-Planck-Institut für Meteorologie 1989.



- 1665 Hendriks, C., Forsell, N., Kiesewetter, G., Schaap, M., and Schöpp, W.: Ozone concentrations and damage for realistic
1666 future European climate and air quality scenarios, *Atmospheric Environment*, 144, 208-219, 2016.
- 1667 Hertel, O., Christensen, J., Runge, E. H., Asman, W. A., Berkowicz, R., Hovmand, M. F., and Hov, Ø.: Development and
1668 testing of a new variable scale air pollution model—ACDEP, *Atmospheric Environment*, 29, 1267-1290, 1995.
- 1669 Hervig, M. E., Russell III, J. M., Gordley, L. L., Park, J. H., and Drayson, S. R.: Observations of aerosol by the HALOE
1670 experiment onboard UARS: A preliminary validation, *Geophysical research letters*, 20, 1291-1294, 1993.
- 1671 Hicks, B., Baldocchi, D., Meyers, T., Hosker, R., and Matt, D.: A preliminary multiple resistance routine for deriving dry
1672 deposition velocities from measured quantities, *Water, Air, and Soil Pollution*, 36, 311-330, 1987.
- 1673 Hodzic, A., Kasibhatla, P. S., Jo, D. S., Cappa, C. D., Jimenez, J. L., Madronich, S., and Park, R. J.: Rethinking the global
1674 secondary organic aerosol (SOA) budget: stronger production, faster removal, shorter lifetime, *Atmospheric Chemistry and
1675 Physics*, 16, 7917-7941, 2016.
- 1676 Hollingsworth, A.: Toward a monitoring and forecasting system for atmospheric composition: The GEMS Project, *Bull.
1677 Amer. Meteor. Soc.*, 89, 1147-1164, <https://doi.org/10.1175/2008BAMS2355.1>, 2008.
- 1678 Hollingsworth, A. and Lönnberg, P.: The statistical structure of short-range forecast errors as determined from radiosonde
1679 data. Part I: The wind field, *Tellus A*, 38, 111-136, 1986.
- 1680 Holtslag, A., Van Meijgaard, E., and De Rooy, W.: A comparison of boundary layer diffusion schemes in unstable
1681 conditions over land, *Boundary-Layer Meteorology*, 76, 69-95, 1995.
- 1682 Holtslag, A. A. and Nieuwstadt, F. T.: Scaling the atmospheric boundary layer, *Boundary-Layer Meteorology*, 36, 201-209,
1683 1986.
- 1684 Horálek, J., Schreiberová, M., Vlasáková, L., Hamer, P., Schneider, P., and Marková, J.: Interim European air quality maps
1685 for 2020. PM₁₀, NO₂ and ozone spatial estimates based on non-validated UTD data., NILU, Oslo,
1686 [https://www.eionet.europa.eu/etcs/etc-atni/products/etc-atni-report-19-2021-interim-european-air-quality-maps-for-2020-
1687 pm10-no2-and-ozone-spatial-estimates-based-on-non-validated-utd-data](https://www.eionet.europa.eu/etcs/etc-atni/products/etc-atni-report-19-2021-interim-european-air-quality-maps-for-2020-pm10-no2-and-ozone-spatial-estimates-based-on-non-validated-utd-data), 2022.
- 1688 Huang, G., Brook, R., Crippa, M., Janssens-Maenhout, G., Schieberle, C., Dore, C., Guizzardi, D., Muntean, M., Schaaf, E.,
1689 and Friedrich, R.: Speciation of anthropogenic emissions of non-methane volatile organic compounds: a global gridded data
1690 set for 1970–2012, *Atmospheric Chemistry and Physics*, 17, 7683-7701, 2017.
- 1691 Huijnen, V., Eskes, H., Poupkou, A., Elbern, H., Boersma, K., Foret, G., Sofiev, M., Valdebenito, A., Flemming, J., and
1692 Stein, O.: Comparison of OMI NO₂ tropospheric columns with an ensemble of global and European regional air quality
1693 models, *Atmospheric Chemistry and Physics*, 10, 3273-3296, 2010.
- 1694 Hunt, B. R., Kostelich, E. J., and Szunyogh, I.: Efficient data assimilation for spatiotemporal chaos: A local ensemble
1695 transform Kalman filter, *Physica D: Nonlinear Phenomena*, 230, 112-126, <https://doi.org/10.1016/j.physd.2006.11.008>,
1696 2007.
- 1697 Jaeglé, L., Quinn, P. K., Bates, T. S., Alexander, B., and Lin, J.-T.: Global distribution of sea salt aerosols: new constraints
1698 from in situ and remote sensing observations, *Atmospheric Chemistry and Physics*, 11, 3137, 2011.



- 1699 Janjic, Z. and Gall, L.: Scientific documentation of the NCEP nonhydrostatic multiscale model on the B grid (NMMB). Part
1700 1 Dynamics, NCAR/TN-489+STR, 2012.
- 1701 Jöckel, P., Tost, H., Pozzer, A., Brühl, C., Buchholz, J., Ganzeveld, L., Hoor, P., Kerkweg, A., Lawrence, M., and Sander,
1702 R.: The atmospheric chemistry general circulation model ECHAM5/MESSy1: consistent simulation of ozone from the
1703 surface to the mesosphere, *Atmospheric Chemistry and Physics*, 6, 5067-5104, 2006.
- 1704 Joly, M. and Peuch, V.-H.: Objective classification of air quality monitoring sites over Europe, *Atmospheric Environment*,
1705 47, 111-123, 2012.
- 1706 Jorba, O., Dabdub, D., Blaszcak-Boxe, C., Pérez, C., Janjic, Z., Baldasano, J., Spada, M., Badia, A., and Gonçalves, M.:
1707 Potential significance of photoexcited NO₂ on global air quality with the NMMB/BSC chemical transport model, *Journal of*
1708 *Geophysical Research: Atmospheres*, 117, 2012.
- 1709 Kahnert, M.: Variational data analysis of aerosol species in a regional CTM: background error covariance constraint and
1710 aerosol optical observation operators, *Tellus B: Chemical and Physical Meteorology*, 60, 753-770, 2008.
- 1711 Kain, J. S. and Fritsch, J. M.: A one-dimensional entraining/detraining plume model and its application in convective
1712 parameterization, *Journal of Atmospheric Sciences*, 47, 2784-2802, 1990.
- 1713 Kaiser, J., Heil, A., Andreae, M., Benedetti, A., Chubarova, N., Jones, L., Morcrette, J.-J., Razinger, M., Schultz, M., and
1714 Suttie, M.: Biomass burning emissions estimated with a global fire assimilation system based on observed fire radiative
1715 power, *Biogeosciences*, 9, 527-554, 2012.
- 1716 Kawka, M., Struzewska, J., and Kaminski, J. W.: Spatial and Temporal Variation of NO₂ Vertical Column Densities
1717 (VCDs) over Poland: Comparison of the Sentinel-5P TROPOMI Observations and the GEM-AQ Model Simulations,
1718 *Atmosphere*, 12, 896, 2021.
- 1719 Klose, M., Jorba, O., Gonçalves Ageitos, M., Escribano, J., Dawson, M. L., Obiso, V., Di Tomaso, E., Basart, S., Montané
1720 Pinto, G., and Macchia, F.: Mineral dust cycle in the Multiscale Online Nonhydrostatic Atmosphere Chemistry model
1721 (MONARCH) version 2.0, *Geoscientific Model Development*, 14, 6403-6444, 2021.
- 1722 Köble, R. and Seufert, G.: Novel maps for forest tree species in Europe, *Proceedings of the 8th European symposium on the*
1723 *physico-chemical behaviour of air pollutants: “a changing atmosphere*, 17-20,
- 1724 Korhonen, H., Carslaw, K. S., Spracklen, D. V., Mann, G. W., and Woodhouse, M. T.: Influence of oceanic dimethyl sulfide
1725 emissions on cloud condensation nuclei concentrations and seasonality over the remote Southern Hemisphere oceans: A
1726 global model study, *Journal of Geophysical Research: Atmospheres*, 113, 2008.
- 1727 Kouznetsov, R. and Sofiev, M.: A methodology for evaluation of vertical dispersion and dry deposition of atmospheric
1728 aerosols, *Journal of Geophysical Research: Atmospheres*, 117, 2012.
- 1729 Kouznetsov, R., Sofiev, M., Vira, J., and Stiller, G.: Simulating age of air and the distribution of SF₆ in the stratosphere
1730 with the SILAM model, *Atmospheric Chemistry and Physics*, 20, 5837-5859, 2020.
- 1731 Kuenen, J., Visschedijk, A., Jozwicka, M., and Denier Van Der Gon, H.: TNO-MACC_II emission inventory; a multi-year
1732 (2003–2009) consistent high-resolution European emission inventory for air quality modelling, *Atmospheric Chemistry and*
1733 *Physics*, 14, 10963-10976, 2014.



- 1734 Kuenen, J., Dellaert, S., Visschedijk, A., Jalkanen, J.-P., Super, I., and Denier van der Gon, H.: CAMS-REG-v4: a state-of-
1735 the-art high-resolution European emission inventory for air quality modelling, *Earth System Science Data*, 14, 491-515,
1736 2022.
- 1737 Kukkonen, J., Savolahti, M., Palamarchuk, Y., Lanki, T., Nurmi, V., Paunu, V.-V., Kangas, L., Sofiev, M., Karppinen, A.,
1738 and Maragkidou, A.: Modelling of the public health costs of fine particulate matter and results for Finland in 2015,
1739 *Atmospheric Chemistry and Physics*, 20, 9371-9391, 2020.
- 1740 Kylling, A., Stamnes, K., and Tsay, S.-C.: A reliable and efficient two-stream algorithm for spherical radiative transfer:
1741 Documentation of accuracy in realistic layered media, *Journal of Atmospheric Chemistry*, 21, 115-150, 1995.
- 1742 Lahoz, W., Geer, A., Bekki, S., Bormann, N., Ceccherini, S., Elbern, H., Errera, Q., Eskes, H., Fonteyn, D., and Jackson, D.:
1743 The Assimilation of Envisat data (ASSET) project, *Atmospheric Chemistry and Physics*, 7, 1773-1796, 2007.
- 1744 Lambert, J. D.: *Numerical methods for ordinary differential systems*, Wiley New York 1991.
- 1745 Lana, A., Bell, T., Simó, R., Vallina, S., Ballabrera-Poy, J., Kettle, A., Dachs, J., Bopp, L., Saltzman, E., and Stefels, J.: An
1746 updated climatology of surface dimethylsulfide concentrations and emission fluxes in the global ocean, *Global*
1747 *Biogeochemical Cycles*, 25, 2011.
- 1748 Landgraf, J. and Crutzen, P.: An efficient method for online calculations of photolysis and heating rates, *Journal of the*
1749 *atmospheric sciences*, 55, 863-878, 1998.
- 1750 Lange, R.: Transferability of a three-dimensional air quality model between two different sites in complex terrain, *Journal of*
1751 *Applied Meteorology and Climatology*, 28, 665-679, 1989.
- 1752 Langner, J., Bergström, R., and Pleijel, K.: European scale modeling of sulphur, oxidized nitrogen and photochemical
1753 oxidants. Model development and evaluation for the 1994 growing season, *Swedish Met. and Hydrol. Inst., Norrköping,*
1754 *Sweden*, 1998.
- 1755 Lansø, A. S., Smallman, T. L., Christensen, J. H., Williams, M., Pilegaard, K., Sørensen, L.-L., and Geels, C.: Simulating the
1756 atmospheric CO₂ concentration across the heterogeneous landscape of Denmark using a coupled atmosphere–biosphere
1757 mesoscale model system, *Biogeosciences*, 16, 1505-1524, 2019.
- 1758 Lefevre, F., Brasseur, G., Folkins, I., Smith, A., and Simon, P.: Chemistry of the 1991–1992 stratospheric winter: Three-
1759 dimensional model simulations, *Journal of Geophysical Research: Atmospheres*, 99, 8183-8195, 1994.
- 1760 Lehtomäki, H., Korhonen, A., Asikainen, A., Karvosenoja, N., Kupiainen, K., Paunu, V.-V., Savolahti, M., Sofiev, M.,
1761 Palamarchuk, Y., and Karppinen, A.: Health impacts of ambient air pollution in Finland, *International journal of*
1762 *environmental research and public health*, 15, 736, 2018.
- 1763 Li, Y., Elbern, H., Lu, K., Friese, E., Kiendler-Scharr, A., Mentel, T. F., Wang, X., Wahner, A., and Zhang, Y.: Updated
1764 aerosol module and its application to simulate secondary organic aerosols during IMPACT campaign May 2008,
1765 *Atmospheric chemistry and physics*, 13, 6289-6304, 2013.
- 1766 Liu, D. C. and Nocedal, J.: On the limited memory BFGS method for large scale optimization, *Mathematical programming*,
1767 45, 503-528, 1989.



- 1768 Louis, J.-F.: A parametric model of vertical eddy fluxes in the atmosphere, *Boundary-Layer Meteorology*, 17, 187-202,
1769 1979.
- 1770 Lurmann, F. W., Lloyd, A. C., and Atkinson, R.: A chemical mechanism for use in long-range transport/acid deposition
1771 computer modeling, *Journal of Geophysical Research: Atmospheres*, 91, 10905-10936, 1986.
- 1772 Maas, R. and Grennfelt, P.: Towards Cleaner Air - Scientific Assessment Report 2016, EMEP-Steering body and Working
1773 Group on Effects - Convention on Long-Range Transboundary Air Pollution 2016.
- 1774 Madronich, S.: Photodissociation in the atmosphere: 1. Actinic flux and the effects of ground reflections and clouds, *Journal*
1775 *of Geophysical Research: Atmospheres*, 92, 9740-9752, 1987.
- 1776 Madronich, S. and Weller, G.: Numerical integration errors in calculated tropospheric photodissociation rate coefficients,
1777 *Journal of atmospheric chemistry*, 10, 289-300, 1990.
- 1778 Manders, A. M. M., Bultjes, P. J. H., Curier, L., Denier van der Gon, H. A. C., Hendriks, C., Jonkers, S., Kranenburg, R.,
1779 Kuenen, J., Segers, A. J., Timmermans, R. M. A., Visschedijk, A., Wichink Kruit, R. J., Van Pul, W. A. J., Sauter, F. J., van
1780 der Swaluw, E., Swart, D. P. J., Douros, J., Eskes, H., van Meijgaard, E., van Ulft, B., van Velthoven, P., Banzhaf, S., Mues,
1781 A., Stern, R., Fu, G., Lu, S., Heemink, A., van Velzen, N., and Schaap, M.: Curriculum Vitae of the LOTOS-EUROS (v2.0)
1782 chemistry transport model, *Geosci. Model Dev. Discuss.*, 2017, 1-53, 10.5194/gmd-2017-88, 2017.
- 1783 Marécal, V., Peuch, V. H., Andersson, C., Andersson, S., Arteta, J., Beekmann, M., Benedictow, A., Bergstrom, R.,
1784 Bessagnet, B., Cansado, A., Chéroux, F., Colette, A., Coman, A., Curier, R. L., Denier van der Gon, H. A. C., Drouin, A.,
1785 Elbern, H., Emili, E., Engelen, R. J., Eskes, H. J., Foret, G., Friese, E., Gauss, M., Giannaros, C., Guth, J., Joly, M.,
1786 Jaumouilla, E., Josse, B., Kadyrov, N., Kaiser, J. W., Krajsek, K., Kuenen, J., Kumar, U., Liora, N., Lopez, E., Malherbe,
1787 L., Martinez, I., Melas, D., Meleux, F., Menut, L., Moinat, P., Morales, T., Parmentier, J., Piacentini, A., Plu, M., Poupkou,
1788 A., Queguiner, S., Robertson, L., Rouil, L., Schaap, M., Segers, A., Sofiev, M., Tarasson, L., Thomas, M., Timmermans, R.,
1789 Valdebenito, A., van Velthoven, P., van Versendaal, R., Vira, J., and Ung, A.: A regional air quality forecasting system over
1790 Europe: the MACC-II daily ensemble production, *Geosci. Model Dev.*, 8, 2777-2813, 2015.
- 1791 Mari, C., Jacob, D. J., and Bechtold, P.: Transport and scavenging of soluble gases in a deep convective cloud, *Journal of*
1792 *Geophysical Research: Atmospheres*, 105, 22255-22267, 2000.
- 1793 Martensson, E., Nilsson, E., de Leeuw, G., Cohen, L., and Hansson, H.-C.: Laboratory simulations and parameterisation of
1794 the primary marine aerosol production, *J. Geophys. Res.*, 108, 4297, doi:10.1029/2002JD002263, 2003.
- 1795 Martet, M., Peuch, V., Laurent, B., Marticorena, B., and Bergametti, G.: Evaluation of long-range transport and deposition
1796 of desert dust with the CTM MOCAGE, *Tellus B: Chemical and Physical Meteorology*, 61, 449-463, 2009.
- 1797 Marticorena, B. and Bergametti, G.: Modeling the atmospheric dust cycle: 1. Design of a soil-derived dust emission scheme,
1798 *Journal of geophysical research: atmospheres*, 100, 16415-16430, 1995.
- 1799 Marticorena, B., Bergametti, G., Aumont, B., Callot, Y., N'Doumé, C., and Legrand, M.: Modeling the atmospheric dust
1800 cycle: 2. Simulation of Saharan dust sources, *Journal of Geophysical Research: Atmospheres*, 102, 4387-4404, 1997.
- 1801 Maul, P., Barber, F., and Martin, A.: Some observations of the meso-scale transport of sulphur compounds in the rural East
1802 Midlands, *Atmospheric Environment (1967)*, 14, 339-354, 1980.



- 1803 McRae, G. J., Goodin, W. R., and Seinfeld, J. H.: Numerical solution of the atmospheric diffusion equation for chemically
1804 reacting flows, *Journal of Computational Physics*, 45, 1-42, 1982.
- 1805 Meleux, F., Solmon, F., and Giorgi, F.: Increase in summer European ozone amounts due to climate change, *Atmospheric*
1806 *Environment*, 41, 7577-7587, 2007.
- 1807 Memmesheimer, M., Friese, E., Ebel, A., Jakobs, H., Feldmann, H., Kessler, C., and Piekorz, G.: Long-term simulations of
1808 particulate matter in Europe on different scales using sequential nesting of a regional model, *International Journal of*
1809 *Environment and Pollution*, 22, 108-132, 2004.
- 1810 Ménégoz, M., Salas y Melia, D., Legrand, M., Teyssède, H., Michou, M., Peuch, V.-H., Martet, M., Josse, B., and
1811 Dombrowski-Etchevers, I.: Equilibrium of sinks and sources of sulphate over Europe: comparison between a six-year
1812 simulation and EMEP observations, *Atmospheric Chemistry and Physics*, 9, 4505-4519, 2009.
- 1813 Menut, L., Bessagnet, B., Briant, R., Cholakian, A., Couvidat, F., Mailler, S., Pennel, R., Siour, G., Tuccella, P., and
1814 Turquety, S.: The CHIMERE v2020r1 online chemistry-transport model, *Geoscientific Model Development*, 14, 6781-6811,
1815 2021.
- 1816 Metzger, S., Dentener, F., Pandis, S., and Lelieveld, J.: Gas/aerosol partitioning: 1. A computationally efficient model, *J.*
1817 *Geophys. Res.*, 107, 4312, 2002.
- 1818 Michou, M., Laville, P., Serça, D., Fotiadi, A., Bouchou, P., and Peuch, V.-H.: Measured and modeled dry deposition
1819 velocities over the ESCOMPTE area, *Atmospheric Research*, 74, 89-116, 2005.
- 1820 Mircea, M., Ciancarella, L., Briganti, G., Calori, G., Cappelletti, A., Cionni, I., Costa, M., Cremona, G., D'Isidoro, M.,
1821 Finardi, S., Pace, G., Piersanti, A., Righini, G., Silibello, C., Vitali, L., and Zanini, G.: Assessment of the AMS-MINNI
1822 system capabilities to simulate air quality over Italy for the calendar year 2005, *Atmospheric Environment*, 48, 178-188,
1823 <https://doi.org/10.1016/j.atmosenv.2013.11.006>, 2014.
- 1824 Miyoshi, T. and Yamane, S.: Local Ensemble Transform Kalman Filtering with an AGCM at a T159/L48 Resolution,
1825 *Monthly Weather Review*, 135, 3841-3861, [10.1175/2007MWR1873.1](https://doi.org/10.1175/2007MWR1873.1), 2007.
- 1826 Monahan, E. C.: The ocean as a source of atmospheric particles, in: *The Role of Air-Sea Exchange in Geochemical Cycling*,
1827 Kluwer Academic Publishers, Dordrecht, Holland, 129-163, 1986.
- 1828 Morcrette, J. J., Boucher, O., Jones, L., Salmond, D., Bechtold, P., Beljaars, A., Benedetti, A., Bonet, A., Kaiser, J., and
1829 Razinger, M.: Aerosol analysis and forecast in the European Centre for medium-range weather forecasts integrated forecast
1830 system: Forward modeling, *Journal of Geophysical Research: Atmospheres*, 114, 2009.
- 1831 Mozurkewich, M.: The dissociation constant of ammonium nitrate and its dependence on temperature, relative humidity and
1832 particle size, *Atmospheric Environment. Part A. General Topics*, 27, 261-270, [http://dx.doi.org/10.1016/0960-](http://dx.doi.org/10.1016/0960-1686(93)90356-4)
1833 [1686\(93\)90356-4](http://dx.doi.org/10.1016/0960-1686(93)90356-4), 1993.
- 1834 Nenes, A., Pandis, S., and Pilinis, C.: ISORROPIA: A New Thermodynamic Equilibrium Model for Multiphase
1835 Multicomponent Inorganic Aerosols, *Aquatic Geochemistry*, 4, 123-152, 1998.
- 1836 Nho-Kim, E.-Y., Michou, M., and Peuch, V.-H.: Parameterization of size-dependent particle dry deposition velocities for
1837 global modeling, *Atmospheric Environment*, 38, 1933-1942, 2004.



- 1838 Nho-Kim, E., Peuch, V., and Oh, S.: Estimation of the global distribution of Black Carbon aerosols with MOCAGE, the
1839 CTM of Météo-France, *J. Korean Meteor. Soc.*, 41, 587-598, 2005.
- 1840 Nieradzik, L.: Application of a high dimensional model representation on the atmospheric aerosol module MADE of the
1841 EURAD-CTM, Institut für Geophysik und Meteorologie der Universität zu Köln, 2005.
- 1842 Nieuwstadt, F.: The steady-state height and resistance laws of the nocturnal boundary layer: Theory compared with Cabauw
1843 observations, *Boundary-Layer Meteorology*, 20, 3-17, 1981.
- 1844 Nocedal, J.: Updating quasi-Newton matrices with limited storage, *Mathematics of computation*, 35, 773-782, 1980.
- 1845 Noilhan, J. and Planton, S.: A simple parameterization of land surface processes for meteorological models, *Monthly
1846 weather review*, 117, 536-549, 1989.
- 1847 Omstedt, G., Bringfelt, B., and Johansson, C.: A model for vehicle-induced non-tailpipe emissions of particles along
1848 Swedish roads, *Atmospheric environment*, 39, 6088-6097, 2005.
- 1849 Pai, S. J., Heald, C. L., Pierce, J. R., Farina, S. C., Marais, E. A., Jimenez, J. L., Campuzano-Jost, P., Nault, B. A.,
1850 Middlebrook, A. M., Coe, H., Shilling, J. E., Bahreini, R., Dingle, J. H., and Vu, K.: An evaluation of global organic aerosol
1851 schemes using airborne observations, *Atmos. Chem. Phys.*, 20, 2637-2665, 10.5194/acp-20-2637-2020, 2020.
- 1852 Parrish, D. F. and Derber, J. C.: The National Meteorological Center's spectral statistical-interpolation analysis system,
1853 *Monthly Weather Review*, 120, 1747-1763, 1992.
- 1854 Passant, N.: Speciation of UK emissions of non-methane volatile organic compounds, AEA Technology2002.
- 1855 Pepper, D., Kern, C., and Long Jr, P.: Modeling the dispersion of atmospheric pollution using cubic splines and chapeau
1856 functions, *Atmospheric Environment (1967)*, 13, 223-237, 1979.
- 1857 Pérez, C., Hausteijn, K., Jorba, O., Janjic, Z., Huneeus, N., Baldasano, J. M., Black, T., Basart, S., Nickovic, S., Miller, R. L.,
1858 Perlwitz, J., Schulz, M., and Thomson, M.: Atmospheric dust modeling from meso to global scales with the online
1859 NMMB/BSC-Dust model—Part 1: Model description, annual simulations and evaluation, *Atmospheric Chemistry and
1860 Physics*, 11, 13001-13027, 2011.
- 1861 Petersen, A. K., Brasseur, G. P., Bouarar, I., Flemming, J., Gauss, M., Jiang, F., Kouznetsov, R., Kranenburg, R., Mijling,
1862 B., and Peuch, V.-H.: Ensemble forecasts of air quality in eastern China—Part 2: Evaluation of the MarcoPolo—Panda
1863 prediction system, version 1, *Geoscientific Model Development*, 12, 1241-1266, 2019.
- 1864 Peterson, J. T.: Calculated actinic fluxes (290-700 nm) for air pollution photochemistry applications, US Environmental
1865 Protection Agency, Office of Research and Development ... 1976.
- 1866 Petroff, A. and Zhang, L.: Development and validation of a size-resolved particle dry deposition scheme for application in
1867 aerosol transport models, *Geoscientific Model Development*, 3, 753-769, 2010.
- 1868 Peuch, V.-H., Engelen, R., Rixen, M., Dee, D., Flemming, J., Suttie, M., Ades, M., Agustí-Panareda, A., Ananasso, C.,
1869 Andersson, E., Armstrong, D., Barré, J., Bousseres, N., Dominguez, J. J., Garrigues, S., Inness, A., Jones, L., Kipling, Z.,
1870 Letertre-Danczak, J., Parrington, M., Razinger, M., Ribas, R., Vermoote, S., Yang, X., Simmons, A., Garcés de Marcilla, J.,



- 1871 and Thépaut, J.-N.: The Copernicus Atmosphere Monitoring Service: From Research to Operations, *Bulletin of the*
1872 *American Meteorological Society*, 103, E2650-E2668, <https://doi.org/10.1175/BAMS-D-21-0314.1>, 2022.
- 1873 Peuch, V., Engelen, R., Simmons, A., Lahoz, W., Laj, P., and Galmarini, S.: Monitoring atmospheric composition and
1874 climate, research in support of the Copernicus/GMES atmospheric service, *Special Issue, Atmos. Chem. Phys.*, [http://www.](http://www.atmos-chem-phys.net/special_issue310.html)
1875 [atmos-chem-phys.net/special_issue310.html](http://www.atmos-chem-phys.net/special_issue310.html), 2014.
- 1876 Poupkou, A., Giannaros, T., Markakis, K., Kioutsioukis, I., Curci, G., Melas, D., and Zerefos, C.: A model for European
1877 Biogenic Volatile Organic Compound emissions: Software development and first validation, *Environmental Modelling &*
1878 *Software*, 25, 1845-1856, 2010.
- 1879 Prank, M., Chapman, D. S., Bullock, J. M., Belmonte, J., Berger, U., Dahl, A., Jäger, S., Kovtunen, I., Magyar, D., and
1880 Niemelä, S.: An operational model for forecasting ragweed pollen release and dispersion in Europe, *Agricultural and forest*
1881 *meteorology*, 182, 43-53, 2013.
- 1882 Rabitz, H. and Aliş, Ö. F.: General foundations of high-dimensional model representations, *Journal of Mathematical*
1883 *Chemistry*, 25, 197-233, 1999.
- 1884 Rappenglück, B., Lubertino, G., Alvarez, S., Golovko, J., Czader, B., and Ackermann, L.: Radical precursors and related
1885 species from traffic as observed and modeled at an urban highway junction, *Journal of the Air & Waste Management*
1886 *Association*, 63, 1270-1286, 2013.
- 1887 Rémy, S., Kipling, Z., Flemming, J., Boucher, O., Nabat, P., Michou, M., Bozzo, A., Ades, M., Huijnen, V., Benedetti, A.,
1888 Engelen, R., Peuch, V. H., and Morcrette, J. J.: Description and evaluation of the tropospheric aerosol scheme in the
1889 European Centre for Medium-Range Weather Forecasts (ECMWF) Integrated Forecasting System (IFS-AER, cycle 45R1),
1890 *Geosci. Model Dev.*, 12, 4627-4659, [10.5194/gmd-12-4627-2019](https://doi.org/10.5194/gmd-12-4627-2019), 2019.
- 1891 Robertson, L., Langner, J., and Engardt, M.: An Eulerian limited-area atmospheric transport model, *Journal of Applied*
1892 *Meteorology and Climatology*, 38, 190-210, 1999.
- 1893 Robichaud, A. and Ménard, R.: Multi-year objective analyses of warm season ground-level ozone and PM 2.5 over North
1894 America using real-time observations and Canadian operational air quality models, *Atmospheric Chemistry and Physics*, 14,
1895 1769-1800, 2014.
- 1896 Roselle, S. J. and Binkowski, F. S.: Cloud dynamics and chemistry, *Science algorithms of the EPA Models-3 Community*
1897 *multiscale air quality (CMAQ) modeling system*, 1999.
- 1898 Rouil, L., Honore, C., Vautard, R., Beekmann, M., Bessagnet, B., Malherbe, L., Meleux, F., Dufour, A., Elichegaray, C.,
1899 Flaud, J. M., Menut, L., Martin, D., Peuch, A., Peuch, V. H., and Poisson, N.: PREV'AIR An Operational Forecasting and
1900 Mapping System for Air Quality in Europe, *Bulletin of the American Meteorological Society*, 90, 73-83,
1901 [10.1175/2008bams2390.1](https://doi.org/10.1175/2008bams2390.1), 2009.
- 1902 Salameh, T., Drobinski, P., Menut, L., Bessagnet, B., Flamant, C., Hodzic, A., and Vautard, R.: Aerosol distribution over the
1903 western Mediterranean basin during a Tramontane/Mistral event, *Annales Geophysicae*, 25, 2271-2291, 2007.
- 1904 Sander, S., Golden, D., Kurylo, M., Moortgat, G., Wine, P., Ravishankara, A., Kolb, C., Molina, M., Finlayson-Pitts, B., and
1905 Huie, R.: Chemical kinetics and photochemical data for use in atmospheric studies evaluation number 15, Pasadena, CA: Jet
1906 Propulsion Laboratory, National Aeronautics and Space ..., 2006.



- 1907 Sandu, A. and Sander, R.: Simulating chemical systems in Fortran90 and Matlab with the Kinetic PreProcessor KPP-2.1,
1908 Atmospheric Chemistry and Physics, 6, 187-195, 2006.
- 1909 Sarwar, G., Simon, H., Bhawe, P., and Yarwood, G.: Examining the impact of heterogeneous nitryl chloride production on
1910 air quality across the United States, Atmospheric Chemistry and Physics, 12, 6455-6473, 2012.
- 1911 Schaap, M., Van Loon, M., Ten Brink, H., Dentener, F., and Builtjes, P.: Secondary inorganic aerosol simulations for Europe
1912 with special attention to nitrate, Atmospheric Chemistry and Physics, 4, 857-874, 2004.
- 1913 Schaap, M., Kranenburg, R., Curier, L., Jozwicka, M., Dammers, E., and Timmermans, R.: Assessing the sensitivity of the
1914 OMI-NO₂ product to emission changes across Europe, Remote Sensing, 5, 4187-4208, 2013.
- 1915 Schaap, M., Manders, A. M. M., Hendriks, E. C. J., Cnossen, J. M., Segers, A. J. S., Denier van der Gon, H., Jozwicka, M.,
1916 Sauter, F. J., Velders, G. J. M., Matthijssen, J., and Builtjes, P. J. H.: Regional Modelling of Particulate Matter for the
1917 Netherlands Netherlands Research Program on Particulate Matter, ISSN: 1875-2314, 2009.
- 1918 Schell, B., Ackermann, I. J., Hass, H., Binkowski, F. S., and Ebel, A.: Modeling the formation of secondary organic aerosol
1919 within a comprehensive air quality model system, Journal of Geophysical Research: Atmospheres, 106, 28275-28293,
1920 2001a.
- 1921 Schell, B., Ackermann, I. J., Hass, H., Binkowski, F. S., and Ebel, A.: Modelling the formation of secondary organic within a
1922 comprehensive air quality model system, J. Geophys. Res., 106, 28275-28293, 2001b.
- 1923 Schutgens, N. A. J., Miyoshi, T., Takemura, T., and Nakajima, T.: Applying an ensemble Kalman filter to the assimilation of
1924 AERONET observations in a global aerosol transport model, Atmos. Chem. Phys., 10, 2561-2576, 10.5194/acp-10-2561-
1925 2010, 2010.
- 1926 Seinfeld, J. H. and Pandis, S. N.: Atmospheric Chemistry and Physics, From Air Pollution to Climate Change., New York,
1927 USA.1998.
- 1928 Shaddick, G., Salter, J. M., Peuch, V.-H., Ruggeri, G., Thomas, M. L., Mudu, P., Tarasova, O., Baklanov, A., and Gumy, S.:
1929 Global air quality: An inter-disciplinary approach to exposure assessment for burden of disease analyses, Atmosphere, 12,
1930 48, 2020.
- 1931 Shrivastava, M. K., Lane, T. E., Donahue, N. M., Pandis, S. N., and Robinson, A. L.: Effects of gas particle partitioning and
1932 aging of primary emissions on urban and regional organic aerosol concentrations, Journal of Geophysical Research:
1933 Atmospheres, 113, 2008.
- 1934 Sič, B., El Amraoui, L., Marécal, V., Josse, B., Arteta, J., Guth, J., Joly, M., and Hamer, P.: Modelling of primary aerosols in
1935 the chemical transport model MOCAGE: Development and evaluation of aerosol physical parameterizations, Geoscientific
1936 Model Development, 8, 381-408, 2015.
- 1937 Silibello, C., Calori, G., Brusasca, G., Giudici, A., Angelino, E., Fossati, G., Peroni, E., and Buganza, E.: Modelling of
1938 PM₁₀ concentrations over Milano urban area using two aerosol modules, Environmental Modelling & Software, 23, 333-
1939 343, 2008.



- 1940 Silver, J. D., Christensen, J. H., Kahnert, M., Robertson, L., Rayner, P. J., and Brandt, J.: Multi-species chemical data
1941 assimilation with the Danish Eulerian hemispheric model: system description and verification, *Journal of Atmospheric*
1942 *Chemistry*, 73, 261-302, 2016.
- 1943 Simpson, D., Guenther, A., Hewitt, C., and Steinbrecher, R.: Biogenic emissions in Europe 1. Estimates and uncertainties, *J.*
1944 *Geophys. Res.*, 100, 22875–22890, 1995.
- 1945 Simpson, D., Fagerli, H., Jonson, J., Tsyro, S., Wind, P., and Tuovinen, J.-P.: The EMEP Unified Eulerian Model. Model
1946 Description, The Norwegian Meteorological Institute, EMEP, Oslo, 2003.
- 1947 Simpson, D., Bergström, R., Briolat, A., Imhof, H., Johansson, J., Priestley, M., and Valdebenito, A.: GenChem v1. 0—a
1948 chemical pre-processing and testing system for atmospheric modelling, *Geoscientific Model Development*, 13, 6447-6465,
1949 2020a.
- 1950 Simpson, D., Benedictow, A., Berge, H., Bergstrom, R., Emberson, L. D., Fagerli, H., Flechard, C. R., Hayman, G. D.,
1951 Gauss, M., Jonson, J. E., Jenkin, M. E., Nyiri, A., Richter, C., Semeena, V. S., Tsyro, S., Tuovinen, J. P., Valdebenito, A.,
1952 and Wind, P.: The EMEP MSC-W chemical transport model - technical description, *Atmos. Chem. Phys.*, 12, 7825-7865,
1953 2012.
- 1954 Simpson, D., Fagerli, H., Colette, A., Denier van der Gon, H., Dore, C., Hallquist, M., Hansson, H.-C., Maas, R., Rouil, L.,
1955 Allemand, N., Bergström, B., Bessagnet, B., Couvidat, F., El Haddad, I., Genberg Safont, J., Goile, F., Grieshop, A.,
1956 Fraboulet, I., Hallquist, A., Hamilton, J., Juhlich, K., Klimont, Z., Kregar, Z., Mawdsely, I., Megaritis, A., Ntziachristos, L.,
1957 Pandis, S., Prévôt, A. S. H., Schindlbacher, S., Seljeskog, M., Sirina-Leboine, N., Sommers, J., and Åström, S.: How should
1958 condensables be included in PM emission inventories reported to EMEP/CLRTAP?, EMEP, Oslo, 2020b.
- 1959 Slinn, W., Hasse, L., Hicks, B., Hogan, A., Lal, D., Liss, P., Munnich, K., Sehmel, G., and Vittori, O.: Some aspects of the
1960 transfer of atmospheric trace constituents past the air-sea interface, *Atmospheric Environment (1967)*, 12, 2055-2087, 1978.
- 1961 Slinn, W. G. N.: Precipitation scavenging, US. Department of Energy, Washington, D.C., 1983.
- 1962 Smagorinsky, J.: General circulation experiments with the primitive equations: I. The basic experiment, *Monthly weather*
1963 *review*, 91, 99-164, 1963.
- 1964 Soares, J., Sofiev, M., Geels, C., Christensen, J. H., Andersson, C., Tsyro, S., and Langner, J.: Impact of climate change on
1965 the production and transport of sea salt aerosol on European seas, *Atmospheric Chemistry and Physics*, 16, 13081-13104,
1966 2016.
- 1967 Sofiev, M.: A model for the evaluation of long-term airborne pollution transport at regional and continental scales,
1968 *Atmospheric Environment*, 34, 2481-2493, 2000.
- 1969 Sofiev, M.: Extended resistance analogy for construction of the vertical diffusion scheme for dispersion models, *Journal of*
1970 *Geophysical Research: Atmospheres*, 107, ACH 10-11-ACH 10-18, 2002.
- 1971 Sofiev, M.: On possibilities of assimilation of near-real-time pollen data by atmospheric composition models, *Aerobiologia*,
1972 35, 523-531, 2019.
- 1973 Sofiev, M., Galperin, M., and Genikhovich, E.: Construction and evaluation of Eulerian dynamic core for the air quality and
1974 emergency modelling system SILAM



- 1975 NATO Science for peace and security, Series C: Environmental Security, Air pollution modelling and its application, XIX,
1976 Springer, 699-701 pp.2008.
- 1977 Sofiev, M., Genikhovich, E., Keronen, P., and Vesala, T.: Diagnosing the surface layer parameters for dispersion models
1978 within the meteorological-to-dispersion modeling interface, *Journal of applied meteorology and climatology*, 49, 221-233,
1979 2010.
- 1980 Sofiev, M., Soares, J., Prank, M., de Leeuw, G., and Kukkonen, J.: A regional-to-global model of emission and transport of
1981 sea salt particles in the atmosphere, *J. Geophys. Res.*, 116, doi:10.1029/2010JD014713, 2011.
- 1982 Sofiev, M., Vira, J., Kouznetsov, R., Prank, M., Soares, J., and Genikhovich, E.: Construction of an Eulerian atmospheric
1983 dispersion model based on the advection algorithm of M. Galperin: dynamic cores v. 4 and 5 of SILAM v. 5.5, *Geoscientific
1984 Model Development Discussions*, 8, 2015a.
- 1985 Sofiev, M., Siljamo, P., Ranta, H., Linkosalo, T., Jaeger, S., Rasmussen, A., Rantio-Lehtimäki, A., Severova, E., and
1986 Kukkonen, J.: A numerical model of birch pollen emission and dispersion in the atmosphere. Description of the emission
1987 module, *International journal of biometeorology*, 57, 45-58, 2013.
- 1988 Sofiev, M., Berger, U., Prank, M., Vira, J., Arteta, J., Belmonte, J., Bergmann, K. C., Chéroux, F., Elbern, H., Friese, E.,
1989 Galan, C., Gehrig, R., Khvorostyanov, D., Kranenburg, R., Kumar, U., Marécal, V., Meleux, F., Menut, L., Pessi, A. M.,
1990 Robertson, L., Rittenberga, O., Rodinkova, V., Saarto, A., Segers, A., Severova, E., Sauliene, I., Siljamo, P., Steensen, B. M.,
1991 Teinmaa, E., Thibaudon, M., and Peuch, V. H.: MACC regional multi-model ensemble simulations of birch pollen
1992 dispersion in Europe, *Atmos. Chem. Phys.*, 15, 8115-8130, 10.5194/acp-15-8115-2015, 2015b.
- 1993 Sofieva, S., Asmi, E., Atanasova, N. S., Heikkinen, A. E., Vidal, E., Duplissy, J., Romantschuk, M., Kouznetsov, R.,
1994 Kukkonen, J., and Bamford, D. H.: Effects of temperature and salinity on sea-spray-aerosol formation simulated with a
1995 bubble-generating chamber, *Atmospheric Measurement Techniques Discussions*, 2022, 1-40, 2022.
- 1996 Spada, M.: Development and evaluation of an atmospheric aerosol module implemented within the NMMB/BSC-CTM,
1997 2015.
- 1998 Spada, M., Jorba, O., Pérez García-Pando, C., Janjic, Z., and Baldasano, J. M.: Modeling and evaluation of the global sea-
1999 salt aerosol distribution: sensitivity to size-resolved and sea-surface temperature dependent emission schemes, *Atmos. Chem.
2000 Phys.*, 13, 11735-11755, 10.5194/acp-13-11735-2013, 2013.
- 2001 Stockwell, W. R., Kirchner, F., Kuhn, M., and Seefeld, S.: A new mechanism for regional atmospheric chemistry modeling,
2002 *Journal of Geophysical Research: Atmospheres*, 102, 25847-25879, 1997.
- 2003 Strand, A. and Hov, O.: A two-dimensional global study of tropospheric ozone production, *J Geophys Res* 99, 22877-22895,
2004 1994.
- 2005 Struzewska, J. and Kaminski, J.: Formation and transport of photooxidants over Europe during the July 2006 heat wave—
2006 observations and GEM-AQ model simulations, *Atmospheric Chemistry and Physics*, 8, 721-736, 2008.
- 2007 Struzewska, J. and Kaminski, J.: Impact of urban parameterization on high resolution air quality forecast with the GEM-AQ
2008 model, *Atmospheric Chemistry and Physics*, 12, 10387-10404, 2012.



- 2009 Struzewska, J., Kaminski, J., and Jefimow, M.: Application of model output statistics to the GEM-AQ high resolution air
2010 quality forecast, *Atmospheric Research*, 181, 186-199, 2016.
- 2011 Struzewska, J., Zdunek, M., Kaminski, J., Łobocki, L., Porebska, M., Jefimow, M., and Gawuc, L.: Evaluation of the GEM-
2012 AQ model in the context of the AQMEII Phase 1 project, *Atmospheric Chemistry and Physics*, 15, 3971-3990, 2015.
- 2013 Szymankiewicz, K., Kaminski, J. W., and Struzewska, J.: Interannual variability of tropospheric NO₂ column over Central
2014 Europe—Observations from SCIAMACHY and GEM-AQ model simulations, *Acta Geophysica*, 62, 915-929, 2014.
- 2015 Thürkow, M., Kirchner, I., Kranenburg, R., Timmermans, R., and Schaap, M.: A multi-meteorological comparison for
2016 episodes of PM₁₀ concentrations in the Berlin agglomeration area in Germany with the LOTOS-EUROS CTM, *Atmospheric
2017 Environment*, 244, 117946, 2021.
- 2018 Tie, X., Madronich, S., Walters, S., Zhang, R., Rasch, P., and Collins, W.: Effect of clouds on photolysis and oxidants in the
2019 troposphere, *Journal of Geophysical Research: Atmospheres*, 108, 2003.
- 2020 Timmermans, R., van Pinxteren, D., Kranenburg, R., Hendriks, C., Fomba, K., Herrmann, H., and Schaap, M.: Evaluation of
2021 modelled LOTOS-EUROS with observational based PM₁₀ source attribution, *Atmospheric Environment: X*, 14, 100173,
2022 2022.
- 2023 Troen, I. and Mahrt, L.: A simple model of the atmospheric boundary layer: Sensitivity to surface evaporation, *Bound.-Layer
2024 Meteorol.*, 37, 129-148, 1986.
- 2025 Tsyro, S., Aas, W., Soares, J., Sofiev, M., Berge, H., and Spindler, G.: Modelling of sea salt concentrations over Europe: key
2026 uncertainties and comparison with observations, *Atmos. Chem. Phys.*, 11, 10367–10388, doi:10.5194/acp-11-10367-2011,
2027 2011.
- 2028 Tuovinen, J.-P., Ashmore, M., Emberson, L., and Simpson, D.: Testing and improving the EMEP ozone deposition module,
2029 *Atmos. Environ.*, 38, 2373–2385, 2004.
- 2030 van Leer, B.: Multidimensional explicit difference schemes for hyperbolic conservation laws, in: *Computing Methods in
2031 Applied Sciences and Engineering VI*, edited by: Lions, R. G. a. J. L., Elsevier, Amsterdam, 1984.
- 2032 Van Ulden, A. and Holtslag, A.: Estimation of atmospheric boundary layer parameters for diffusion applications, *Journal of
2033 Applied Meteorology and Climatology*, 24, 1196-1207, 1985.
- 2034 Van Zanten, M., Sauter, F., RJ, W. K., Van Jaarsveld, J., and Van Pul, W.: Description of the DEPAC module: Dry
2035 deposition modelling with DEPAC_GCN2010, RIVM rapport 680180001, 2010.
- 2036 Vautard, R., Bessagnet, B., Chin, M., and Menut, L.: On the contribution of natural Aeolian sources to particulate matter
2037 concentrations in Europe: Testing hypotheses with a modelling approach, *Atmospheric Environment*, 39, 3291-3303,
2038 <https://doi.org/10.1016/j.atmosenv.2005.01.051>, 2005.
- 2039 Venkatram, A.: Estimating the Monin-Obukhov length in the stable boundary layer for dispersion calculations, *Boundary-
2040 Layer Meteorology*, 19, 481-485, 1980.
- 2041 Venkatram, A., Karamchandani, P., and Misra, P.: Testing a comprehensive acid deposition model, *Atmospheric
2042 Environment (1967)*, 22, 737-747, 1988.



- 2043 Vira, J. and Sofiev, M.: On variational data assimilation for estimating the model initial conditions and emission fluxes for
2044 short-term forecasting of SO_x concentrations, *Atmospheric environment*, 46, 318-328, 2012.
- 2045 Vira, J. and Sofiev, M.: Assimilation of surface NO₂ and O₃ observations into the SILAM chemistry transport model,
2046 *Geoscientific Model Development*, 8, 191-203, 2015.
- 2047 Wang, X., Zhang, L., and Moran, M. D.: Development of a new semi-empirical parameterization for below-cloud
2048 scavenging of size-resolved aerosol particles by both rain and snow, *Geoscientific Model Development*, 7, 799-819, 2014.
- 2049 Weaver, A. and Courtier, P.: Correlation modelling on the sphere using a generalized diffusion equation, *Quarterly Journal*
2050 *of the Royal Meteorological Society*, 127, 1815-1846, 2001.
- 2051 Wesely, M. L.: Parameterization of surface resistances to gaseous dry deposition in regional-scale numerical models,
2052 *Atmospheric Environment (1967)*, 23, 1293-1304, 1989.
- 2053 Wild, O., Zhu, X., and Prather, M. J.: Fast-J: Accurate Simulation of In- and Below-Cloud Photolysis in Tropospheric
2054 Chemical Models, *Journal of Atmospheric Chemistry*, 37, 245-282, 10.1023/A:1006415919030, 2000.
- 2055 Williams, E., Guenther, A., and Fehsenfeld, F.: An inventory of nitric oxide emissions from soils in the United States,
2056 *Journal of Geophysical Research: Atmospheres*, 97, 7511-7519, 1992.
- 2057 Williamson, D. L. and Rasch, P. J.: Two-dimensional semi-Lagrangian transport with shape-preserving interpolation,
2058 *Monthly Weather Review*, 117, 102-129, 1989.
- 2059 Willis, P. T. and Tattelman, P.: Drop-size distributions associated with intense rainfall, *Journal of Applied Meteorology and*
2060 *Climatology*, 28, 3-15, 1989.
- 2061 Xian, P., Reid, J. S., Hyer, E. J., Sampson, C. R., Rubin, J. I., Ades, M., Asencio, N., Basart, S., Benedetti, A., and
2062 Bhattacharjee, P. S.: Current state of the global operational aerosol multi-model ensemble: An update from the International
2063 Cooperative for Aerosol Prediction (ICAP), *Quarterly Journal of the Royal Meteorological Society*, 145, 176-209, 2019.
- 2064 Yamartino, R., Scire, J., Carmichael, G., and Chang, Y.: The CALGRID mesoscale photochemical grid model—I. Model
2065 formulation, *Atmospheric Environment. Part A. General Topics*, 26, 1493-1512, 1992.
- 2066 Yamartino, R. J., Flemming, J., and Stern, R.: Adaptation of analytic diffusivity formulations to Eulerian grid model layers
2067 of finite thickness, in: *Air Pollution Modeling and Its Application XVII*, Springer, 468-477, 2007.
- 2068 Yarwood, G., Rao, S., Yocke, M., and Whitten, G. Z.: Updates to the Carbon Bond chemical mechanism: CB05,
2069 http://www.camx.com/publ/pdfs/CB05_Final_Report_120805.pdf, 2005.
- 2070 Yienger, J. and Levy, H.: Empirical model of global soil-biogenic NO_x emissions, *Journal of Geophysical Research:*
2071 *Atmospheres*, 100, 11447-11464, 1995.
- 2072 Yuan, H., Dai, Y., Xiao, Z., Ji, D., and Shangguan, W.: Reprocessing the MODIS Leaf Area Index Products for Land
2073 Surface and Climate Modelling, *Remote Sensing of Environment*, 155, 1171-1187, doi:10.1016/j.rse.2011.01.001, 2011.
- 2074 Zare, A., Christensen, J., Irannejad, P., and Brandt, J.: Evaluation of two isoprene emission models for use in a long-range
2075 air pollution model, *Atmospheric Chemistry and Physics*, 12, 7399-7412, 2012.



- 2076 Zare, A., Christensen, J., Gross, A., Irannejad, P., Glasius, M., and Brandt, J.: Quantifying the contributions of natural
2077 emissions to ozone and total fine PM concentrations in the Northern Hemisphere, *Atmospheric Chemistry and Physics*, 14,
2078 2735-2756, 2014.
- 2079 Zender, C. S., Bian, H., and Newman, D.: Mineral Dust Entrainment and Deposition (DEAD) model: Description and 1990s
2080 dust climatology, *Journal of Geophysical Research: Atmospheres*, 108, 10.1029/2002jd002775, 2003.
- 2081 Zhang, K. M., Knipping, E. M., Wexler, A. S., Bhave, P. V., and Tonnesen, G. S.: Size distribution of sea-salt emissions as a
2082 function of relative humidity, *Atmospheric Environment*, 39, 3373-3379, <https://doi.org/10.1016/j.atmosenv.2005.02.032>,
2083 2005.
- 2084 Zhang, L., Brook, J. R., and Vet, R.: A revised parameterization for gaseous dry deposition in air-quality models, *Atmos.*
2085 *Chem. Phys.*, 3, 2067–2082, 2003.
- 2086 Zhang, L., Gong, S., Padro, J., and Barrie, L.: A size-segregated particle dry deposition scheme for an atmospheric aerosol
2087 module, *Atmospheric Environment*, 35, 549-560, 2001.
- 2088 Zhang, Y., Bocquet, M., Mallet, V., Seigneur, C., and Baklanov, A.: Real-time air quality forecasting, part I: History,
2089 techniques, and current status, *Atmospheric Environment*, 60, 632-655, 2012a.
- 2090 Zhang, Y., Bocquet, M., Mallet, V., Seigneur, C., and Baklanov, A.: Real-time air quality forecasting, part II: State of the
2091 science, current research needs, and future prospects, *Atmospheric Environment*, 60, 656-676,
2092 <https://doi.org/10.1016/j.atmosenv.2012.02.041>, 2012b.
- 2093 Zilitinkevich, S. and Mironov, D. V.: A multi-limit formulation for the equilibrium depth of a stably stratified boundary
2094 layer, *Boundary-Layer Meteorology*, 81, 325-351, 1996.
2095